Probabilistic Evaluation of Distribution Network Reliability in the Presence of Renewable Energy Sources, Energy Storage and Electric Vehicles

By

Anand Maniyam Pariyarath

A Thesis submitted to the Faculty of Graduate Studies of
The University of Manitoba
in partial fulfillment of the requirements of the degree of
DOCTOR OF PHILOSOPHY

Department of Electrical and Computer Engineering
Faculty of Engineering
University of Manitoba
Winnipeg, Manitoba, Canada

April 2021

Abstract

Increased penetration of electric vehicles (EVs) and renewable energy sources (RESs) in power systems can directly affect the system reliability and impose additional complexities to planning and operation due to their uncertainties. The traditional planning methods based on deterministic analysis fail to accurately capture the impact of the aforementioned uncertainty on the system reliability.

In this thesis, a reliability-oriented distribution system analysis methodology that captures the complex interactions between EVs, photovoltaic (PV) power production, and energy storage is proposed. Firstly, a two-layer stochastic EV charging demand estimation model is proposed. The model comprises of a traffic layer representing the spatial-temporal distributions of EVs and an electrical network layer describing the impact of EV charging demand on electrical network. A Dynamic Hidden Markov model is used to capture the EV movements in the traffic layer. The ability of the traffic layer model to faithfully represent the random travel pattern of actual vehicles used by different types of drivers is examined. Secondly, a novel stochastic solar irradiance model based on probability distributions of the first-order differences of hourly global solar horizontal irradiance is proposed to calculate the stochastic power output of the PV system. Measured solar irradiance data from four different locations with varying climate characteristics were used to evaluate the proposed model in comparison to two previously reported models. Additionally, various computational models such as the EV charging station model, reliability evaluation model, and economic evaluation model are developed to support the reliability and economic evaluation with necessary inputs.

Monte Carlo simulation (MCS) is used to analyze a range of best to worst-case scenarios for more optimal outcomes. A range of sensitivity analysis is performed to illustrate the reliability and economic impact due to EV charging, PV power production and various operating strategies. Several new reliability indices are proposed to quantify the impact of EV charging characteristics, RES penetration, and energy storage system (ESS) on the reliability performance of distribution systems. Finally, an optimization algorithm along with developed stochastic models and MCS framework is used for the optimization of the resource sizes considering EV charging stations (EVCSs) life-cycle costs, reliability and emissions.

Use of Copyrighted Material

I like to confirm the approval from all the authors and hereby acknowledge the use of the following publications during the preparation of this thesis. Only the contents of the publications where I am the first author are included in this thesis.

Publication in Elsevier Journals

- **M. P. Anand,** B. Bagen, and A. Rajapakse, "Reliability Oriented Distribution System Analysis Considering Electric Vehicles and Hybrid Energy Resources," *Int. J. Electr. Power Energy Syst., (Under Review)*
- **M. P. Anand,** B. Bagen, and A. Rajapakse, "Probabilistic reliability evaluation of distribution systems considering the spatial and temporal distribution of electric vehicles," *Int. J. Electr. Power Energy Syst.*, vol. 117, no. July 2019, p. 105609, 2020.

Publication in International Energy Journal

- **M. P. Anand,** A. Rajapakse, and B. Bagen, "Stochastic Model for Generating Synthetic Hourly Global Horizontal Solar Radiation Data Sets Based on Auto Regression Characterization," *Int. Energy J.*, vol. 20, pp. 181–200, 2020.

Publications in IEEE Conference

- **M.P. Anand,** A. D. Rajapakse, and B. Bagen, "Analysis of the quality of long-term synthetic solar radiation data generated from stochastic models," *2018 Int. Conf. Probabilistic Methods Appl. to Power Syst. PMAPS 2018 - Proc.*, pp. 1–6, 2018.
- **M.P. Anand**, A. Rajapakse, S. Muthukumarana, and B. Bagen, "Evaluation of a Stochastic Vehicle Travel Pattern Generation Model with the Real-World Travel Data," *2020 IEEE Electr. Power Energy Conf.*, vol. 3, pp. 8–13, 2020.

Regarding the copyright policy of Elsevier, the following is endorsed;

"Authors can use their articles, in full or in part, for a wide range of scholarly, non-commercial purposes as outlined below:

- Use by an author in the author's classroom teaching (including distribution of copies, paper or electronic)
- Distribution of copies (including through e-mail) to known research colleagues for their personal use (but not for Commercial Use)
- **Inclusion in a thesis or dissertation (provided that this is not to be published commercially)**
- Use in a subsequent compilation of the author's works
- Extending the Article to book-length form
- Preparation of other derivative works (but not for Commercial Use)
- Otherwise using or re-using portions or excerpts in other works

These rights apply to all Elsevier authors who publish their article as either a subscription article or an open-access article. In all cases, we require that all Elsevier authors always include a full acknowledgement and, if appropriate, a link to the final published version hosted on Science Direct."

Regarding the copyright policy of IEEE, following is endorsed;

"In reference to IEEE copyrighted material, which is used with permission in this thesis, the IEEE does not endorse any of University of Manitoba's products or services. Internal or personal use of this material is permitted. If interested in reprinting/republishing IEEE copyrighted material for advertising or promotional purposes or for creating new collective works for resale or redistribution, please go to ***http://www.ieee.org/ publications_standards/ publications/rights/rights_link.html*** to learn how to obtain a License from RightsLink. If applicable, University Microfilms and/or ProQuest Library, or the Archives of Canada may supply single copies of the dissertation."

Acknowledgments

I would like to express my deepest gratitude and thanks to my advisor Dr. Athula Rajapakse and co-advisor Dr. Bagen Bagen for their invaluable guidance, and continuous encouragement throughout the research work. It was a great privilege to work under their supervision. I also wish to thank all academic, administrative, and technical staff at the Department of Electrical and Computer Engineering, especially Traci Gledhill and Amy Dario for their assistance.

I wish to express my sincere gratitude to the Advisory Committee members for their helpful comments and feedback to improve the quality of the thesis. I like to acknowledge the financial supports received from Manitoba Hydro, Mitacs accelerate program and the University of Manitoba. Also, I like to thank all my colleagues in the Department of Electrical and Computer Engineering for their continuous encouragement.

I extend my deepest gratitude and pranams to my guru His Holiness Sri Sri Ravi Shankar, humanitarian, spiritual leader and founder of the organization The Art of Living for showering his blessings, guidance and support during my difficult times. I thankfully remember all my Art of Living family members for making these years of my stay in Canada one of the best experiences of my life. I also like to thank Mr. Mohan K Vedkumar, Vedic Astrologer, the Astro research centre, Palakkad, Kerala, India for giving me such an extraordinary direction in my career and constant backing during challenging times. I also like to pay my thankfulness to all my essential educators and supporters of my academic life.

Last but not least, I would like to extend my gratitude to my beloved parents and grandparents for all their love and guidance throughout my life. Without them, I would not be the person I am today. The biggest acknowledgement goes to my loving wife for her patience, understanding, and encouragement whenever I most needed them.

Anand Maniyam Pariyarath

December 2020

Dedication

To my beloved mother, father, and my dear wife

Contents

List of Tables

List of Figures

List of Abbreviations

ASAI	Average System Availability Index
BEV	Battery Electric Vehicle
CC	Commercial Center
CDF	Cumulative Distribution Function
CL	Charge Level
DER	Distributed Energy Resource
DHMM	Dynamic Hidden Markov Model
DN	Distribution Network
ED	Euclidean Distance
EDECI	Expected Duration of EV Charging Index
EECL	Expected EV Charging Load
EENS	Expected Energy Not Supplied
EFECI	Expected Frequency of EV Charging Index
ESS	Energy Storage System
EV	Electric Vehicle
GHI	Global Horizontal Irradiance
HMM	Hidden Markov Model
IEA	International Energy Agency
MCMC	Markov Chain Monte Carlo Simulation
MCS	Monte Carlo Simulation
NRC	Natural Resources Canada
PCC	Pearson Correlation Coefficient
PV	Photovoltaic
RA	Residential Areas
RES	Renewable Energy Resources

RL	Random Location
SAIDI	System Average Interruption Duration Index
SAIFI	System Average Interruption Frequency Index
SM	Shopping Mall
SOC	State of Charge
TMY	Typical Meteorological Year
V2G	Vehicle to Grid
WP	Workplace

Chapter 1

Introduction

1.1 Background

Climate change, environmental pollution, and energy crisis have motivated all nations to cater to the utilization of renewable energy sources (RESs) instead of fossil fuels and to adopt sustainable transportation by including more electric vehicles (EVs) in their fleet [1]. The penetration of RESs and other emerging technologies such as energy storage systems (ESSs) and EVs has rapidly increased during the past decade, particularly in the electrical distribution systems [2], [3]. The undergoing growth of small-scale generation and ESSs connected to the distribution network, commonly referred to as the distributed energy resources (DERs), along with EV charging infrastructure has resulted in considerable changes to the distribution network concerning the structure, operation, regulation, and modernization [4].

Figure 1.1 shows a conceptual diagram illustrating a modern distribution system with RESs, ESSs, and EVs along with traditional consumer loads. The factors such as increased RESs utilization, achieving better energy efficiency and improving grid reliability drive

DERs integration. Therefore, the power distribution systems need to be planned considering these changes and the new investments should be allocated to the right infrastructure that facilitates harnessing the perceived benefits of RESs, ESSs, and EVs [5]. Hence, it is imperative to develop appropriate models and methodologies for accurate and realistic evaluation of the reliability of distribution networks considering the roles of RESs, ESSs, and EVs.

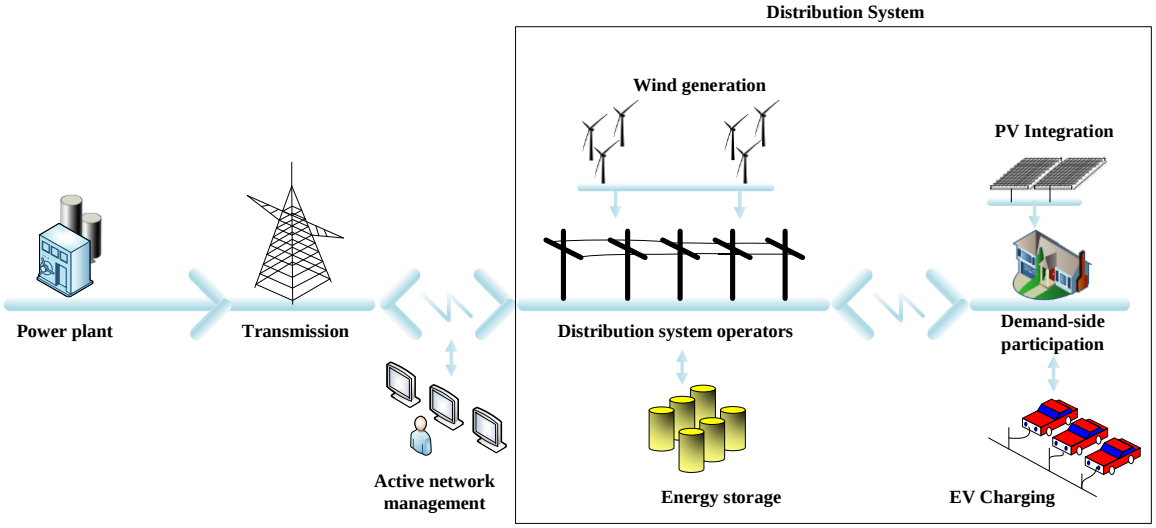

Figure 1.1. Features of a modern distribution system

1.2 Probabilistic analysis of power systems

The conventional deterministic planning methods are challenged by the intermittent nature of distributed generation (DG) based on wind, solar energy and non-traditional loads like EV charging loads. Probabilistic analysis is considered the most suitable approach for modelling the power system uncertainty since the uncertainties associated with the output of the generator or load is quantified by conducting a statistical analysis of the corresponding data. A random

variable (RV) and a particular probability density function (PDF) are used to represent the uncertainty associated with each system input. Two major propositions for probabilistic analysis of power systems have been put forward in the literature, namely, i) analytical methods, and ii) simulation methods

The application of analytical methods such as point estimation method (PEM) and copulas estimation technique to deal with load and generation uncertainty is described in several publications. PEM involves the use of sample data to calculate a single value which is to serve as the best estimate of an unknown population parameter. For example, a probabilistic power flow based on PEM has been employed to estimate the uncertainty associated with wind turbine-based DGs, load demand, PV power and EV charging behaviour in [6]. The copula is a function which couples a multivariate distribution function to its marginal distribution functions, generally called marginals or simply margins. Compared with PEM they are great tools for modelling and simulating correlated random variables. The copulas estimation technique has been used in [7] to predict the EV demand by considering the randomness in EV travel distance as well as the plug-in time of EVs.

On the other hand, simulation-based methods rely on repeated random sampling to obtain numerical results. Monte Carlo simulation (MCS) is the most popular simulation-based method. There are many MCS methods, but in general, they involve (i) defining a domain of each input; (ii) generating inputs randomly from a probability distribution over its domain; (iii) computation of some objective functions (deterministically) from the random inputs; and (iv) aggregation of the results. In the application of MCS to a particular

problem, the major concern is the development of the problem-specific models required in step (iii), obtaining the proper probability density functions of inputs, and computational time required to the convergence of the simulation. Thus, the implementation of the MCS analysis for a given problem can differ depending on the modelling approach. A common technique is to use a pool of scenarios to represent the stochastic inputs. For example, in [8] a set of 10 probabilistic wind and solar power profiles have been used to analyze the operational challenges associated with the integration of intermittent sources using MCS. A similar approach has been used to model the stochastic behaviour of wind turbines [9], to analyze the uncertainties associated with the plug-in EVs, wind-based DG, EV driving patterns and energy consumption [10], [11], [12].

The survey of the literature shows that although analytical approaches are less computationally demanding, they require many simplifying assumptions in formulating the problem in a manner amenable for analytical solutions. On the other hand, MCS methods are proven to be able to handle the effect of uncertainties without many simplifying assumptions. They are also flexible enough to incorporate complex network management strategies.

1.3 Stochastic models and operating strategies

Non-traditional load patterns due to massive EVs penetration along with stochastic power output from RESs have been reported to cause various distribution system challenges such voltage deviations, quality of supply degradation, increased power losses, transformers and line overloads, harmonics and fault current increase in distribution

networks [13]. Hence, it is imperative to model the original characteristics of EV charging and RESs for the evaluation of distribution system reliability.

From the power system context, EVs can be considered as non-traditional loads as the EV owners have the freedom to charge their vehicle whenever there is an opportunity. This brings forward the relevance to consider the spatial-temporal aspects in the EV charging demand estimation models. Additionally, EV modeling also presents complexities due to various aspects such as varying charging patterns during the weekends and weekdays, different charging behaviour of the EV drivers, variations in the travel distances, disparities in the battery state of charge (SOC) depending on the type of EVs and their battery size. There are detailed EV models [14]–[17] that have considered both major and minor details pertained to EV charging. These models are proven to be efficient in EV charging demand estimation, electrical network analysis, charging station planning etc. However, these models are highly complex and can be computationally exhaustive to use in MCS-based planning approaches which require thousands of simulations over long planning horizons. On the other hand, there are simple models [18]–[21] which partially ignore the important spatial-temporal distribution while estimating the EV charging demand. Hence, a stochastic EV charging demand estimation model that finds an appropriate trade-off between the details and simplifications helps back the probabilistic evaluation.

While considering the RESs like solar energy systems in the probabilistic planning studies, MCS requires a distinct time series of solar irradiance for each trial over the planning horizon as an input to fully characterize the randomness. Historical data over a short period may not fully capture the full stochastic nature of the variations in solar

irradiance over a long planning period. Therefore, synthetic solar irradiance generators are often used to support MCS and similar probabilistic approaches. A significant effort has been devoted in the past to develop various stochastic solar irradiance models capable of generating synthetic sets of solar irradiance [22]. Different solar prediction models have been proposed to generate solar irradiance in short, medium and long-term horizons [23]–[25]. Many of the existing long-term solar irradiance models have deficiencies either in accurately representing the site-specific random variations or in computational efficiency, limiting their utility in MCS. A solar irradiance model suitable for generating long-term synthetic solar irradiance data can be helpful for MCS-based power system planning studies [22].

It can be challenging to ensure secure, economic, and reliable power system operation under the penetration of stochastic power sources like RESs and non-traditional loads due to EV charging. To tackle this, various operating strategies are adopted by the distribution system operators. The adverse effects of uncontrolled EV charging on distribution system challenges are catalogued in [13], where adopting smart-charging approaches to efficiently manage the EV charging-related challenges is advocated. For distribution system operators/utilities, finding an optimal operating approach can be formulated as a multi-objective optimization problem. For example, the reduction in the operating cost with the minimization of the difference between average and maximum power demand is considered in formulating the optimization problem in [26]. In the beginning, many approaches ignored the presence of RESs uncertainties in their operating strategies.

On the other hand, distribution system operators/power utilities can use a coordinated approach for power dispatch in the presence of RESs and ESSs to efficiently manage the EV charging-related challenges on the distribution system planning. As demonstrated in [27], EVs charging/discharging potential can be utilized for balancing the power production and demand for a micro-grid with wind power and EV charging loads. The operating flexibility of the distribution system greatly increases when the vehicle to grid (V2G) energy transfer is enabled. A comparison of different types of EV charging management strategies in distribution systems including uncontrolled and smart charging approaches along with demand response and V2G energy transfer is presented in [28] for day-ahead scheduling of smart grid with intensive penetration of DGs and EVs. It is also shown in [29] that when the owners of EVs and controllable loads participate in energy and reserve scheduling, the operational flexibility improves further.

Many of the proposed approaches in [13], [26]–[29] address the issue of short-term operational planning of active distribution networks to achieve various technical, economic, environmental and reliability goals and are generally too complicated to use in long-term planning studies. However, distribution system operating strategies are required to optimally utilize the available resources to effectively maintain a reliable system operation while considering RESs and EVs charging.

1.4 Distribution system reliability

The reliability of an electrical network is the ability of the power system to supply consumers continuously with acceptable quality. The result of distribution system

reliability assessment is various reliability indices such as Loss of Load Expectation (LOLE), Expected Energy Not Served (EENS), System's Average Interruption Frequency Index (SAIFI), System's Average Interruption Duration Index (SAIDI), and other similar indices [30].

Presently, the main concern for distribution system reliability is the stochastic nature of the power output of RESs, EV charging loads, and controllable loads used in demand-side management. The growth of the EV fleet increases the system loading resulting in the weakening of the system reliability and the EV charging/discharging strategy has a strong influence on the power system reliability indices like LOLE and EENS [11]. Recent literature reports some efforts to incorporate these effects into the models and methods used for reliability evaluation. An explicit evaluation of the impact of DSM on power system reliability has been reported in [31]. The load profile of major residential appliances, flexibility associated with individual load profiles, appliance level load profiles and different contingencies are used to assess the system reliability. While some interesting work has been carried out in this area, there are many more aspects to explore, especially related to the incorporation of EV charging. The models need to be improved considering driving patterns, different charging methods, and differences in the EVs of different manufactures.

1.5 Problem definition

The traditional distribution planning adopts the least-cost approach for meeting the peak system demand while satisfying some reliability criteria. However, due to stochastic

generation sources such as wind and PV energy systems, and loads such as EVs, this approach will not lead to the best solution. On the other hand, the existing distribution planning models are not flexible enough to incorporate the intermittent generation due to the DERs and non-traditional loads such as EVs. Hence, probabilistic planning approaches that can incorporate uncertainties into the distribution system planning are gaining increased attention. MCS methods are one of the approaches for probabilistic evaluation of distribution systems that have flexibility in modelling uncertainties such as the output of RESs or EV loads. This approach mimics the actual operating history of power systems by random sampling to obtain numerical results. Hence, reliability-centred planning using MCS is an attractive approach to incorporate uncertainties, random influences, and complex network management strategies [32].

As discussed earlier, suitable stochastic models that represent the uncertainties of the power system components and operational practices are required to perform MCS. It is imperative to have accurate computational models capable of estimating the possible variations associated with RESs and EV charging to obtain trustworthy results. These models are then used to evaluate quantitative indicators of reliability or their distributions. It is expected that any stochastic models developed for backing the MCS-based probabilistic evaluation should be able to preserve the original characteristics of the designated modeling element (RESs, ESSs, EVs) while being compatible to generate long-term, non-repetitive datasets.

As presented in Section 1.1, some interesting work has been carried out in the past to develop stochastic EV models to account for the charging demand on the power system.

Similarly, many stochastic solar irradiance models have been developed to generate synthetic solar irradiance datasets for use in MCS. Although the representation of renewable energy generation in planning studies is somewhat established, there are several aspects to be explored when incorporating renewable energy sources with EV charging. For example, an emerging trend in renewable-based EV charging has been reported in the literature [33]. The EVCSs equipped with PV energy systems and ESSs are often considered as they can be easily incorporated into urban settings. Systems that combine RESs and ESSs are referred to as distributed energy resources (DERs). The distribution system reliability is an important factor but many of the reported stochastic planning approaches that consider RESs, ESSs, and EVs are heavily focused on the cost of emission reductions and pay less attention to reliability aspects. Reliability-centred electrical network analysis is sensitive to random parameters such as stochastic power output of RESs, EV driver's charging characteristics. This randomness can only be tackled using efficient stochastic models.

In summary, the main research gaps identified to address in this thesis are:

- A dearth of research that study and quantify the impact of EV charging on the distribution system reliability as most previous studies mostly focussed on objectives such as cost and emission reduction or finding optimal charging station locations.
- Limitations of the models used to generate spatial and temporal distributions of EV charging patterns in probabilistic planning methods. The existing models are either computationally exhaustive or too simple to capture some important aspects related to

EV charging, such as the day type, driving patterns, different charging methods, and differences in the EVs.

- Deficiencies in synthetic solar irradiance generating models used in probabilistic planning studies in preserving the stationary and sequential properties of measured solar irradiance.

Thus, the proposed research will advance the state-of-the-art in the probabilistic evaluation of distribution networks (DNs) containing RESs, ESSs, and EVs by developing appropriate models and techniques. These models and techniques will be developed to facilitate the use of the MCS approach and to incorporate various efficient algorithms for the optimization of system reliability and costs. The proposed approach is expected to facilitate a more realistic evaluation of distribution system reliability under the changing industry environment and help the power industry to perform probabilistic analysis in distribution system reliability assessment and integrated resource planning.

1.6 Objectives of the research

The main goal of the proposed research is to develop appropriate models for accurate and realistic evaluation of the reliability of distribution networks considering the role of RESs, ESSs and EVs. To achieve the main goal of this research, the following sub-objectives are proposed:

a) To develop a suitable model to estimate the stochastic power output of PV energy systems that is usable for MCS based long-term planning studies, including a model capable of generating long-term, non-repetitive, synthetic sets of solar irradiance.

b) To develop a suitable stochastic model for generating the EV charging demand patterns considering the spatial-temporal distribution of EVs while incorporating the parameters pertaining to individual EVs such as driving range, charging locations, driving distances, and driver's charging habits.

c) To develop a complete methodology to examine the impact of EV penetration on distribution network reliability by utilizing the stochastic EV model developed in (b).

d) Development of a comprehensive methodology for distribution system reliability evaluation considering the complex interactions among EVs, PV systems, and energy storage.

e) Development of an economic evaluation model to calculate the total cost pertained to EVCS equipped DERs considering the capital cost, operation cost, emission cost, and cost of unreliability.

f) Application of the developed stochastic models and MCS framework for optimization of the resource sizes of EVCSs considering the life-cycle costs, reliability and emissions.

1.7 Thesis overview

Figure 1.2 illustrates the individual chapters included in this thesis and their inter-relationship in leveraging the development of different models and methodologies as the research progresses. Each chapter consists of a focused literature review pertaining to the context addressed in the chapter, and therefore the thesis does not contain a separate chapter

devoted to the literature review, except for the background provided in this introduction. The contents of each chapter represent a major publication or a combination of several publications.

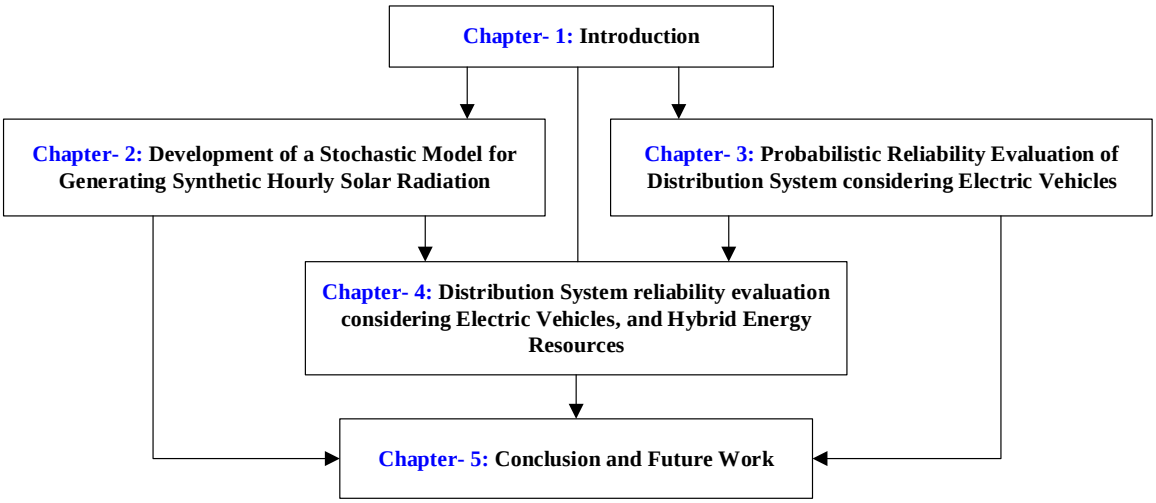

Figure 1.2. Flow diagram illustrating the overview of the thesis

Chapter 1 provides the introduction giving the necessary background, motivation, and objectives of this thesis along with the details of the thesis organization. The next three chapters present the main contributions of the thesis with each chapter addressing one or more objectives: Objective (a) is addressed in Chapter 2; objectives (b) and (c) are addressed in Chapter 3; and objectives (d), (e), and (f) are addressed in Chapter 4.

Chapter 2 develops a novel stochastic solar irradiance model to generate long-term, non-repetitive synthetic sets of solar irradiance data. The chapter contains a detailed literature review on the existing solar irradiance models which leads to the identification of several areas for improvement, the development and validation of a novel synthetic solar irradiance generation model and its comparison with two other existing models.

Chapter 3 presents the development of a stochastic model to quantify the additional power demand due to EV charging. It reviews the existing models that attempted to quantify the EV charging demand and identifies key research gaps over the existing state of the art. Furthermore, this chapter develops a methodology to perform distribution system reliability analysis using the developed stochastic EV charging demand estimation model and MCS. The application of the models is demonstrated by performing various studies and sensitivity analyses to examine the impact of EV penetration on distribution system reliability.

Chapter 4 combines the stochastic EV model from Chapter 2 and the stochastic solar irradiance model from Chapter 3 for distribution reliability evaluation considering the presence of both EVs and PV power generation. The chapter presents a complete methodology to perform distribution system reliability evaluation considering RESs, ESSs, EVs using the developed stochastic models to generate synthetic patterns of PV power output and EV energy consumption patterns while analyzing the best to worst-case scenarios using the MCS. This framework is incorporated into an optimization algorithm to choose optimal DERs sizes.

Chapter 5 provides the conclusions of the research along with the directions for improvements through further research.

Chapter 2

Stochastic Model for Generating Synthetic Solar Irradiance Data

2.1 Introduction

The typical approach used for designing solar energy systems is to use a short period of historical weather data or typical meteorological year (TMY) data for the particular location to evaluate the performance of the system being designed. However, a short period of historical data or TMY data may not capture the full stochastic nature of the variations in solar irradiance over the long design life of solar energy systems. To overcome this limitation and reliably evaluate the feasibility of design alternatives and the impact of different operational strategies associated with solar energy systems, probabilistic methods like Monte Carlo simulation (MCS) is used [34]. Each trial of MCS requires a distinct time series of solar irradiance over the design life cycle of the system as an input to fully characterize the randomness. MCS typically requires hundreds, if not thousands, of trails before convergence, and the simulation input demands non-repetitive datasets of solar

irradiance for each simulation trial [35]. Therefore, synthetic solar irradiance generators are often used to support MCS and similar probabilistic analysis approaches to perform design studies associated with the siting and sizing of solar collectors and energy storage requirements of both solar thermal and PV systems [36].

In this chapter, a novel stochastic solar irradiance model based on probability distributions of the first-order differences of hourly global solar horizontal irradiance is proposed. The first-order differences are modeled using a trend component and a stochastic component represented using the cumulative distribution functions, both extracted from historical data taken over a window of 31 days around the considered day of the year. Measured solar irradiance data from four different locations with varying climate characteristics were used to evaluate the proposed model in comparison to two previously reported models. The same approach can be extended to model diffuse horizontal irradiance and beam normal irradiance values.

2.2 Background and literature Review

Various methodologies have been employed by different authors in the development of synthetic solar irradiance generators. However, not every solar irradiance model is suitable for MCS which requires long-term, non-repetitive, synthetic solar irradiance values while preserving the original characteristics of the measured solar irradiance values. A brief review of existing solar irradiance generation models is presented in this section.

The method of calculating the clear sky solar irradiance based on the day of the year, time, and location is well established and many models are available [37]. This typically

involves the calculation of solar altitude, extraterritorial solar radiation, and attenuation due to aerosol concentration, water vapour, and various other atmospheric conditions and involves the use of well-studied geometrical and empirical relationships developed through long-term measurements. Clear sky direct normal solar radiation is predictable using deterministic models. However, the actual solar irradiance at a given location at a given time deviates from this due to random cloud cover and generally consists of both direct radiation and diffuse radiation due to scattering and reflections by clouds and atmospheric particles.

In one of the earliest attempts to model solar irradiance, Jordan and Liu proposed a model to determine the horizontal surface diffuse irradiance, the long-term average hourly and daily sums of diffused solar irradiance considering varying levels of cloudiness [38]. Another approach is proposed to generate sequences of global horizontal irradiance utilizing the probability of sunshine and cloudiness in [39]. The performance of this model has been validated by comparing the characteristics of the daily simulated solar irradiance to the observed daily data. Procedures for generating random but coherent sequences of daily global insolation values, and then decompose daily irradiance to hourly irradiance values are presented in [40], [41]. These models use a library of Markov transition matrices generated from long-term measurements for this purpose [42]. A similar stochastic procedure has been proposed for generating synthetic sets of hourly solar irradiance values in [43]. All these models primarily use the clearness index as a measure to capture the cloudiness during the sunshine hours while generating synthetic sets of solar irradiance. The clearness index is calculated as the ratio of measured solar irradiance to extraterrestrial

solar radiation. The extraterrestrial solar radiation is calculated based on the solar geometry and is assumed to be having higher values compared to the measured solar irradiance at the earth's surface. Thus the maximum value of the clearness index will be 1 which is calculated as a ratio of measured solar irradiance to the extra-terrestrial solar radiation [41]. However, it has been reported in [44] that cloud reflected radiation added to the direct solar radiation could sometimes make the measured solar irradiance values higher than the extraterrestrial solar radiation, especially near the sunrise and sunset. These instances can make the clearness index values greater than 1 and introduce errors to the models which use the clearness index as a primary measure [44].

The multi-scale methodology is proposed in [45] for generating long-term series of solar irradiance at a particular location involves generating annual and monthly global horizontal irradiance (GHI) and direct normal irradiance (DNI). Then, these outputs are used to generate hourly and sub-hourly solar irradiance. According to the results, these models can reproduce the main characteristics of the natural time series of measured solar irradiance data. Many publications including [43], [46] further validate these models for different locations, and they generally tend to preserve the statistical characteristics in the solar irradiance estimations. Additionally, some of the existing models intend to produce time series of hourly clearness index from the average values using stochastic procedures like average value decomposition [40] and Markov models [47], [48] to generate hourly clearness index from daily clearness index. However, solar system studies based on average values sometimes yield incorrect results [49].

There are attempts to develop solar irradiance generators capable of generating synthetic irradiance values at sub-hour time intervals for short periods such as 10-min [23], 5-min [24], 1-min [25] from mean hourly meteorological observation inputs. The motivation for developing these models is derived from the need for models that are essential in capturing the short-term temporal dynamics associated with solar irradiance which can bring huge operational benefits such as real-time power system scheduling [50]. However, short-term synthetic solar irradiance generators are less applicable to long-term planning studies.

Sizing, design, and performance evaluation of solar energy systems with dynamic characteristics and ESS at any location under consideration require accurate and detailed information on both the stationarity and sequential properties of hourly solar irradiance [51]. Analysis of the sequential characteristics of assorted meteorological variables, such as cloud cover, air temperature, wind speed, and relative humidity [23], [49] reveal very strong correlations at the one-hour time lag. A similar trend is revealed in a time series analysis of hourly GHI for a wide range of climatic stations that span temperate and tropic conditions [52]. The examination of the sequential behavior of hourly solar irradiance revealed strong correlations over long persistence times nearly equal to the entire daylight period. The solar irradiance time series input should reproduce not only the frequency of occurrence of various solar irradiance levels for each hour of the day but also the persistence times and persistence strengths of hour-to-hour variations of irradiance[51]. This is highly important with respect to the design of system including ESS. Hence, a simple model capable of generating synthetic, non-repetitive, long-term solar irradiance

datasets that replicates both the stationary and sequential characteristics of measured irradiance would be helpful for long-term planning studies.

2.3 Basis of the new model: first-order difference in solar irradiance

A strong correlation between the hourly solar irradiance over long persistence time periods has been reported by [51]. Similarly, the autocorrelation values are shown in Figure 2.1 (a) reveals the correlative structure of hourly GHI data measured at La Grange, USA. The strong correlation between the current hour solar irradiance with those of three past hours can be seen in the partial correlation shown in Figure 2.1 (b).

The relationship of this natural time series with respect to its immediate time steps is therefore evident from these correlation values. A similar trend in the autocorrelation and partial correlation values was observed for other locations considered in this work. Therefore, a new property named the "first-order difference in solar irradiance" which simply represents the rise or fall of solar irradiance at the current time step (t) with respect to the previous time step (t-1) is proposed in this work. This change in the global horizontal solar irradiance between two adjacent time steps can be represented as:

$$\Delta H_G(t) = H_G(t) - H_G(t-1) \qquad 2.1$$

where, $H_G(t)$ is the global horizontal solar irradiance measured at the current time step t and $H_G(t-1)$ is the value measured at the previous time step.

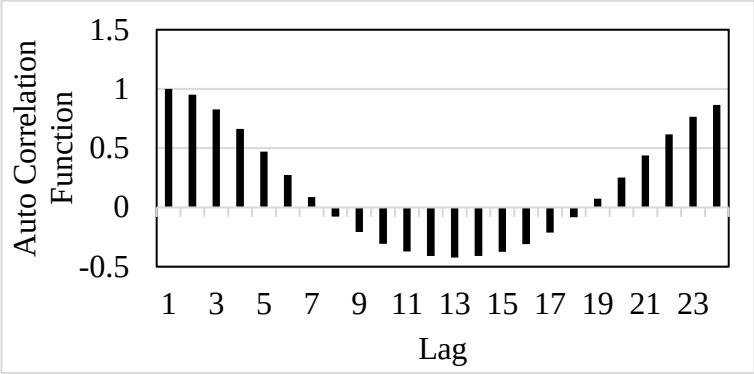

(a)

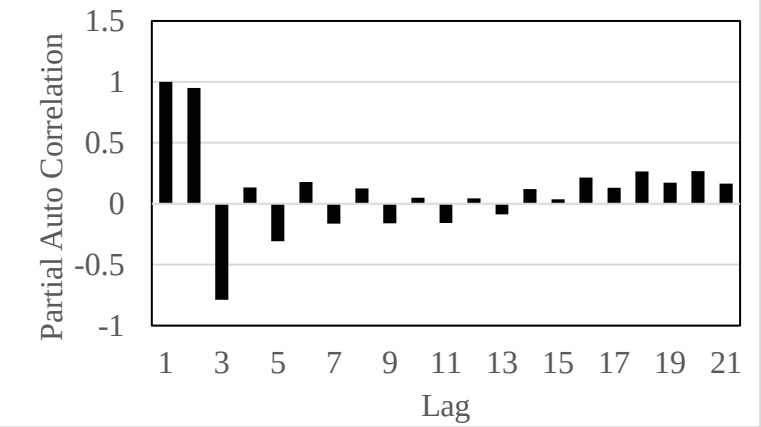

(b)

Figure 2.1. (a) Autocorrelation and (b) partial correlation of measured solar irradiance from La Grange, USA

2.3.1 Inter-annual ΔH_G probability distributions

To demonstrate the relevance of hourly ΔH_G values, the probability distributions of ΔH_G values calculated at three different time periods for 10 different years measured at La Grange, USA are shown in Figure 2.2. The trend line in Figure 2.2 represents the distribution when all 10 years of data are considered together. Figure 2.2 shows that ΔH_G

values at a given hour in a given date has a characteristic distribution that does not change significantly from year to year. Similar distributions could be observed for ΔH_G values computed for other time periods too.

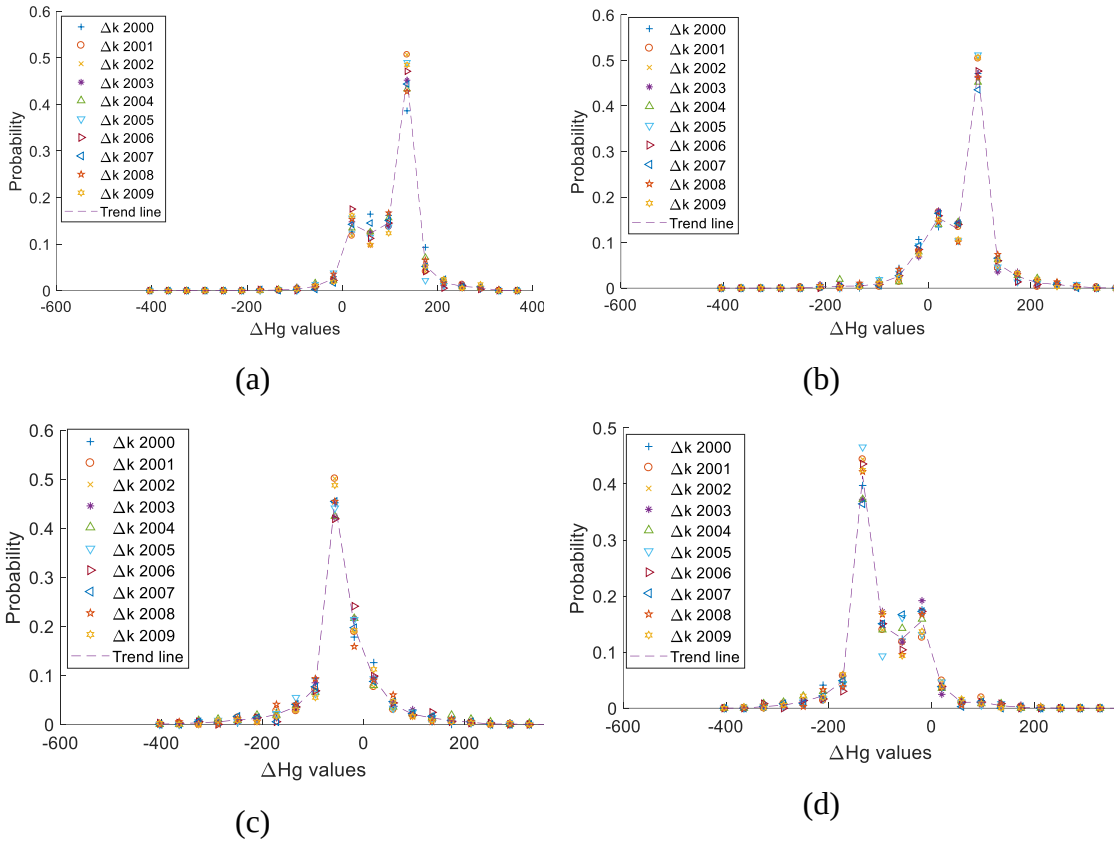

Figure 2.2. Comparison of ΔH_G inter-annual probability distributions for three different years for the periods (a) 10.00-11.00 (b) 11.00-12.00 hours (c) 12.00-13.00 hours, and (d) 16.00-17.00 hours.

Almost identical probability values for different years point to the fact that even though random variation exists with respect to measured solar irradiance, annual probability distributions of ΔH_G values are similar and predictable. Even though the primary location considered in Figure 2.2 is La Grange, USA, a similar pattern of ΔH_G probability values

were observed for other locations such as Leavenworth, in the USA and Division 23/21 in Manitoba, Canada.

To quantify the similarity of the distributions of ΔH_G values, the two-sample Kolmogorov Smirnov test (KS-II) with varying confidence levels was used. The test was applied to all possible distinct pairs of years (10 years of data results in 45 distinct pairs) taking ΔH_G values for the respective pair of years as the samples from the two distributions. Figure 2.3 shows the passing rates of the KS-II test for four different times as shown in Figure 2.2 considering three significance levels of 1%, 5%, and 3%. Over 95% of pairs of years passed the test (i.e. confirmed the null hypothesis that two distributions are the same) even when a 5% significance level is considered.

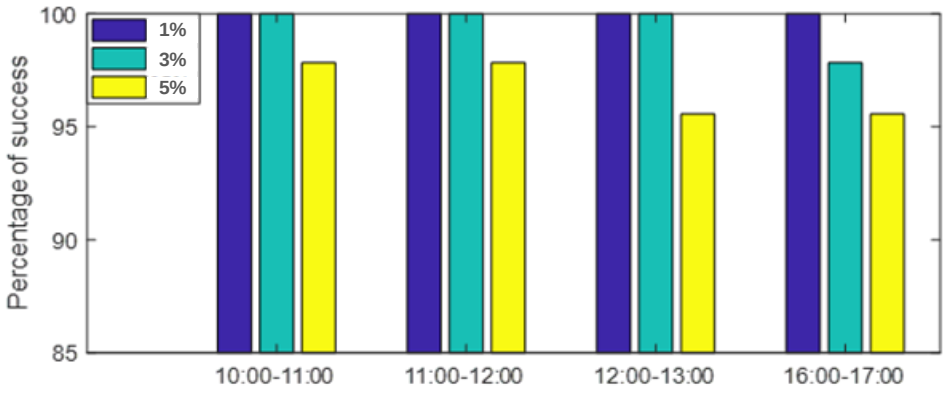

Figure 2.3 Percentage of pairs of years that passed the KS-II test for asserting the similarity between the distributions of inter-annual ΔH_G values computed at four different time periods.

Therefore, it can be deduced that this characteristic distribution of ΔH_G values can be a useful metric to compare the accuracy of prediction models while comparing with the measured solar irradiance data. In other words, any good synthetic solar irradiance

generator should be able to preserve these characteristic distributions, in addition to the other statistical properties commonly considered.

2.3.2 Intra-annual ΔH_G probability distributions

To examine the feasibility of utilizing the "first-order differences" in generating synthetic sets of solar irradiance, the intra-annual characteristics distribution of first-order differences were obtained considering ΔH_G values from a 31-day window around the given date. These distributions for 10 different years are shown in Figure 2.4.

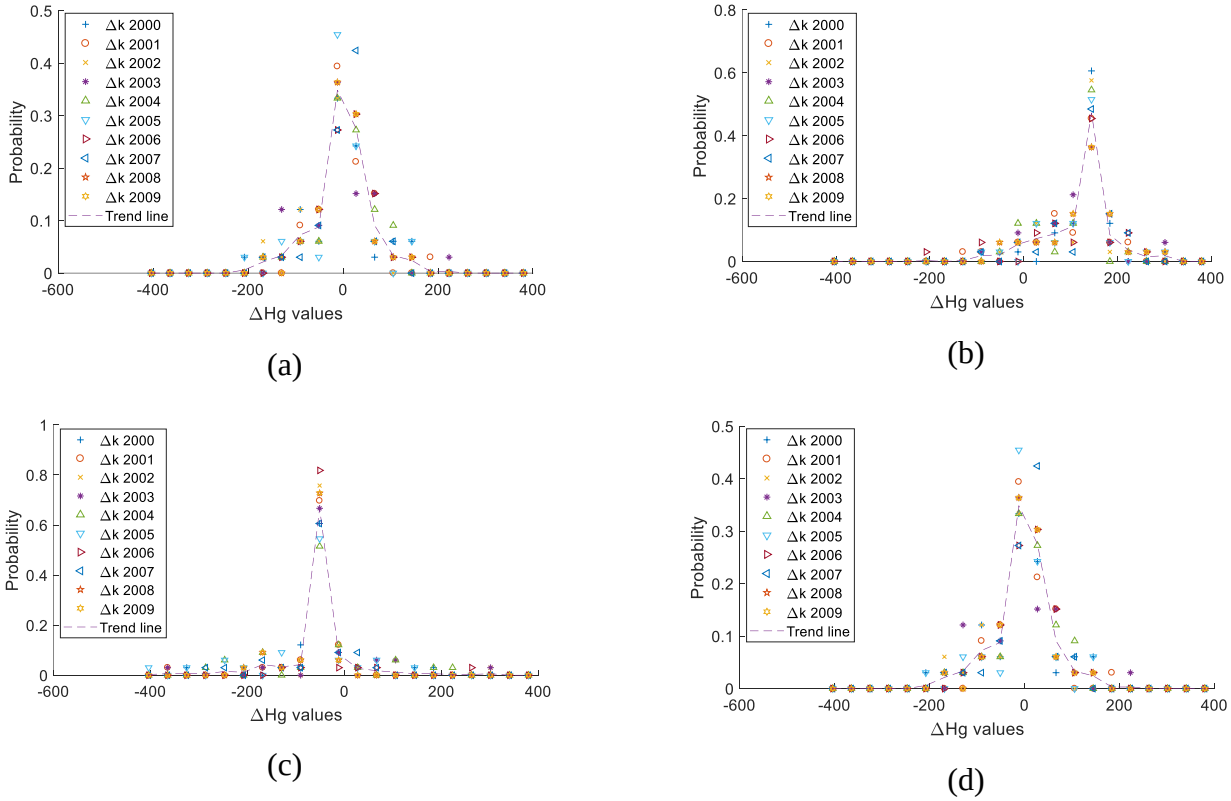

Figure 2.4. Comparison of intra-annual ΔH_G probability distributions for three different years for the month and periods (a) Feb 14:00-15:00 (b) May 11:00-12:00 (c) July 15.00-16.00 (d) Dec 14.00-15.00

It can be observed that the probability distributions for different years are similar, although the random deviations among them are higher when considered a 31-day window, instead of the whole year. Since these distributions are generated using a fewer number of samples of ΔH_G values, such differences are expected. Similar to the annual ΔH_G probability distributions, KS-II test was used to quantify the similarity of the probability distributions with varying significance levels. As evident from Figure 2.5, over 90% passing rate was observed for the KS-II test, for all pairs of years, at all three significance levels (1%, 3%, and 5%) considered. Therefore, it is proposed to use a window of 31 days centred around the current day to obtain the probability distributions of the first-order differences (ΔH_G values) for developing a synthetic hourly solar irradiance data generation model. The characteristic obtained with a 31-day window would be more consistent with monthly average characteristics that are considered in most solar irradiance models [41].

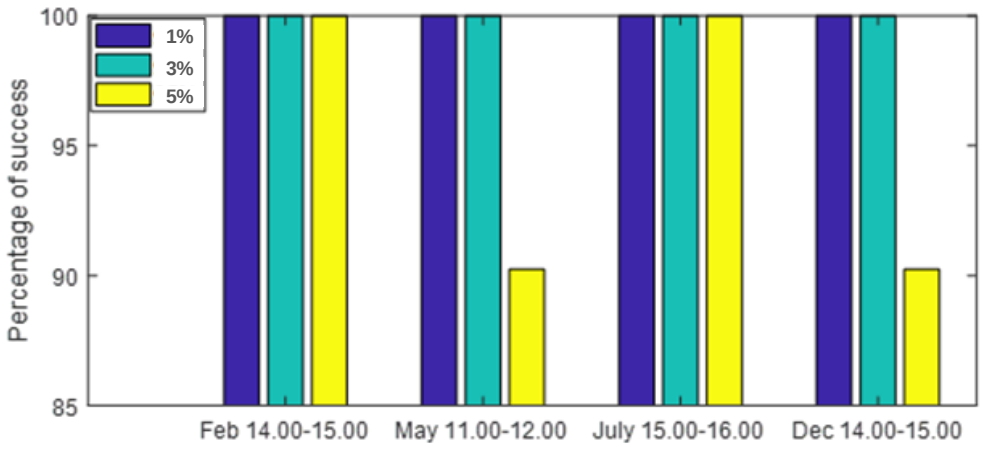

Figure 2.5 Percentage of pairs of years that passed the KS-II test for asserting the similarity between the distributions of intra-annual ΔH_G values computed at four different time periods.

2.4 Modelling solar irradiance based on first-order differences

The main target application of the proposed synthetic solar irradiance generation model is the MCS-based long-term energy planning studies. Since the solar irradiance databases are becoming available for most locations in the world, the focus is on a model that can be easily developed using a sufficient length of measured hourly solar irradiance data for the location of interest. In contrast to most previously published approaches that primarily model the solar irradiance expected at a given hour or hourly clearness index, the new model proposed in this chapter attempts to model the expected change in solar irradiance at a given hour, ΔH_G. Then the solar irradiance at hour *t*, $H_G(t)$ is obtained by adding the change of solar irradiance generated for hour *t*, $\Delta H_G(t)$ to the previous hour solar irradiance $H_G(t-1)$ as shown in (2.2). By continuing this process, a time series of solar irradiance data can be obtained recursively.

$$H_G(t) = H_G(t-1) + \Delta H_G(t) \qquad 2.2$$

As per the proposed model, the current hour solar irradiance is calculated as the previous time-step solar irradiance $H_G(t-1)$ plus the difference $\Delta H_G(t)$. Hence, each hour of solar irradiance is resulting from a sequence of past solar irradiance values. Therefore, the model automatically incorporates the relationship of the current hour solar irradiance value to all past values in the day. This is inherent in the model and contributes to preserving the auto-correlation property for several time-lags.

2.4.1 Modeling ΔH_G using the trend and stochastic components

The first order differences ΔH_G can be considered as a combination of trend and stochastic components as shown in (2.3).

$$\Delta H_G(t) = \Delta H_T(t) + \Delta H_S(t) \quad 2.3$$

The trend component ΔH_T represents the general trend in the pattern of the first-order differences in solar irradiance and the stochastic component ΔH_S represents the random deviations from the trend component. The trend component $\Delta H_T(t)$ for hour *t* in a given day can be obtained from the historical data. It is the mean of $\Delta H_G(t)$ values observed during a sliding window (31-days window was considered in this study) centred on the given day typically averaged over several years. Once the trend component is determined, the stochastic component $\Delta H_S(t)$ can be calculated from historical data using (2.4). Figure 2.6 shows some sample time series plots of ΔH_G, ΔH_T and ΔH_S values for several different seasons in a year. The trend component ΔH_T values are calculated beforehand based on the measured solar irradiance and CDFs are used to model the stochastic component ΔH_S. Several examples of CDFs of ΔH_S are shown in Figure 2.6.

$$\Delta H_S(t) = \Delta H_T(t) - \Delta H_G(t) \quad 2.4$$

Since the model need to store a large number of CDFs to generate the ΔH_S values, it is more computationally efficient to fit CDF data to a model and store the model coefficients. It was found that polynomial functions are appropriate to approximate the inverse relationships of the CDFs. Trials with the data for the selected locations showed that 3rd

order polynomials, as given in (2.5) result in Pearson correlation coefficients (PCC) greater than 0.95 for all CDFs.

$$\Delta H_S(x) = a_0^t + a_1^t x + a_2^t x^2 + a_3^t x^3 \qquad 2.5$$

where $x \in [0-1]$ is the cumulative probability, and $\Delta H_S \in [\Delta H_{S,min}(t), \Delta H_{S,max,}(t)]$ at hour *t*. The coefficients $a_0^t, \ldots, a_3^t$ are found by the least-square fitting [53].

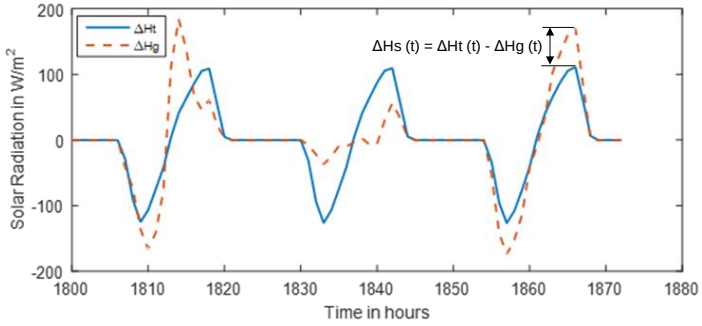

(a)

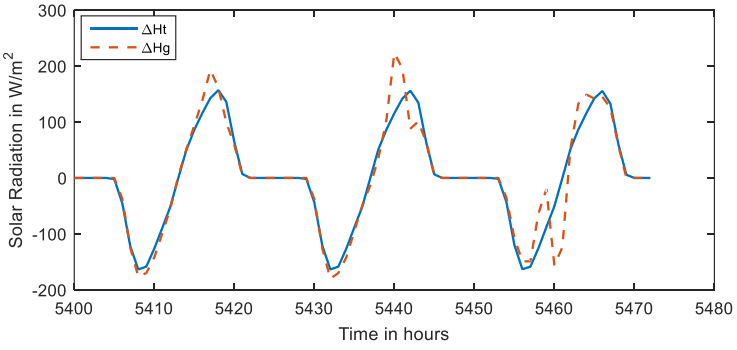

(b)

Figure 2.6 Sample time series plot illustrating the trend (ΔH_T) and actual (ΔH_G) component of first order difference in solar irradiance for (a) March 2012, (b) July 2012

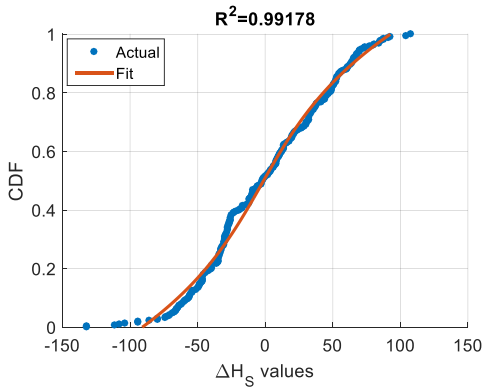

(a)

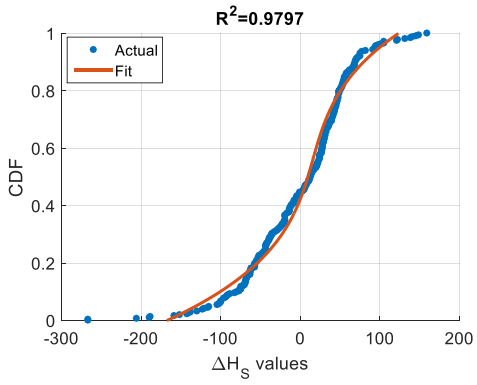

(b)

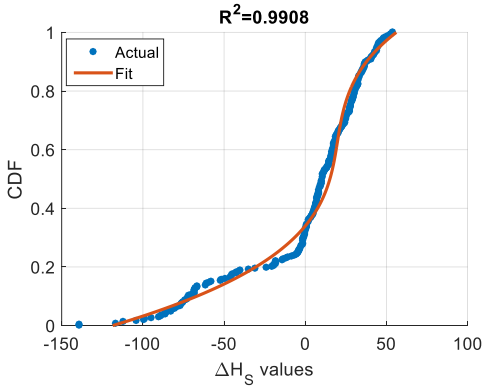

(c)

Figure 2.7. Cumulative distribution functions (CDFs) of ΔH_S values developed for (a) Jan 25, 11.00-12.00, (b) March 15, 16.00-17.00, and (c) September 10, 18.00-19.00 measured at La Grange, USA

Other approaches such as bootstrapping the error of data used for obtaining CDFs can be applied to generate random samples of ΔH_S values. However, if measured data for a sufficiently long period of time (>10 years) is available, with a 31 days window, there are enough data samples to generate a reliable CDF. Therefore, fitting a curve to represent a CDF is a more computationally efficient approach.

2.5 Procedures for building the proposed model and generation of synthetic solar irradiance values

The proposed model is developed based on the following hypotheses:

1. Due to the sinusoidal variation of clear sky irradiance, solar irradiance values of two consecutive time steps are highly correlated. Thus, the current hour solar irradiance is highly relevant when generating the next hour solar irradiance and forms the basis for (2.2).
2. Characteristics of solar irradiance within 31 days centred around the current day are similar. Thus, cumulative distribution functions required for the model are developed on a daily basis with a sliding window of 31 days similar to [54].
3. Annual first-order differences of the hourly solar irradiance representing the trend and random component, calculated at a given hour, for different years, have a unique distribution that does not change from year to year. Therefore, synthetic values generated from a good solar irradiance model would preserve this characteristic distribution.

As per the hypothesis derived, trend and random components of solar irradiance are needed to determine the hourly synthetic solar irradiance at any time period t. The trend component ΔH_T is an averaged value over the years with a 31-days moving window while random component ΔH_S are modeled and generated using probability distribution functions (CDFs).

2.5.1 Building of the synthetic solar radiation model

Figure 2.8 demonstrates the step-by-step procedure followed in building the model. The following steps explain in detail the procedure carried out in building the proposed model using the measured solar irradiance.

- **Step-1:** From the historical data, calculate ΔH_G values, and then considering a 31-day sliding window, calculate the trend component (ΔH_T) for each hour of the year. Using the trend component, calculate the stochastic component (ΔH_S) values. Record $H_{G,min}(\mathrm{t})$ and $H_{G,max}(t)$ representing minimum and maximum solar irradiance for hour t observed in the historical data (31-day moving window).
- **Step-2:** Segregate ΔH_S values corresponding to a given hour t (within the 31-day sliding data window, of all years) into bins. Develop the CDFs $F(\Delta H_S)$ for each hour.
- **Step-3:** The coefficient values of the 3rd order polynomials for each hour t is calculated using the least square estimation.

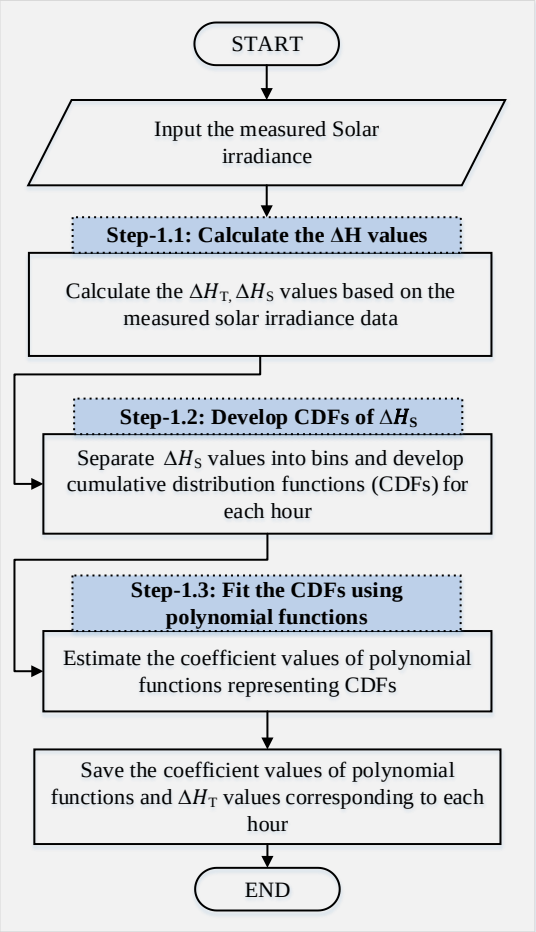

Figure 2.8. Procedural flowchart for building the proposed synthetic solar irradiance model

After constructing the model, the estimated coefficient values are stored in 8760 × 4 arrays. Note that all coefficients corresponding to nighttime hours are zero, indicating a 100% probability of having $\Delta H_S = 0$ in these hours. However, these zero coefficients are also kept in the array for the convenience of programming.

2.5.2 Generation of synthetic solar irradiance data

To generate synthetic hourly solar irradiance data, the coefficient values, synthetic data starting date/time and end date/time are given as inputs. Figure 2.9 illustrates the flowchart used in generating synthetic hourly global horizontal solar irradiance.

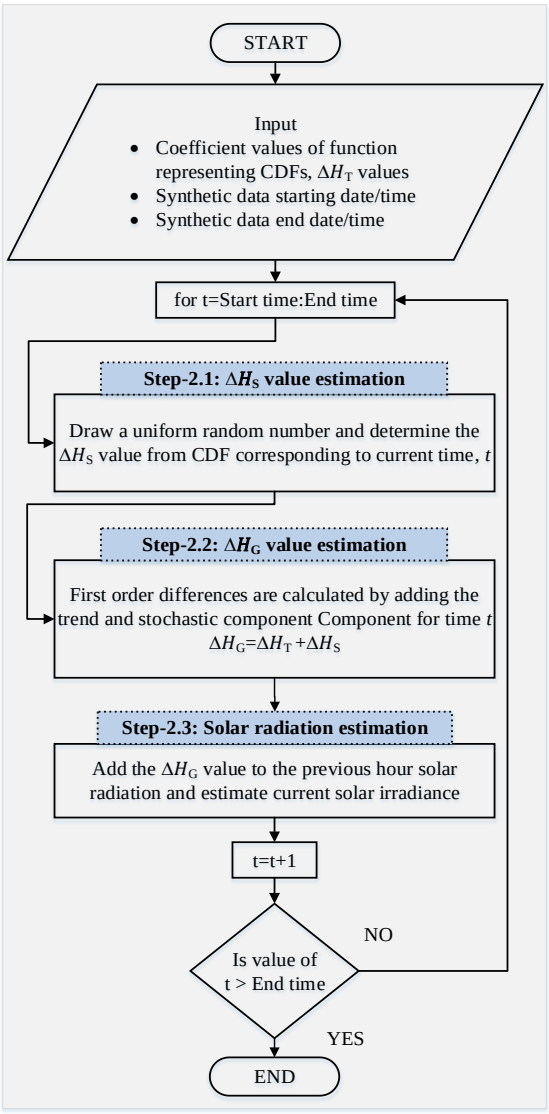

Figure 2.9. Procedural flowchart for generating synthetic solar irradiance data.

The following are the simple steps followed to complete the data generation.

- **Step-1:** Recall the CDF coefficients (a_i^t) corresponding to the current hour (t). Then draw a uniformly distributed random number in the range [0.0 -1.0] and use it as the cumulative probability in (2.5) to obtain a value for the stochastic component of the first-order difference in solar irradiance (say $\widehat{\Delta H_S}(t)$). The initial value of $H_G(t-1)$ in (2.2) is assumed be to zero due to the sunset hour. Therefore, the initial value of solar irradiance$H_G(t)$ also will be zero.
- **Step-2:** The estimated $\widehat{\Delta H_S}(t)$ value is added to the trend component of solar irradiance $\Delta H_T(t)$ to estimate the first-order difference in solar irradiance $\widehat{\Delta H_G}(t)$ as in (2.3).
- **Step-3:** To estimate the solar irradiance of hour *t*, the generated first-order difference in solar irradiance $\widehat{\Delta H_G}(t)$ is added to the previous hour solar irradiance $\widehat{H}(t-1)$ as in (2.2). If the estimated solar irradiance $\widehat{H_G}(t)$ is out of the range $[H_{G,min}, H_{G,max}]$, the procedure is repeated by randomly drawing another $\widehat{\Delta H_S}(t)$ until $\widehat{\Delta H_G}(t)$ will become within the limits. Continue the procedure until solar irradiance generation has been completed for the required duration.

2.6 The extended solar irradiance model

Hourly solar irradiance values reported are the average of solar irradiance values, usually measured in more frequent intervals, during the past one hour. The intra-hour fluctuations in solar irradiance are thus averaged into a single value. This is usually quite

sufficient for solar thermal applications. However, for certain applications, simulation of solar irradiance values at shorter intervals is desired. In such applications, assuming a constant value of solar irradiance for an hour would make under or over-valuation of energy collected. Specific applications like EVs demands 30-minutes time steps in the simulation due to their dynamic state changes [55]. Thus, models simulating solar energy systems together with EVs may need 30-mins solar irradiance values. Hence, a method is proposed to obtain 30-mins solar irradiance values from hourly solar irradiance values. This requires the prediction of two data points with random variations, in such a way that the average of the two data points is equal to the hourly average solar irradiance value. Table 2.1 shows the PCC values that indicate the correlation between the hourly irradiance and 30 min irradiance values, for different times of the day. Higher correlation values calculated in Table 2.1 demonstrate the dependency of intermediate irradiance values on the hourly solar irradiance values.

Thus, the main hypothesis behind the proposed procedure is:

- There is a strong correlation between average hourly solar irradiance with respective to 30-min measured solar irradiance. So, the hourly solar irradiance can be used to predict 30-mins solar irradiance values.

This procedure is useful when the historical data is available only in hourly intervals, which is the case for most locations. Consider an hourly GHI value, $\widehat{H}_G(t)$ predicted using the proposed model based on the ΔH_G values. Also, assume $\widehat{H}_G^{30}(t)$ and $\widehat{H}_G^{60}(t)$ are the intermediate 30-minute GHI values corresponding to 30th min and 60th min respectively during the time period t. According to the hypothesis, they are highly correlated to $\widehat{H}_G(t)$.

Table 2.1 PCC values between hourly average solar irradiance and 30 mins intermediate solar irradiance

Hourly solar irradiance	**To**	
	$\widehat{H}_G^{30}(t)$	$\widehat{H}_G^{60}(t)$
Hour-6	0.84835	0.99246
Hour-7	0.97136	0.97503
Hour-8	0.97835	0.96945
Hour-9	0.97751	0.96193
Hour-10	0.9762	0.95759
Hour-11	0.96895	0.95807
Hour-12	0.96466	0.94632
Hour-13	0.95523	0.93861
Hour-14	0.95424	0.93128
Hour-15	0.9659	0.94555
Hour-16	0.97012	0.93795
Hour-17	0.97664	0.95888
Hour-18	0.98521	0.94054
Hour-19	0.98924	0.88801
Average PCC Values	0.963	0.95012

Figure 2.10 shows a plot of 30 min measured GHI values for three sample days, with superimposed hourly irradiance values. Based on the above hypothesis, 30 min solar irradiance data are estimated from the predicted hourly solar irradiance values, using (2.6)-(2.7):

$$\widehat{H}_G^{30}(t) = \beta^{30}(t).\widehat{H}_G(t) + \in^t \quad 2.6$$

$$\widehat{H}_G^{60}(t) = \beta^{60}(t).\widehat{H}_G(t) + \in^t \quad 2.7$$

where $\beta^{30}(t)$ and $\beta^{60}(t)$ represent a set of coefficients corresponding to each hour, which can be estimated from a sample of measured data, and $\in^t$ are random changes specific to a given hour modeled as a random number with zero mean and constant variance.

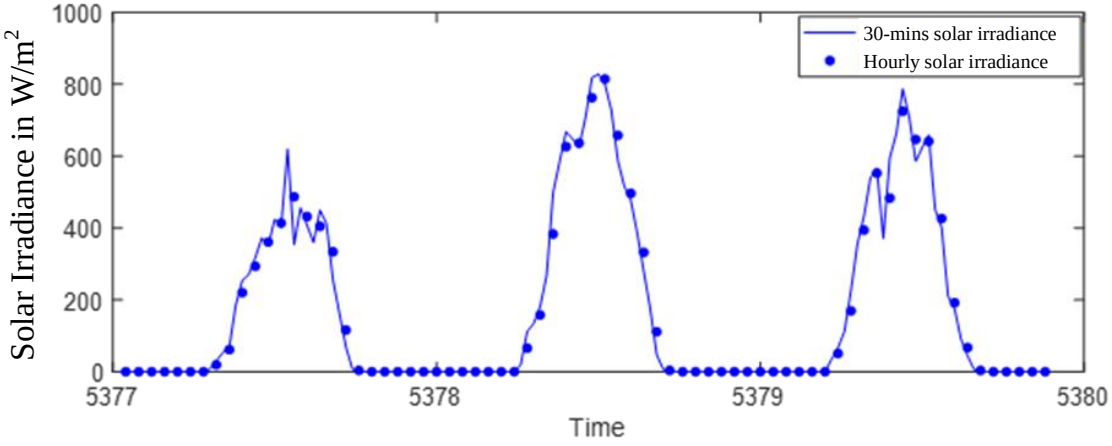

Figure 2.10. Measured solar irradiance with 30-mins and hourly intervals

2.7 Components of solar radiation

There are essentially two main components of solar irradiance considered while calculating the output of solar energy systems. These components are direct normal or direct beam solar irradiance (DNI) represented as H_B, and the diffuse horizontal solar irradiance (DHI) represented as H_{DH}. The global horizontal solar irradiance (GHI) represented as H_G is the total irradiance on a horizontal plane due to both direct and diffuse radiation.

DNI or H_B is measured at the surface of the Earth at a given location with a surface element perpendicular to the Sun. It excludes diffuse solar radiation (radiation that is scattered or reflected by atmospheric components). Direct irradiance is equal to the extraterrestrial irradiance above the atmosphere minus the atmospheric losses due to absorption and scattering. DHI or H_{DH} is the radiation at the Earth's surface from light scattered by the atmosphere. It is measured on a horizontal surface with radiation coming

from all points in the sky excluding circumsolar radiation. GHI or H_G is the total irradiance from the sun on a horizontal surface on Earth. It is the sum of DNI (after accounting for the altitude angle β_t of the sun) and DHI [56].

$$H_G(t) = H_{DH}(t) + H_B(t).\sin(\beta_t) \quad 2.8$$

In this work, synthetic values are generated independently using the proposed solar irradiance model to calculate the values using (2.9). Thus, with the measurements of H_G and H_B, H_{DH} can be obtained as:

$$H_{DH}(t) = H_G(t) - H_B(t).\sin(\beta_t) \quad 2.9$$

2.8 Calculation of photovoltaic power generation

The calculation of power output from PV panels $P^{pv,t}$ at any time period t can be calculated using (2.10) [57], [58]:

$$P^{pv,t} = P^{dc,t}.\eta_{conv}.\eta_{dirt}.\eta_{mismatch} \quad 2.10$$

where DC power output $P^{dc,t}$ can be calculated using (2.11) with the cell temperature $T^{cell,t}$ obtained from (2.12).

$$P^{dc,t} = \frac{IC_t}{1000}.P^{pv-m}.N^{pv}.[1-\gamma.(T^{cell,t}-25)] \quad 2.11$$

$$T^{cell,t} = T^{amb,t} + \left(\frac{NOTC-20}{800}\right).IP^t \quad 2.12$$

The total solar irradiance on the solar collector IC^t during time period t can be found using (2.13) considering the values of direct beam radiation on the solar collector IB^t,

diffuse radiation on the solar collector ID^t, and the reflected radiation on the solar collector IR^t [56].

$$IC^t = IB^t + ID^t + IR^t \quad (2.13)$$

where IB can be calculated using the following equation:

$$IB = H_B . \cos(\theta) \quad (2.14)$$

where, H_B is the DNI measured normal to the rays and θ is the incident angle.

The incident angle θ and azimuth angle $\emptyset_s$ can be calculated using (2.15) - (2.16):

$$\cos(\theta) = \cos(\beta) . \cos(\emptyset_s - \emptyset_c) . \sin(\Sigma) + \sin(\beta) \cos(\Sigma) \quad (2.15)$$

$$\emptyset_s = asin. \left(\frac{\cos(\delta_d) . \sin(H)}{\cos(\beta)} \right) \quad (2.16)$$

where,

β = altitude angle

$\emptyset_c$ = the azimuth angle of the collector

$\emptyset_s$ = solar azimuth angle

Σ the tilt angle of the collector

δ_d = declination angle

H = hour angle

The solar declination angle δ_d, hour angle H, solar time ST, equation of time E, and altitude angle β can be calculated using Eqns. (2.17)-(2.22):

$$\delta_d = deg.23.45.sin\left[\frac{360}{365}.(n_j - 81)\, deg\right] \quad 2.17$$

$$H = 15deg.(12 - ST) \quad 2.18$$

$$ST = CT + \frac{4}{60}(MstdT - Mlocal) + E - DL \quad 2.19$$

$$E = 9.87.\sin(2B) - 7.53.\cos(B) - 1.5.\sin(B) \quad 2.20$$

$$B = \frac{360}{365}.(n_j - 81) \quad 2.21$$

$$\beta = \text{asin}\,(\cos(Lat).\cos(H) + \sin(Lat).\sin(\delta_d)) \quad 2.22$$

In Eqns. (2.17) - (2.22),

n_j = Julian date

$MstdT$ = local time

$Mlocal$ = local standard time meridian

The diffuse solar irradiance on the solar collector ID can be calculated using the following equation:

$$ID = \lambda_S.H_{DH} \quad 2.23$$

where, H_{DH} represents DHI on a horizontal surface and λ_S is the sky view factor. λ_S can be calculated using Eqn. (2.24):

$$\lambda_S = \frac{1}{2}.(1 + \cos(\Sigma)) \quad 2.24$$

The reflected solar irradiance IR can be calculated using the following equation:

$$IR = \lambda_g.\rho.[I_B.\sin(\beta) + H_{DH}] \quad 2.25$$

where ρ is the ground reflectivity and λ_g is the ground view factor. λ_g values can be calculated using (2.26)

$$\lambda_g = \frac{1}{2}.(1 - \cos(\Sigma)) \qquad 2.26$$

2.9 Generation of synthetic DNI, DHI, and GHI values

Even though the proposed model is trained and validated using GHI values, the model is also capable of generating other solar irradiance components such as DNI and DHI too. To generate all three solar radiation components, the following steps are used:

- **Step-1:** Train the designated model using the measured H_G and H_B values. Record the observed maximum $\overline{H_G}(t)$, $\overline{H_B}(t)$ and minimum $\underline{H_G(t)}$, $\underline{H_B(t)}$ values for each time period t.
- **Step-2:** Generate the synthetic values of $H_G(t)$ and $H_B(t)$ for each time period *t* using the proposed solar irradiance model.
- **Step-3:** Substitute the $H_G(t)$ and $H_B(t)$ values in (2.9) to compute $H_{DH}(t)$. Check for minimum or maximum boundary condition violations using $\overline{H_G}(t)$, $\overline{H_B}(t)$ and $\underline{H_G(t)}$, $\underline{H_B(t)}$. If a violation is noticed, repeat Step-2, else proceed to Step-4.
- **Step-4:** Calculate the total solar irradiance on the collector, IC^t using (2.13). If the $IC^t > \overline{IC^t}$ repeat Step-2, else proceed to Step-5. In this work, it was assumed $\overline{IC^t} = 1000$ W/m^2 .

- **Step-5:** Continue Step-2 to Step-5 until $t = T$.

2.10 Description of models used for comparison

There are many stochastic solar irradiance models developed in the past that are capable of generating synthetic solar irradiance datasets. Among many of those, the models proposed in [41], [43] account for the autocorrelation between hourly solar irradiance in the modeling of solar irradiance through a stochastic disaggregation procedure to convert daily solar irradiance to hourly solar irradiance. Additionally, the models have used clear sky indices as a primary factor to develop the model and average-decomposition procedures are utilized to estimate the hourly clearness index from daily and/or monthly clearness index [40], [41]. To compare the performance of models that primarily use k-values and decomposition procedures to build synthetic solar irradiance generators with the proposed approach, these models are representative. Moreover, these models have been validated using the solar irradiance data collected from Europe, the USA and Canadian cities [42], [43]. The proposed model has also used the measured solar irradiance data collected from the USA and Canada for model development and testing. For the convenience of representation, these models have been denoted as SHSRG [43] and SISIM [41] models in this thesis. The results associated with these models are used to compare the efficiency of the proposed model.

2.11 Solar irradiance data

The measured hourly GHI data collected from four different locations with varying climate characteristics are used to develop and test the proposed model. Solar irradiance data from four different locations, which includes two locations from Canada and two locations from the USA as shown in Table 2.2, were collected. The open database from Natural resources Canada (NRC) [59] is used to obtain the solar irradiance data of Canadian locations and Solar anywhere [60] is used to get the solar irradiance data of US locations. The distinction between the climate characteristics of the chosen locations is defined based on Köppen-Geiger climate classification [52], and these locations can be classified as subarctic, warm summer humid continental, temperate Mediterranean climate, warm oceanic climates respectively. The motivation behind choosing different locations is to ensure the generic applicability of the developed model.

The NRC's dataset [59] includes solar irradiance data of 492 Canadian locations and solar irradiance values are primarily based on satellite-derived solar estimates using methods developed at the State University of New York. As per the database information, the average standard error for all sites is calculated as 5%. Solar anywhere database [60] generates solar irradiance data from geostationary satellite images using the Perez Model [61]. The database utilizes satellite images to generate GHI measurements in resolutions as high as 1 km. As per the database, the standard error for annual solar irradiance at all sites is close to 5%.

Table 2.2 Location, data period, database and climate classification for the four locations

Location	Data period	Database	Köppen-Geiger climate classification
Division 23, Manitoba (DM-23) (Lat: 57.95, Long: -100.05)	January 2004 to December 2014	Natural resources Canada [59]	Subarctic
Division 21, Manitoba (DM-21) (Lat: 54.45, Long: -100.05)	January 2004 to December 2014	Natural resources Canada [59]	Warm summer humid continental
Leavenworth, Washington (LW-W) (Lat: 47.75, Long: -120.65)	January 2000 to December 2014	Solar anywhere [60]	Temperate Mediterranean climate
La Grange, Georgia (LG-G) (Lat: 41.65, Long: -104.45)	January 2000 to December 2014	Solar anywhere [60]	Warm oceanic climates

2.12 Results and discussions

A good synthetic solar irradiance generation model should be able to:

- Follow the characteristic diurnal and seasonal variations,
- Include the random variations due to clouds and atmospheric conditions,
- Preserve statistical measures such as mean, standard deviation, etc.,
- Preserve correlation among consecutive time steps.

In order to examine the above aspects, the simulated results are compared with measured solar irradiance data and existing solar irradiance models in terms of comparison plots, autocorrelation, probability distributions, and mean values. All the simulated results were computed using the commercial software package MATLAB R2017a [62].

2.12.1 Training the model and generation of synthetic data

Figure 2.11 illustrates a time series plot of a part (three years) of the long-term measured hourly solar irradiance data used for building the model (plotted in blue) followed by simulated hourly solar irradiance data using the developed model (plotted in orange). It can be observed from Figure 2.11 that the designed model is able to maintain the general trend of actual data over the time period of one year.

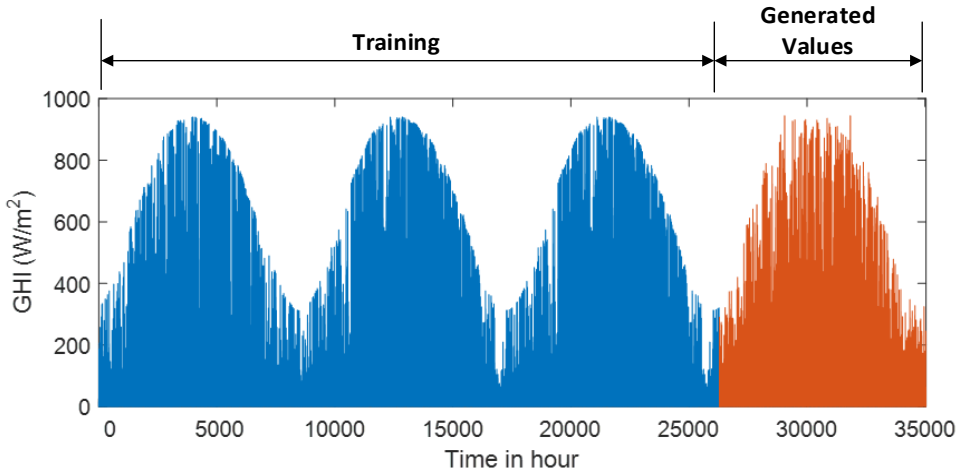

Figure 2.11. Training and Generated values of solar irradiance using the proposed solar irradiance model for La Grange, USA.

Since the proposed model is not meant to predict the solar irradiance at a given hour on a given day, it is highly important to compare the main descriptive parameters such as

autocorrelation, probability distributions, and average values of the simulated and actual solar irradiance [63]. Also, it is important to investigate whether the model captures diurnal and seasonal variation on average.

2.12.2 Autocorrelation and partial autocorrelation values

There is a strong correlation between consecutive hourly solar irradiance values. The autocorrelation and partial correlation functions of the measured solar irradiance data shown in Figure 2.12 and Figure 2.13 underline this fact. Both SHSRG [43] and SISIM [41] solar irradiance models consider the correlation between clearness indices of consecutive days and hours in generating random solar irradiance values.

Additionally, the models try to preserve the time correlation by considering previous hour solar irradiance values while generating the current hour irradiance values. Based on this character, it is expected that these models can preserve the time correlation of the natural time series of measured solar irradiance. However, the generated solar irradiance data from SHSRG and SISIM models show a lower correlation compared to the correlation seen in the measured irradiance at all lags for both locations shown in the plots. On the other hand, the autocorrelation and partial correlation functions of the simulated data from the proposed model are more similar to those of the measured solar irradiance data.

This is because, in the proposed model, the current hour solar irradiance is calculated as the previous time-step solar irradiance$\widehat{H}(t-1)$ plus the difference $\Delta\widehat{H_G}(t)$. Hence, each hour of solar irradiance is calculated considering a sequence of past solar irradiance values. Therefore, the model automatically incorporates the relationship of the current hour solar

irradiance value to all past values in the day. This is inherent in the model and contributes to preserving the auto-correlation property for several time-lags. These comparisons underline the fact that the proposed solar irradiance model better preserves the time correlation properties and performs better than SISIM and SHSRM models in this aspect.

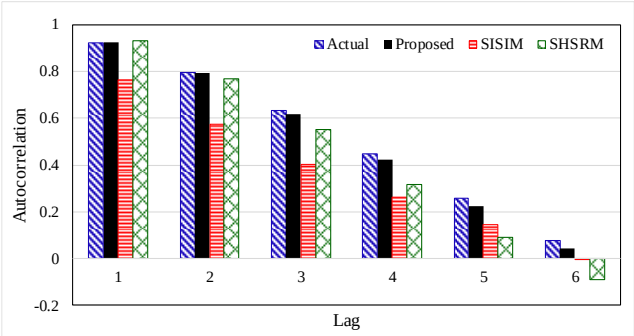

(a)

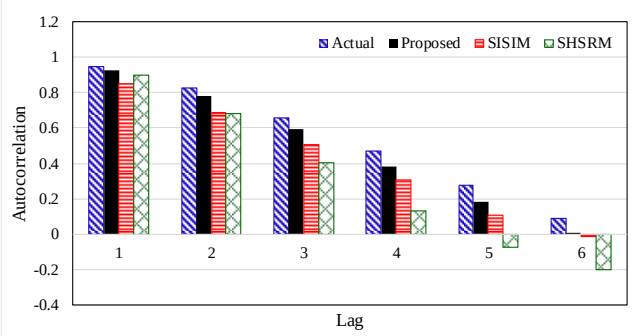

(b)

Figure 2.12. Comparison of the autocorrelation of measured hourly GHI values and generated hourly GHI values using the proposed model, SISIM, and SHSRM for (a) La Grange, USA and (b) Division 23, Manitoba, Canada

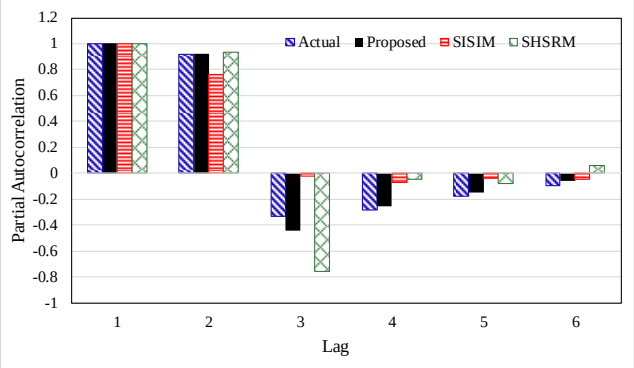

(a)

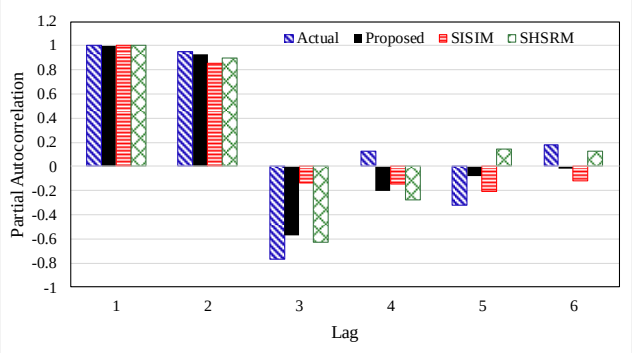

(b)

Figure 2.13. Comparison of partial autocorrelation of measured hourly GHI values and generated hourly GHI values using the proposed model, SISIM, and SHSRM for (a) La Grange, USA and (b) Division 23, Manitoba, Canada

2.12.3 Probability distributions

It is expected that the annual probability distributions of ΔH_G values computed from synthetic solar irradiance values from a good model also demonstrate the same distribution that was found from the measured data illustrated in Figure 2.2. Figure 2.14 compares the distributions of ΔH_G values obtained from the solar irradiance measurements with those

obtained from the synthetic data generated using the proposed model, SISIM model, and SHSRM model, for four different locations at four different time periods. It can be seen from Figure 2.14 that the distributions of ΔH_G values obtained SISIM and SHSRM models significantly differ from the ΔH_G distributions of the actual solar irradiance data.

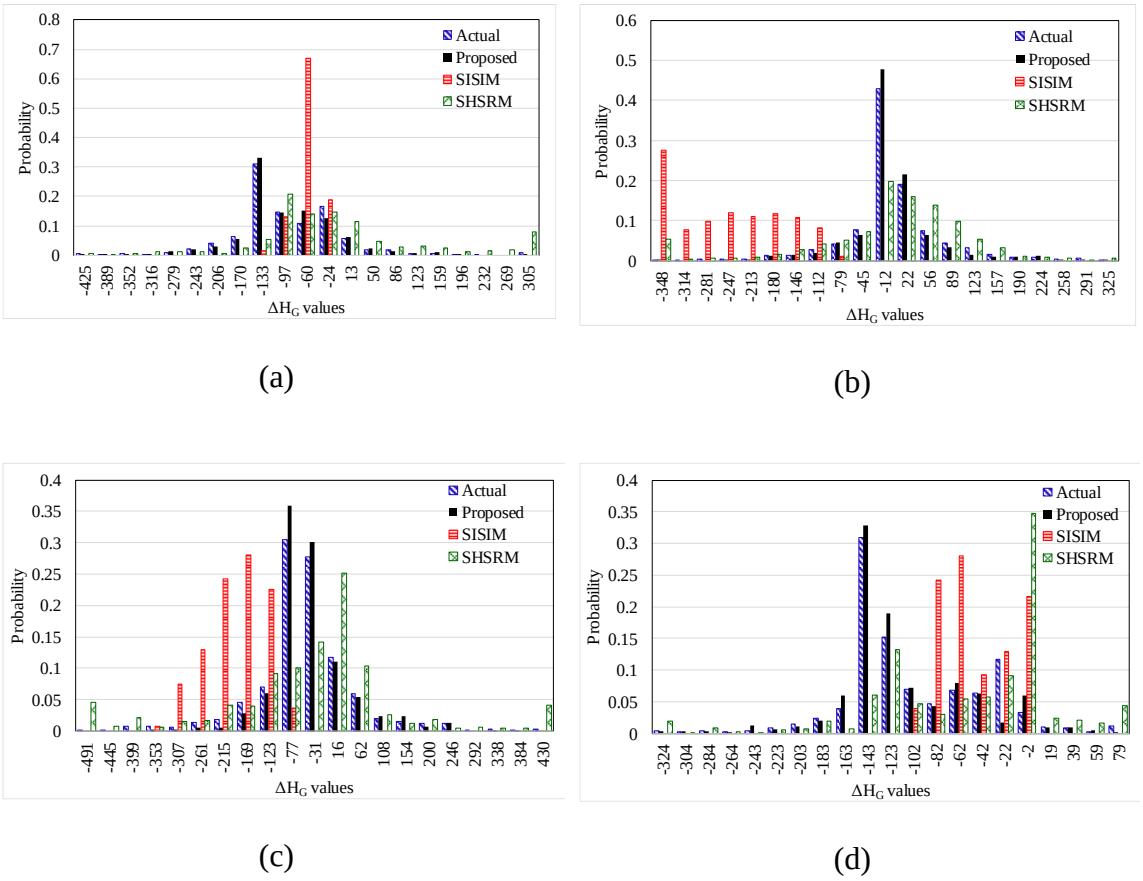

Figure 2.14. Comparison of the probability distributions of ΔHG obtained from the solar irradiance models (SHSRM and SISIM) with those of actual data for the periods (a) 10.00-11.00 at Division 23, Manitoba, Canada, (b) 15.00-16.00 at Division 21, Manitoba, Canada, (c) 11.00-12.00 at Leavenworth, USA, and (d) 15.00-16.00 La Grange, USA

As expected, the probability distribution functions of ΔH_G are similar for the actual and synthetic data generated from the proposed model, because the proposed model for hourly global horizontal irradiance was developed based on the probability distribution functions of the first-order differences of the historical hourly irradiance measurements. The Euclidean distance between two ΔH_G probability distributions can be used to quantify the similarity of distributions. Euclidean distance between two distributions can be defined as shown in (2.27).

$$d(x,y) = \sqrt{\sum_{l=1}^{P}(x_l - y_l)^2} \qquad 2.27$$

where d represents the Euclidean distance (ED), x_l indicates the probability values corresponding to the actual ΔH_G distribution, y_l are probability values corresponding to the simulated ΔH_G distribution values and P indicates the total number of ΔH_G points in the x-axis. The lower the ED, the higher the similarity between the two distributions.

Table 2.3 shows the Euclidean distances between the ΔH_G distributions obtained from the measured solar irradiance and the synthetic data generated using the proposed, SISIM, and SHSRM models. The highest average ED value is seen for the SISIM model. On the other hand, the proposed model has the lowest average ED value for all four locations. This verifies the ability of the proposed model to produce ΔH_G distributions which are more similar to those corresponding to the actual measured solar irradiance data.

Table 2.3. Euclidean distances between the ΔH_G distributions of the actual data and the calculated data (using the proposed, SISIM, and SHSRM models) for different locations.

Time Period	DM-23			DM-21			LW-W			LG-G		
	Proposed	**SISIM**	**SHSRM**	**Proposed**	**SISIM**	**SHSRM**	**Proposed**	**SISIM**	**SHSRM**	**Proposed**	**SISIM**	**SHSRM**
8	0.10	0.19	0.16	0.44	0.57	0.58	0.09	0.39	0.40	0.44	0.57	0.58
9	0.06	0.14	0.16	0.11	0.49	0.41	0.07	0.66	0.40	0.11	0.49	0.41
10	0.06	0.64	0.28	0.06	0.36	0.26	0.05	0.35	0.30	0.07	0.37	0.27
11	0.07	0.78	0.30	0.08	0.55	0.19	0.10	0.57	0.28	0.08	0.56	0.22
12	0.06	0.35	0.33	0.05	0.62	0.26	0.06	0.57	0.40	0.06	0.62	0.27
13	0.10	0.29	0.11	0.05	0.77	0.49	0.09	0.42	0.20	0.06	0.77	0.49
14	0.06	0.61	0.07	0.06	0.28	0.42	0.09	0.74	0.29	0.08	0.29	0.42
15	0.11	0.43	0.25	0.10	0.30	0.35	0.06	0.90	0.30	0.12	0.32	0.35
16	0.19	0.32	0.86	0.13	0.32	0.31	0.13	0.32	0.20	0.13	0.31	0.31
17	0.16	0.53	0.61	0.15	0.32	0.33	0.07	0.57	0.18	0.15	0.31	0.33
18	0.11	0.31	0.37	0.15	0.24	0.58	0.06	0.32	0.18	0.15	0.36	0.58
19	0.11	0.57	0.31	0.09	0.48	0.13	0.09	0.46	0.17	0.07	0.27	0.13
20	0.10	0.40	0.16	0.15	0.31	0.15	0.04	0.22	0.24	0.13	0.30	0.15
21	0.11	0.20	0.06	0.00	0.00	0.33	0.01	0.04	0.22	0.00	0.00	0.33
22	0.00	0.00	0.13	0.00	0.00	0.00	0.00	0.00	0.00	0.00	0.00	0.00
Average of all time periods	**0.09**	**0.38**	**0.28**	**0.11**	**0.37**	**0.32**	**0.07**	**0.43**	**0.25**	**0.11**	**0.37**	**0.32**

2.12.4 Monthly mean solar irradiance values

Comparisons of the simulated and actual solar irradiance data obtained from the models described previously, and the proposed model is shown in Figure 2.15 and Figure 2.16 for monthly mean daily solar energy calculated for four different locations. These averages are taken over 10 years. It can be observed that all the models fairly capture the monthly mean. Even though the proposed model is not characterized to explicitly capture the daily or hourly mean values like [41], [42], it is clear from the figure that simulated and measured hourly global horizontal irradiance values are very close.

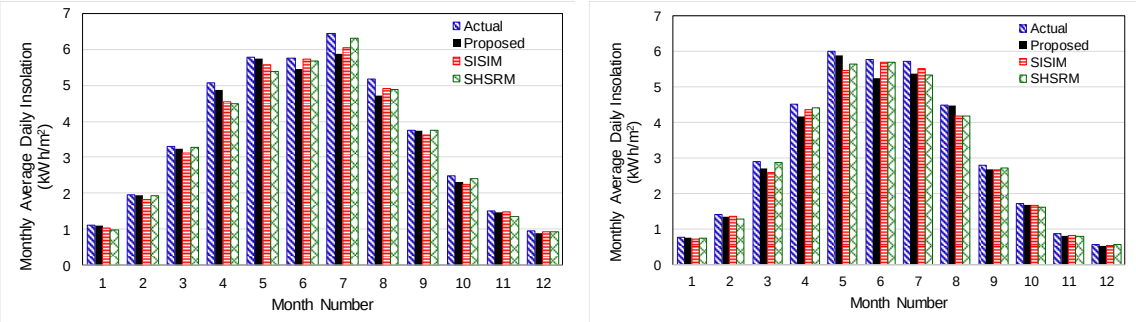

(a) (b)

Figure 2.15. Comparison of monthly mean daily insolation of measured solar irradiance, the proposed, SISIM, and SHSRM models for (a) Division 23, Manitoba, Canada and (b) Division 21, Manitoba, Canada

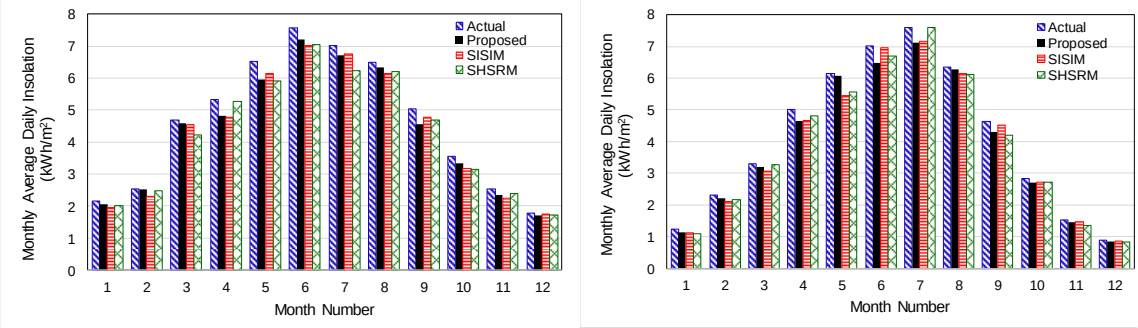

(a) (b)

Figure 2.16. Comparison of monthly mean daily insolation of measured solar irradiance, the proposed, SISIM, and SHSRM models for (a) Leavenworth, USA and (b) La Grange, USA

Additionally, the comparisons of monthly mean hourly solar irradiance between measured solar irradiance, the proposed model, SISIM and SHSRM calculated are shown in Figure 2.17 and Figure 2.18.

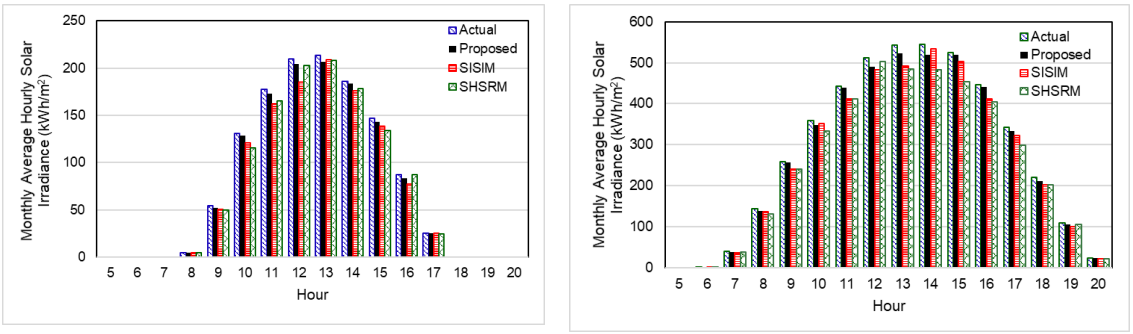

(a) (b)

Figure 2.17. Comparison of monthly mean hourly solar irradiance of measured solar irradiance, the proposed, SISIM, and SHSRM models for (a) Division 23, Manitoba, Canada and (b) Division 21, Manitoba, Canada calculated for the month of (a) February and (b) June

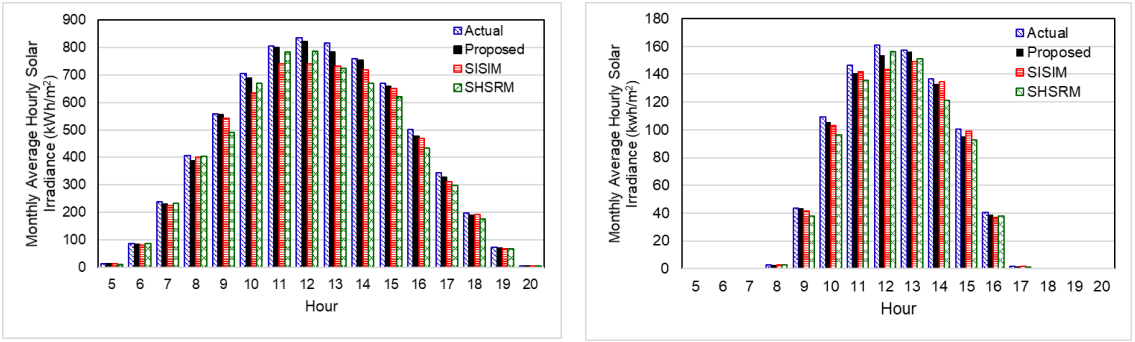

(a) (b)

Figure 2.18. Comparison of monthly mean hourly solar irradiance of measured solar irradiance, the proposed, SISIM, and SHSRM models for (a) Leavenworth, USA and (b) La Grange, the USA calculated for the month of (a) February and (b) June

The values are shown for four different locations and four different seasons where the average is taken over 10 years. It can be seen from the figure that all models were able to

preserve the hourly averages close to the measured solar irradiance data. Figure 2.19 shows the comparison of measured versus synthetic values of monthly average hourly solar irradiance values of IB and ID. The closer actual and synthetic values seen from the figure demonstrate the efficiency of the proposed model to preserve the original characteristics of the measured IB and ID values. These values (IB, ID) can be further used to calculate the reflected solar irradiance IR and total solar irradiance IC on the PV array. Even though four different locations (as shown in Table 2.2) were used to validate the fidelity of the proposed model, the solar data from Division 23, Manitoba (DM-23) (Lat: 57.95, Long: -100.05) is consistently used further in this thesis while calculating the power output of PV systems.

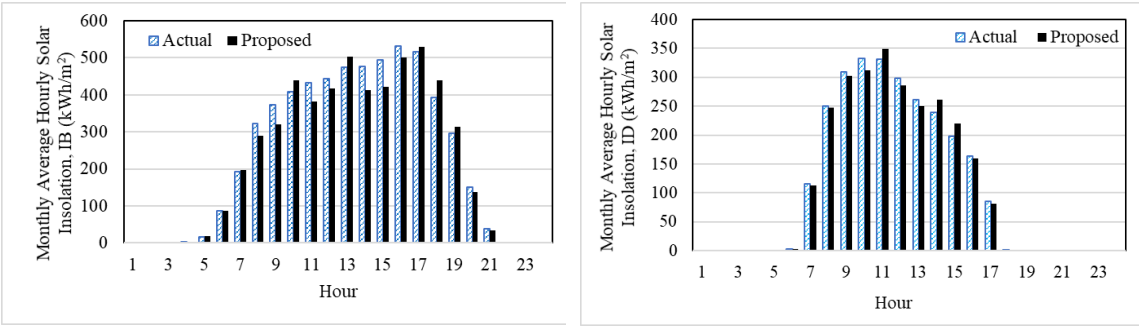

(a) (b)

Figure 2.19. Comparison of monthly mean hourly solar irradiance of measured solar irradiance, the proposed for (a) direct beam solar irradiance values IB (b) diffused solar irradiance ID for Division 23, Manitoba, Canada calculated for the month of May

2.12.5 Calculation of PV power output

The total solar irradiance on the PV array IC and PV power output from a single PV panel calculated for a random day during the year is shown in Figure 2.20.

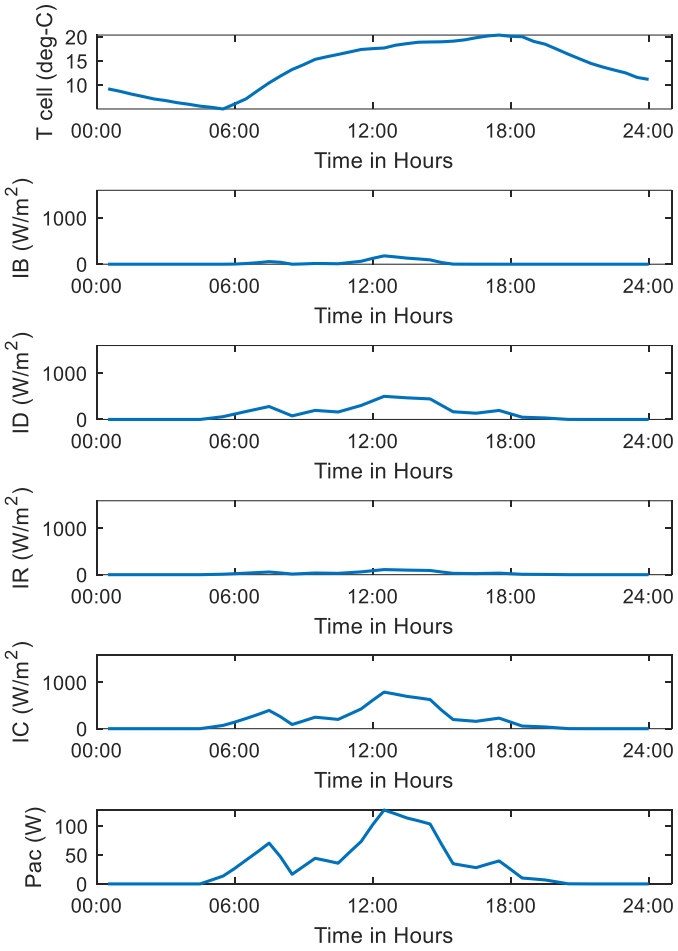

Figure 2.20. Measured hourly temperature, direct beam hourly solar irradiance, diffused hourly solar irradiance, reflected hourly solar irradiance, total hourly solar irradiance, and AC power output of a single PV panel calculated for a random day in the month of May 2012 at Division 23, Manitoba

As inputs, the five-year daily average temperature measured in Winnipeg [64] was used as T_{amb} for various time period t during a year and other input values pertained to the calculation of IC and P_{ac} is given in Table 2.4 [56], [65], [66].

Table 2.4. Necessary inputs pertained to PV power output calculation

Parameter	Value	Parameter	Value
$NOTC$	44.5 °C	$\eta_{mismatch}$	97%
P^{pv-m}	200 W	P^{pv-r}	72 kW
γ	0.5%	$MstdT$	90
η_{conv}	95%	$Mlocal$	100.05
η_{dirt}	96%	$\emptyset_c$	0
N^{pv}	1	Σ	57.95

2.12.6 Generation of 30 mins solar irradiance values

Figure 2.21 illustrates a sample of simulated 30 min solar irradiance data, following the procedure presented in Section 2.6.

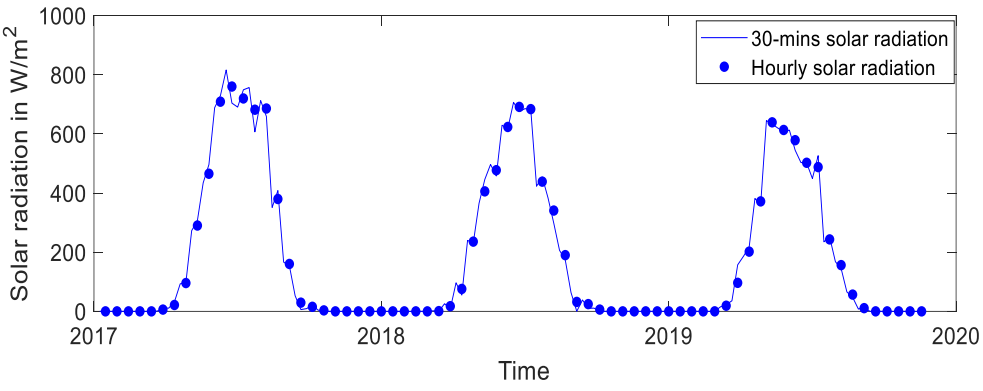

Figure 2.21. Predicted solar irradiance for 30-min time step using the extended solar irradiance model

The scattered points indicate the hourly solar irradiance predicted using the proposed model. The 30 mins solar irradiance have been estimated using (2.6)-(2.7) with the coefficient values computed using the measured data.

The similarity in the pattern along with the ability to include the random variations similar to actual measured 30 min solar irradiance (shown in Figure 2.10) shows the proposed approach for simulating solar irradiance data at 30 min intervals is acceptable.

2.13 Concluding remarks

In this chapter, an analysis of historical hourly global horizontal solar irradiance data revealed that the first-order differences of solar irradiance calculated at a given hour have a characteristic distribution that does not tend to vary from year to year. A new long-term stochastic solar irradiance generation model that utilizes this characteristic distribution function of the first-order differences of hourly solar irradiance was proposed. It was shown that the first-order differences of solar irradiance of a particular hour in a year can be represented in terms of a trend component and a stochastic component characterized using a cumulative distribution function obtained from the historical data. Additionally, an extended model is presented utilizing the strong correlation between hourly to sub-hourly values to generate 30-mins solar irradiance values from hourly solar irradiance values.

As per the analysis presented using data for four distinct locations, synthetic solar irradiance generated from SISIM and SHSRM solar irradiance models failed to accurately reproduce the distribution functions for the first-order differences of global horizontal solar irradiance. In contrast, the proposed model closely reproduced the probability distributions of the first-order differences, while maintaining other statistical properties such as monthly mean daily irradiance and monthly mean hourly irradiance values better or similar to the other two models. Although the generalizability of the developed model to different

locations is limited, building the model from historical data for a given location is simple and straightforward, and useful for applications such as MCS.

Chapter 3

Probabilistic Reliability Evaluation of Distribution Systems Considering Electric Vehicles

3.1 Introduction

Fast-growing EV load could have significant impacts on the reliability performance of electric power systems, particularly distribution networks. Charging a large population of EVs will increase both the overall energy demand and the system load of the local distribution networks. From a power system point of view, EVs can be considered as random moving loads and an appropriate model for estimating the electricity demand and assessing their impacts are therefore necessary and important.

In this chapter, a new probabilistic approach is proposed to evaluate the impacts of EVs on the reliability performance of power distribution systems. A two-layer stochastic EV charging demand estimation model is proposed where the model comprises a traffic layer

representing the spatial-temporal distributions of EVs and an electrical network layer describing the EVs charging demand. A Dynamic Hidden Markov Model (DHMM) is used to capture the EV movements in the traffic layer. EV travel patterns and charging demand are simulated using a sequential MCS approach considering the vehicle distance travelled, the type of charging location and the driver class. The proposed approach and the models are used to perform reliability studies on an example test system, and a series of analysis results are presented.

3.2 Background and literature Review

EVs are non-stationary and the estimation of electricity demand requires consideration of the spatial and temporal distributions of EVs during a particular period. The areas with the denser spatial distribution of EVs indicate the near future upgrades for facilitating the construction of infrastructure such as charging stations. The temporal distribution indicates that the power required for EV charging can be used in developing strategies for the optimal management of distribution system assets [67]. A great deal of effort has been devoted in the past to examine the spatial-temporal distribution of EVs, which is eventually translated to power demand in the electric network. They can generally be classified as simple EV models and detailed EV models.

A stochastic model based on a four-state Markov Chain Monte Carlo (MCMC) simulation was proposed in [18]. The simulated driving patterns were then used to undertake an uncertainty analysis on the network impact due to EV charging. The model assumed four states as home, work, commercial areas (various location types), and drive.

A similar model is presented in [68] to simulate EV motion and to quantify the energy required from the distribution system. The model characterizes the movement of EVs into different parking location types to estimate the aggregated power demand. A Markov model has been developed to obtain an EV charging pattern in [20], where the EV states considered were drive, park, and charging. A discrete-time Markov Chain model is proposed for generating the EV charging profiles in [21]. Detailed analyses were performed by categorizing the EV fleet into a combination of different states such as drive, park, charge, and different levels of state of charge (SOC) such as low, mid, high respectively. The validity of the model is evaluated using real-world data from 2000 cars, and it is concluded that the Markov chain is a suitable tool for modeling large-scale deployment of EVs [21]. The models presented in the existing literature [18], [20], [21], [68] are capable of estimating the EV charging profiles and aggregated power demand. Generally, these models gathered various similar locations into a single location type. For instance, EVs being charged from various residential feeders across the distribution system were classified into a single state in Markov-chain [68]. However, in reality, there would be many residential feeders across a distribution network and classifying them into one simple state would result in neglecting their actual spatiality. Additionally, in the case of states that are bound to actual charging locations, a complete restructuring of the model is needed when adding a new location to the analysis.

There were attempts to develop detailed models using the Markov model considering the traffic network in [14]. It is worth noting that the number of transition probabilities in a Markov model is determined using the total number of Markov model states. Hence,

modeling of traffic network road segments/intersections with a limited number of states for a smaller geographical area would be accurate [14]. However, using the same approach to model a larger traffic network will not be feasible due to the increased complexity. Hence, a more generic model capable of including spatially diverse location types in the charging demand estimation would be an improvement to the existing models.

A rectangular coordinate system is proposed to develop an activity-based traveling schedule to capture the spatial and temporal distributions in [15]. The frequency of travel to individual locations is taken into consideration, and the EV daily travel pattern is determined accordingly. The model used random permutation in deciding the travel destinations of EVs. However, random permutations may not be an accurate way to sample EV spatial distributions when there are multiple charging locations or travel destinations. In reality, the next travel location of an EV can be influenced by the present location, time, day (weekend or weekday), driver's travel behavior, and the SOC of the EV battery. The concept of graph theory is used in [16] to estimate the charging power demand of two fast-charging stations on an urban road network. The nodes of the graph represent the intersections while road segments are represented using the edges. This model is useful under a limited number of EV charging locations or destinations, but the model complexity increases rapidly with the increase in the number of road segments and intersections. There are other traveling schedule models [17] that use optimum route algorithms to simulate the travel behavior of EVs. However, such techniques are computationally exhaustive and unsuitable for multiple simulations involved in MCS.

Therefore, there is a need for a simple and inclusive model that can accurately capture both the macroscopic aspects representing the wide geographical area (where the EVs have the mobility to move freely) and the microscopic aspects representing the specific travel destination or charging location.

Additionally, Fuzzy methods are used in the past to choose optimal sites of EV charging stations [69], [70] and online coordination of plug-in EV charging [71]. However, ordinary Fuzzy systems lack the means to incorporate randomness in the vehicle movements and are often found to be suitable for deterministic approaches. In order to introduce randomness, authors in [30] attempt to predict EV charging profile considering characteristics like arrival time, departure time, daily distance travelled and vehicle parameters using a stochastic fuzzy model of the driving patterns.

In addition to the peak demand increase due to EV charging, higher penetration of EVs creates dynamic changes in demand, which can adversely affect the reliability of the distribution system [15], [72]–[74]. Therefore, it is necessary to quantify these potential reliability impacts to arrive at optimal investment decisions related to future network upgrades. The reliability assessment of integrated transportation and electrical power systems is presented in [15] considering RESs and EVs. A detailed analysis of the generation system adequacy under the bidirectional charging power of EVs under various scenarios is described in [72]. These studies examine the impact of scheduled and unscheduled charging, Vehicle to Grid (V2G) mode operation, integration of PV units with charging stations on distribution system reliability. However, reliability-focused detail

evaluation of EV charging impact on the distribution system would be a beneficial extension to the models and techniques described in the existing literature.

3.3 Proposed models

A new two-layer EV charging demand simulation model consisting of a stochastic traffic network layer and an electrical network layer is proposed in this chapter. Firstly, a traffic network layer considered as the first layer of the model is introduced utilizing the concept of geographical zones to capture the spatial distribution of charging demand in a reasonable manner. While some studies described in the existing literature have completely ignored the spatial distribution, others attempted to take into account all geographical locations in a traffic network leading to an exponentially increasing model complexity. By separating inter-zone and intra-zone EV movements, model complexity is reduced to a manageable level in the proposed traffic network model as detailed in Subsection 3.3.1. A dynamic hidden Markov model (DHMM) that enables capturing the stochastic nature of both spatial and temporal changes in EV movement, as well as the type of charging locations, is proposed to represent the traffic network layer. The states of the DHMM capture the locational aspect while the dynamic transition probabilities model the temporal aspect. Moreover, the observable outputs of the DHMM are utilized to characterize the location types. It is shown that these model parameters can be conveniently obtained from traffic survey data.

Additionally, a novel probability-based method to incorporate the charging behavior of drivers and preferential charging locations is proposed. The model also incorporates trip

cancellations due to a lack of sufficient charge to complete the trip. The separated electrical network layer considered as the second layer of the model allows detailed representation of power distribution system and performing power flow, limit checking, reliability analysis, and simulation of corrective actions such as load shedding. Based on the proposed models, a detailed simulation procedure is developed to assess the impact of EV penetration on distribution system reliability performance using the Monte Carlo approach. Figure 3.1 shows the concept of the proposed two-layer stochastic EV charging demand estimation model with two separate layers which form the basis to build the designated model.

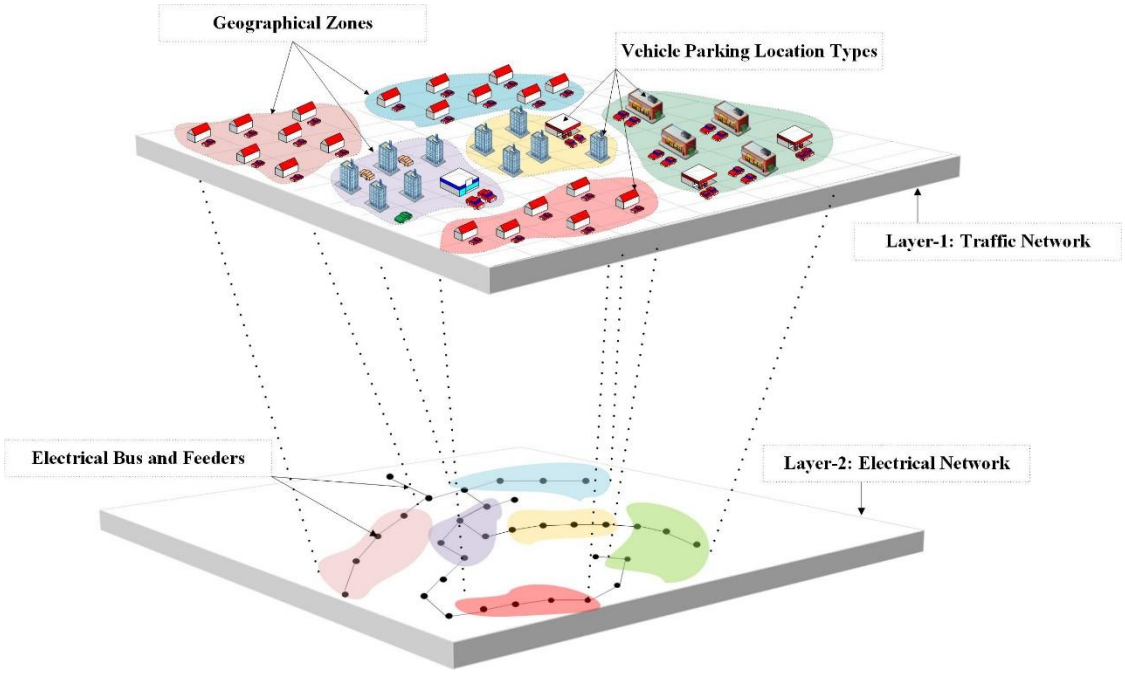

Figure 3.1. Proposed two-layer stochastic EV charging demand estimation Model

3.3.1 EV charging demand estimation models

The models and methods described in this section are associated with the two-layer EV charging demand estimation technique, where the 'traffic layer' represents the spatial distribution of EVs using a set of geographical zones, while the 'electrical network layer' models the electric power distribution network. The model takes into account EV movements, travel distances, charging behavior of drivers, EV battery state to assess the EV charging demand and the reliability of electrical power systems. The basic evaluation models are developed based on the hypothesis that the movement of a large group of EVs within an area consisting of a set of geographical zones can be represented using a Hidden Markov Model (HMM).

In order to capture the macroscopic aspect of EV movement, the interested geographical area is divided into several geographical zones, where each zone contains a cluster of vehicle parking locations. In this way, the macroscopic aspect of EV movement is captured by dividing the interested geographical area (urban area) into various geographical zones, where each zone contains a cluster of vehicle parking locations (microscopic aspect). A DHMM is used to model the movement of an EV, where the hidden states are used to represent the geographical zones, and the visible states are used to capture the type of specific parking location within a given geographical zone. Each prominent parking location is considered as an element in the cluster, which in reality represents a main electrical distribution point such as a distribution transformer for a group of residential customers, a shopping mall, or a fast-charging station. These parking locations can be grouped into various geographical zones based on road connections or

using a clustering algorithm such as k-means clustering or expectation-maximization clustering [75]. A particular geographical zone can contain different types of EV parking/charging locations.

The Hidden Markov Model provides a convenient structure for representing the EV movement and parking location type, although the hidden states are not indeed hidden in the conventional sense, as they are associated with known geographical zones. Figure 3.2 shows the state transition diagram of a discrete-time HMM with $H = Z + 1$ hidden states, where Z is the number of geographical zones, and S_1 ... S_Z are corresponding hidden states.

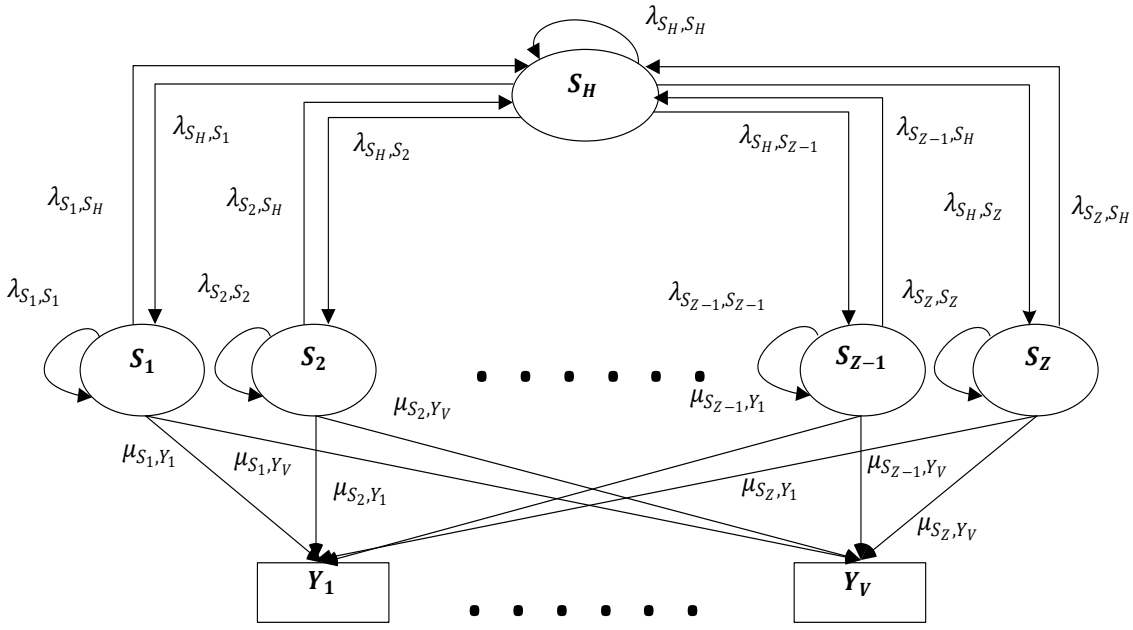

Figure 3.2. Dynamic Hidden Markov Model for EV spatial distribution

In addition to the Z hidden states representing the geographical zones, there is an 'in-movement' state (denoted as S_H). This is an 'intermediate latent state' and the last hidden state. The transition between the hidden states represents the inter-zone commutation of

EVs, and it is framed in such a way that when a vehicle moves from one zone to the other, it always goes through the 'in-movement' state. The state of the n^{th} EV at time t is defined as:

$$S_n^t \in \{S_1, S_2, \dots\dots, S_{Z-1}, S_Z, S_H\} \quad 3.1$$

The V visible states of the HMM, denoted by $Y_1 \dots Y_V$, are the location types within each zone. The parking location type of the n^{th} EV at time t is defined by the observations associated with the HMM.

$$Y_n^t \in \{Y_1, Y_2, \dots, Y_V\} \quad 3.2$$

In (3.1), (3.2), H and V represents the number of hidden states and the number of location types respectively.

3.3.1.1. Time-dependent state transition probabilities

The transition of an EV from its current zone to a new zone ($S_n^t \rightarrow S_n^{t+1}$) or remaining in the same zone is random in nature and it can be described by the probabilities defined in the state transition matrix [76]. According to the model depicted in Figure 3.2, for a given time t, the state transition matrix takes the following form:

$$M^t = \begin{bmatrix} \lambda_{S_1,S_1} & 0 & 0 & 0 & 0 & 0 & \lambda_{S_1,S_H} \\ 0 & \lambda_{S_2,S_2} & 0 & 0 & 0 & 0 & \lambda_{S_2,S_H} \\ 0 & 0 & . & 0 & 0 & 0 & . \\ 0 & 0 & 0 & . & 0 & 0 & . \\ 0 & 0 & 0 & 0 & . & 0 & . \\ 0 & 0 & 0 & 0 & 0 & \lambda_{S_{H-1},S_{H-1}} & \lambda_{S_H,S_{H-1}} \\ \lambda_{S_H,S_1} & \lambda_{S_H,S_2} & . & . & . & \lambda_{S_H,S_{H-1}} & \lambda_{S_H,S_H} \end{bmatrix} \quad 3.3$$

where λ_{S_i,S_j} is the probability of transition from state S_i to S_j. Each entry in the matrix is a non-negative real number representing a probability. The transition probability of a given EV from one zone to the other or remaining in the same zone is dependent on the time of the day. These probabilities are related to the driver's behavior and could be different from a weekday to a weekend day. Thus, the hidden state transition matrix is time-dependent [77], and makes the model a DHMM. The visible states indicating the location type can be assigned using the conditional probabilities provided in the form of an observation matrix as given in (3.4).

$$O^t = \begin{bmatrix} \mu_{S_1,Y_1} & \mu_{S_1,Y_2} & \cdot & \cdot & \cdot & \mu_{S_1,Y_V} \\ \mu_{S_2,Y_1} & \mu_{S_2,Y_2} & \cdot & \cdot & \cdot & \mu_{S_2,Y_V} \\ \cdot & \cdot & \cdot & \cdot & \cdot & \cdot \\ \cdot & \cdot & \cdot & \cdot & \cdot & \cdot \\ \mu_{S_{H-1},Y_1} & \mu_{S_{H-1},Y_2} & \cdot & \cdot & \cdot & \mu_{S_{H-1},Y_V} \\ \mu_{S_H,Y_1} & \mu_{S_H,Y_2} & \cdot & \cdot & \cdot & \mu_{S_H,Y_V} \end{bmatrix} \quad 3.4$$

where $\mu_{S_iY_j}$ is the conditional probability of EV being parked at a location of type Y_j in zone S_i. The elements of the observation matrix represent the conditional probabilities for a given EV to be parked in a particular type of location such as a 'workplace' or a 'home' when it is in a particular zone. These conditional probabilities are also time-dependent. The sum of probabilities in each row of a transition matrix (M^t) and the observation matrix (O^t) is 1, indicating that the hidden states and the location types are assumed to be mutually exclusive for simplicity. A Markov chain is considered periodically stationary or cyclo-stationary when the transition probabilities are periodically repeated [68]. Therefore, it is assumed that the transition probabilities will be repeated periodically in every τ time steps due to the cyclo-stationary properties of Markov chain as expressed mathematically using

Eqns. (3.5) and (3.6). It has been generally assumed that EV movement patterns are similar during the weekdays and it differs for weekends [68]. Hence, the probabilities are assumed to be repeated in a weekly cycle. In practical implementation, λ_{S_i,S_j} and $\mu_{S_iY_j}$ probability values can be calculated from vehicle travel data considering different geographical zones and parking location types. In fact, these probability values act as a medium to train the designated model similar to a machine-learning algorithm to functionally mimic the actual vehicle travel data [78].

$$M^t = M^{t+\tau} \quad 3.5$$

$$O^t = O^{t+\tau} \quad 3.6$$

3.3.1.2. Travel distance

EV travel distance is one of the major parameters in estimating the EV charging load. The distance D^t traveled by an EV within a time period is considered as a summation of inter-zone and intra-zone trip distances as given in (3.7).

$$D^t = d^t_{inter} + d^t_{intra} \quad 3.7$$

where, d^t_{inter}, is the distance traveled between two zones by an EV, and it can be determined from a geographic map of the road network and be reasonably assumed to be fixed for simplicity. This is not a major limitation as the total distance traveled is adjusted by the intra-zone trip distances. The fixed inter-zone travel distances can be represented by a matrix as given in (3.8). In (3.8), d_{S_i,S_j} represents the inter-zone distance between S_i-S_j. The distance traveled within a zone, d^t_{intra} , is modeled as a random variable with a

Gaussian distribution. Each zone can have a specific Gaussian distribution defined by its mean trip distance and standard deviation.

$$d_{inter}^{t} = \begin{bmatrix} 0 & d_{S_1,S_2} & . & . & d_{S_1,S_z} \\ d_{S_2,S_1} & 0 & . & . & d_{S_2,S_z} \\ . & . & . & . & . \\ d_{S_{z-1},S_1} & d_{S_{z-1},S_2} & . & 0 & . \\ d_{S_z,S_1} & d_{S_z,S_2} & . & . & 0 \end{bmatrix} \quad 3.8$$

3.3.1.3. Charging behaviour of drivers

The EV driver's charging preferences play a crucial role in evaluating the impacts of EVs on power system reliability. As per the International Energy Agency (IEA) EV outlook, there is a direct correlation between EV driver charging preferences, parking location, and charging probability [79], [80]. From a power system point of view, it is imperative to capture these attributes associated with the EV charging and their interaction with the power system. In the existing literature, driver's charging behaviors are taken into account by considering their charging locations [19] and various trip types [81]. A different approach is used in this work to model the driver's charging behaviors. It is assumed that each driver class has g preferred location types specified as $g = \{g_1, g_2, \ldots g_G\}$: g_1 represents the most preferred location for charging their EVs, while g_2, g_3,…..g_L are the other locations, in the order of preference, from where drivers in this class would recharge their vehicles. To incorporate this concept in the overall simulation process, the probability of EV to charge at any time t is determined considering the type of the parked location (g_i) and the present charge level (CL). The probability is a conditional probability, $P(CL|g_i)$ that can be assumed constant over a range of SOC values and specified for L discrete CL

designated by the set $CL = \{CL_1, CL_2 \dots CL_L\}$. For example, CL_1 may represent 'low charge level' and corresponds to the SOC range [0% – 40%]. Then the conditional probabilities can be specified in a matrix ($L \times G$) form as shown in (3.9). Each driver class would have a different matrix of conditional probabilities. Battery related parameters such as SOC are important and consistent definitions should be used [82], [83].

$$P(CL|g) = \begin{bmatrix} P(CL_1|g_1) & \cdots & P(CL_1|g_G) \\ \vdots & \ddots & \vdots \\ P(CL_L|g_1) & \cdots & P(CL_L|g_G) \end{bmatrix} \quad 3.9$$

3.3.1.4. Battery energy

The battery energy level E^t at the end of a time point, t depends on whether an EV is in charging, discharging, or parked state during the time period Δt. It is modeled using (3.10):

$$E^t = \begin{cases} E^{t-1} + \eta^{ch}.P^{ch}.\Delta t, & \text{'Charging'} \\ E^{t-1} - \frac{1}{\eta^{dch}}.D^t \cdot E^{dch}, & \text{'In-Movement'} \\ E^{t-1}, & \text{'Parked'} \end{cases} \quad 3.10$$

where η^{ch} and η^{dch} represents the charging and discharging efficiency of each EV. P^{ch} is the power at which an EV is charged, D^t represents the distance traveled and E^{dch} indicates the average energy consumed per unit distance associated with EV movement. P^{ch} represents the average power due to charging over a simulation time step, which may include constant current or constant voltage charging periods. This is a reasonable simplification for MCSs with course time steps, which are typical in planning studies. However, a more sophisticated SOC-dependent EV charging demand model can be

included in MCS, if required. The battery operation is limited within certain boundaries, typically specified by the EV manufacturer as follows:

$$\Psi^{min} \leq E^t \leq \Psi^{max}, \ \forall t = \{1 \dots T\} \qquad 3.11$$

The battery SOC at the end of time step t is computed from E^t. A decision to redirect the Battery Electric Vehicle (BEVs) to a nearby charging location is taken under the situation when an EV does not have enough charge to complete a specific trip.

$$E^t < (D^t \cdot E^{dch}) + \Psi^{min}, \quad \forall t = \{1 \dots T\} \qquad 3.12$$

where Ψ^{min} represents the required energy to maintain a minimum SOC and avoid battery depletion beyond a certain limit.

3.3.1.5. Power demand due to EV charging

To quantify the amount of power EVs draw from a power system, the number of EVs connected to the particular network bus in the charging mode in a given zone need to be determined. The total EV charging power demand $P^{ch,t,b}$ at bus b at time point t is computed by summing the charging power P_k^{ch} of each of the $K^{b,t}$ number of EVs connected at bus b and being charged in the time period considered.

$$P^{ch,t,b} = \sum_{k=1}^{K^{b,t}} P_k^{ch} \qquad 3.13$$

The values of $P^{ch,t,b}$ in (3.13) is assumed as the total three-phase power. Although most residential EV chargers are single-phase type, it is reasonable to assume that the chargers fed from a given distribution transformer are distributed evenly among the phases,

especially in planning studies. If the distribution network consists of single-phase sections, then this should be appropriately treated.

3.4 Calculation of reliability indices

Power system reliability assessment using a probabilistic technique mainly involves two major steps. These EV charging at each time period at each distribution bus can be determined using the models described in Section 3.3.1. The total power demand is the sum of power demand due to EV charging and the power demand due to other loads. Once the state for each time period is selected (in the form of power demand), the next step is to evaluate the consequence of each state by performing a power flow analysis. A backward/forward sweep method that is suitable for distribution system power flow analysis is employed in this work [84]. If overload or voltage issues are found, the appropriate amount of load is shed to eliminate the issue, considering a simple priority-based load shedding algorithm. It is assumed that the power utilities can make an agreement with the consumer to curtail the loads whenever necessary. The following reliability indices are used to evaluate the reliability performance of power systems. The reliability indices computed are System Average Interruption Frequency Index (SAIFI), System Average Interruption Duration Index (SAIDI), Expected Energy Not Supplied (EENS), and Average System Availability Index (ASAI).

$$SAIFI = \frac{\sum_{j=1}^{N_s} \left[\frac{\sum_{t=1}^{T} CI^t}{N_{cust}}\right]}{N_s} \quad 3.14$$

$$SAIDI = \frac{\sum_{j=1}^{N_s}\left[\frac{\sum_{t=1}^{T} CI^t * r^t}{N_{cust}}\right]}{N_s} \quad 3.15$$

$$EENS = \frac{\sum_{i=1}^{N_s}[\sum_{t=1}^{T} P^{curt,t} * \Delta t]}{N_s} \quad 3.16$$

$$ASAI = \left[\frac{1 - \sum_{t=1}^{T} CI^t * r^t}{(N_{cust} \cdot T)}\right] \quad 3.17$$

where,

r^t : Restoration time

CI^t : Number of customers interrupted at time t

$P^{curt,t}$: Power curtailed at time t

N_{cust} : Total number of customers

N_s : Total number of MCS replications

T : Total number of time periods in a year

Three new reliability indices are also proposed to capture and quantify the impact of EV charging due to a mixed group of EVs with different designs as well as driver behaviors. These are the Expected Frequency of EV Charging Index (EFECI), the Expected Duration of EV Charging Index (EDECI), and Expected EV Charging Load (EECL):

$$EFECI = \frac{\sum_{j=1}^{N_s}\frac{\sum_{t=1}^{T} q^t}{N_{ev} * 365}}{N_s} \quad 3.18$$

$$EDECI = \frac{\sum_{j=1}^{N_s}\frac{\sum_{t=1}^{T} q^t * cd^t}{N_{ev} * 365}}{N_s} \quad 3.19$$

$$EECL = \frac{\sum_{j=1}^{N_s} \frac{\sum_{t=1}^{T} \sum_{b=1}^{N_B} P^{ch,t,b}}{T}}{N_s} \quad 3.20$$

where,

q^t : Total number of new EVs-charger connections at time t

cd^t : The charging duration

N_{ev} : The total number of EVs

N_B : The number of buses that are connected to EV in the distribution system at time t.

EFECI values essentially depict the average frequency of charging of an EV per day, EDECI indicates the average charging time of an EV per day and EECL represents the average charging load anticipated over a particular period.

3.5 Simulation process flowchart

Figure 3.3 illustrates the procedural flowchart used to illustrate the overall simulation process. To begin with the simulation, essential inputs with regards to traffic networks such as inter-zone distances, the data related to the type, driver's charging behavior, the initial condition for each EV, the time-dependent transition probability data for the HMM, and data pertaining to the electrical network are provided. After the initialization, the EV state for the next particular time instant $t = 1$ is found using the HMM. The algorithm will then check whether the energy remaining in the battery (only applicable for BEVs) is sufficient to complete the trip. If BEV's charge is not enough, a short detour to a nearby charging facility will be assumed, and the trip will be cancelled for the time being. On the other

hand, if sufficient charge is ensured, then the total inter-zone and intra-zone distance are calculated, and EV SOC is updated.

If EV is not in S_H ('in-movement' state) then the next possible outcome is to park the EV at a particular location within a zone. If the situation is such that EV is parked on the same zone during $t-1$ and t, but the parking locations are different for two-time periods, then the EV would have taken a short trip (intra-zone trip distance) within the same geographical zone for example S_i in Figure 3.3. Then the short-trip distance is drawn from the Gaussian distribution and the SOC of the EV is updated to reflect the short-trip. The algorithm will check for the charging facility at the designated current parking location, and the driver class-dependent charging decision is determined based on a random permutation of the current level of state of charge and the location type.

If the decision is to charge, the EV will be charged, and the EV SOC will be updated based on the EV model and the capacity (level) of the charging facility. The algorithm will update the SOC of EVs, compute the total EV load at each location, and run the power flow analysis. To control the simulation, a minimum number of trails are ensured, and the standard deviation values of total system load per trial beyond a threshold value are used as a criterion to stop the simulation.

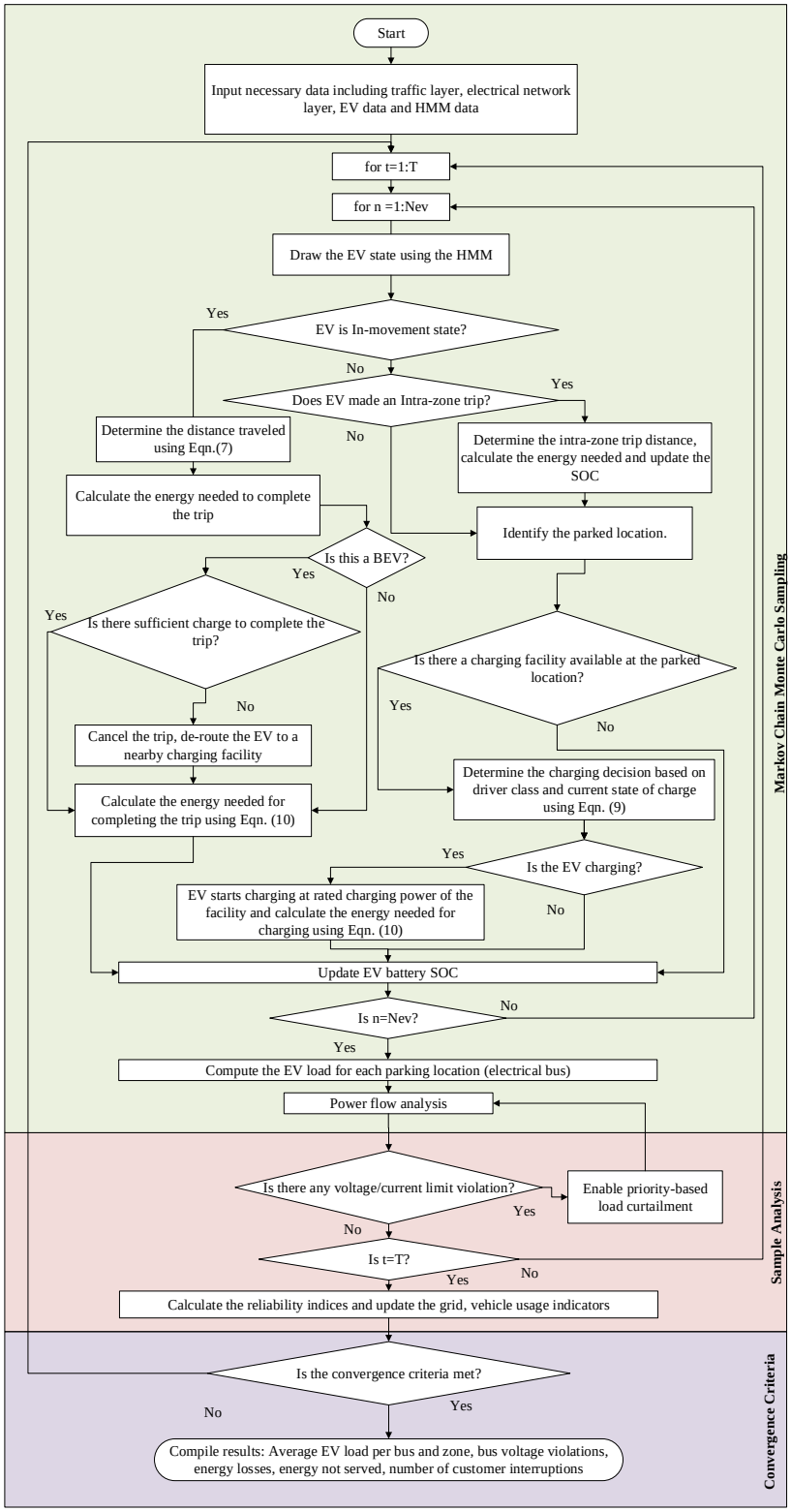

Figure 3.3. Simulation process flowchart of MCMC

3.6 Study system description and data inputs

In order to illustrate the applicability of the proposed models and methodology, studies were performed to evaluate the impact of EV penetration on an example distribution network. A modified version of the IEEE 33 bus system [85] was used as the example electrical network in this chapter. The test system is assumed to be connected to the main grid through a substation transformer rated at 110/13.22 KV, 1.5 MVA as shown in Figure 3.4. The parameters of the test system are provided in Appendix A: Table A.1. It was assumed that there are six different geographical zones and five different location types present as illustrated in Figure 3.4, giving rise to a total of 30 EV parking locations with charging facilities within the designated geographical area.

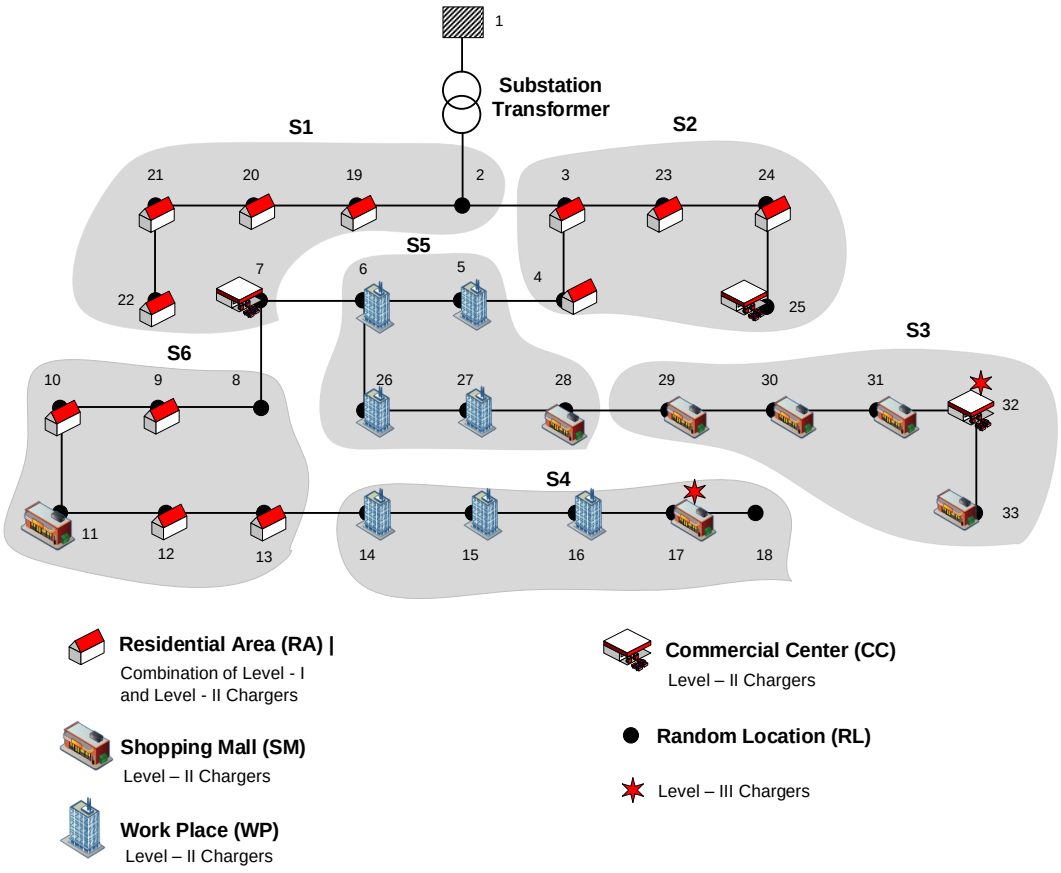

Figure 3.4. Example system representation (modified IEEE 33 bus system)

Table 3.1 summarizes the details of charging locations. Some of the information presented in Figure 3.4 such as the Levels I, II and III chargers will be described later in this section. The inter-zone distances to be used in the matrix d_{inter}^{t} defined in Eqn. (3.8) are given in Table 3.2. The intra-zone travel distances were computed considering a Gaussian distribution with a mean of 2 km and a standard deviation of 1.55 km for all zones in this example. The d_{intra}^{t} values were limited to a range of [0.9 – 6 km]. There are seven hidden states $(S_1 - S_6, S_H)$ representing the geographical zones and in-movement state, and five visible states $(Y_1 - Y_5)$ representing the output of the HMM, which indicate the

vehicle parking location types such as RA, WP, SM, CC, and RL. For simplicity, it is assumed that a charger is available whenever an EV decides to charge. The availability of the chargers is generally not a concern for RA or WP locations. For other location types, it is assumed that enough chargers are available regardless of the number of EVs being charged simultaneously.

Table 3.1 Charging locations in different zones and corresponding electrical buses

Zone	**Number of charging locations type**				
	RA	**WP**	**CC**	**SM**	**RL**
S_1	4 (19, 20, 21, 22)	-	1 (7)	-	-
S_2	4 (3, 4, 23, 24)	-	1 (25)	-	-
S_3	-	-	1 (32)	4 (29, 30, 31, 33)	-
S_4	-	3 (14, 15, 16)	-	1 (17)	1 (18)
S_5	-	4 (5, 6, 26, 27)	-	1 (28)	-
S_6	4 (9, 10, 12, 13)	-	-	1 (11)	1 (8)

Table 3.2 Inter-zone distances (km)

	S_1	**S_2**	**S_3**	**S_4**	**S_5**	**S_6**
S_1	0	6.25	8.75	6.25	7.5	11.75
S_2	6.25	0	6.25	7.5	6.25	7.5
S_3	8.75	6.25	0	11.25	7.5	5
S_4	6.25	7.5	11.25	0	5	8.75
S_5	7.5	6.25	7.5	5	0	5
S_6	11.75	7.5	5	8.75	5	0

Before the simulation, a number of inputs associated with the traffic layer, electrical network layer, HMM and EV need to be provided. The initial zone for each EV is assumed to be located in zones $[S_1, \dots, S_6]$ with probabilities of $[0.33\ 0.33\ 0\ 0\ 0\ 0.34]$. It is also

assumed that each EV is parked at [RA, WP, SM, CC, RL] with probabilities of [0.8 0.05 0.05 0.05 0.05]. This represents a higher probability for an EV to be parked at residential locations (S_1, S_2, and S_6). The values of the transition matrix (M^t) and observation matrix (O^t) are assumed to represent the EV driver travel survey published in [79]. As an example, values of M^t and O^t at $t = 9$ are shown in Table 3.3 and Table 3.4 respectively. Since the patterns were assumed repetitive in weekly cycles, these probability matrices were defined for each time step in a week, considering the differences between weekdays and weekends.

Table 3.3 State transition matrix values for time period $t = 9$

	S_1	**S_2**	**S_3**	**S_4**	**S_5**	**S_6**	**S_7**
S_1	0.98	0	0	0	0	0	0.02
S_2	0	0.98	0	0	0	0	0.02
S_3	0	0	0.02	0	0	0	0.98
S_4	0	0	0	0.02	0	0	0.98
S_5	0	0	0	0	0.02	0	0.98
S_6	0	0	0	0	0	0.98	0.02
S_7	0.33	0.33	0	0	0	0.33	0.01

For each EV, a charging location associated with a residential or workplace location within its 'home' zone was assigned as the preferred charging location. The travel pattern of EVs and their charging from various locations were simulated for a year using the HMM. A simulation time step (Δt) of 30 minutes was used. This results in a total of 17520 simulation time steps in a sample year. The total electrical load in the system consists of the regular electrical load (base caseload) and the EV charging load.

Table 3.4 Observation matrix values for time period $t = 9$

	$\mathbf{Y_1}$	$\mathbf{Y_2}$	$\mathbf{Y_3}$	$\mathbf{Y_4}$	$\mathbf{Y_5}$
$\mathbf{S_1}$	0.95	0	0	0.05	0
$\mathbf{S_2}$	0.95	0	0	0.05	0
$\mathbf{S_3}$	0	0	0.6	0.4	0
$\mathbf{S_4}$	0	0.8	0.15	0	0.05
$\mathbf{S_5}$	0	0.8	0.2	0	0
$\mathbf{S_6}$	0.8	0	0.15	0	0.05
$\mathbf{S_7}$	0	0	0	0	0

The variation in the base caseload is modeled using the demand level factors as per [86]. A 5-year annual load profile data published by ERCOT [87] is used to capture the annual load variation patterns. The battery capacity and driving miles are the two main factors considered in modeling the battery storage of EVs [73]. The standard models of PHEV40 [88], BEV 200 [73] and BEV 100 are used in the studies. Table 3.5 details the major parameters of these standard models. It can be seen from Table 3.5 that the driving range increases along with the battery energy storage capacity. The initial battery SOC values of individual EVs were randomly assigned considering a uniform distribution of initial SOCs within the range of 15% to 90% [89]. Three different charging levels, namely Level-I, Level-II, and Level-III [90] are assumed to represent the rated charging powers 0.2C, 1C, and 2C respectively where the C is the standard charging power. Their rated charging powers and locations are given in Table 3.6.

Table 3.5 Details of PHEV and BEV batteries

	PHEV 40 (USABC)	**BEV 100**	**BEV 200 (MIT)**
Driving range with battery (km)	64.3	160.9	321.8
Peak power (kW)	46	50	80
Energy capacity (kWh)	17	30	48
Charge power at 0.2C (kW)	3.4	3.6	9.6
Charge power at 1C (kW)	17	18	48
Charge power at 2C (kW)	34	36	96
Charging efficiency (%)	85	85	85
Discharging efficiency (%)	85	85	85
Minimum SOC (%)	30	30	30
Maximum SOC (%)	90	90	90

Table 3.6 Details of various charger types used and corresponding electrical buses

Charger Type	**Charging Power**	**Locations (Bus Numbers)**
Level-I Chargers	0.2C	19, 3, 9, 14, 5, 20, 4, 10, 15, 6, 21, 23, 12, 16, 26, 22, 24, 13, 7
Level-II Chargers	1C	7, 25, 32, 29, 17, 28, 11, 30, 31, 33
Level-III Chargers	2C	17, 32

Level-I and Level-II chargers are the most common charger types, and their presence was assumed in most of the electrical buses. Level-III chargers are the fast-charging stations, and they were assumed to be present in a few locations like SM and CC. The parameters used for modeling the EV driver behavior are given in Table 3.7. Four preferred charging locations (g_1, g_2, g_3, g_4) and three discrete charging levels (CL_1, CL_2, CL_3) were considered. Table 3.7 lists the conditional probability $P(CL|g)$ values for each driver class with respective preferred location types. These probability values are assigned to reflect the driver behavior information provided in IEA Outlook 2017 [79]. It should be noted that although the charging events of different EV drivers are considered independent, those

events in the same class are not mutually exclusive. The annual average total active power on the system was taken as the parameter to monitor the convergence of MCS. The simulation is considered to be converged if the standard deviation of annual average total active power on the system is lower than 0.001 kW after completing a minimum number of 100 trails.

Table 3.7 Parameters used for modelling driver behavior

Driver Class	**Charge level**		**(CL_1)**	**(CL_2)**	**(CL_3)**
	SOC range (%)		**0 - 30**	**31 - 70**	**71 - 90**
	Preferred Location	**Location Type**			
Class-1	g_1	RA	0.85	0.82	0.78
	g_2	WP	0.9	0.82	0.74
	g_3	CC	0.76	0.5	0.23
	g_4	SM	0.74	0.45	0.2
Class-2	g_1	WP	0.9	0.85	0.72
	g_2	CC	0.88	0.83	0.71
	g_3	SM	0.73	0.65	0.22
	g_4	RA	0.71	0.6	0.2
Class-3	g_1	SM	0.93	0.83	0.79
	g_2	CC	0.92	0.82	0.77
	g_3	RA	0.73	0.6	0.22
	g_4	WP	0.72	0.58	0.2

3.7 Results and discussions

This section provides the simulation results obtained using the proposed approach. The results are presented in the following order: (i) results related to verification of the traffic layer model, (ii) results related to verification of the electrical network layer model, and (iii) reliability indices calculated including sensitivity analysis.

3.7.1 Validation of the traffic layer using the real-world travel data

It is important to investigate the practicality of obtaining parameters of the proposed model (traffic layer) from actual recorded vehicular data and verify the fidelity of the model in representing the actual driving patterns of vehicle users. The studies described in this chapter utilizes the travel data of 50 vehicles obtained by GPS recording devices, over a period of time in and around the city of Winnipeg, MB, Canada. A few attributes of the data utilized in this work are listed below:

- The data was collected by the University of Winnipeg [91] and contains more than 44 million data points and over 150 000 parking events.
- The vehicle drivers chosen for the study were volunteers from different income brackets, education levels, and gender and from different areas of the city to create a statistical population best representing the drivers within the city of Winnipeg.
- The fleet chosen includes sedans, both full and mid-size (67%), and sport utility vehicles and pickup trucks (33%). The data collected were representing various activities such as commuting, shopping, and socializing.

- This actual data has been transformed to hide the identity of volunteers and their locations, and the database has been used previously by various researchers for EV-related studies in [92], [93].

3.7.1.1. Calculation of transition matrix and observation matrix probability values

Actual vehicle data has been used to calculate the time-dependent probability values of the state transition matrix and the observation matrix for each vehicle. It is assumed that the geographical area of the city of Winnipeg can be divided into nine zones as shown in Figure 3.5 based on a general trend of vehicle movements through the city.

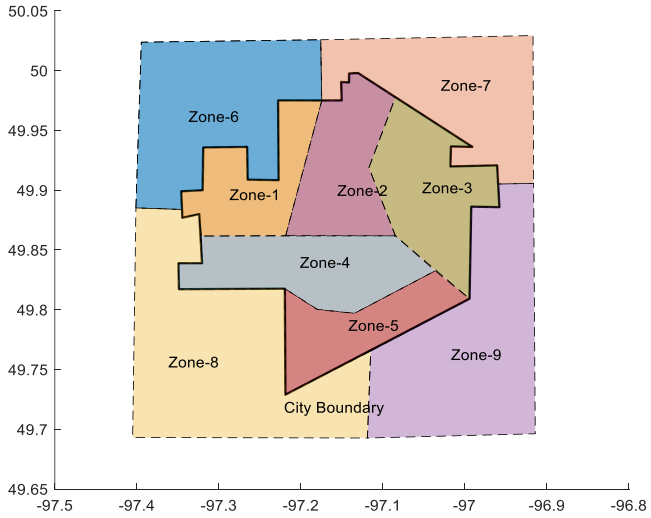

Figure 3.5 Illustration of various geographical zones for the City of Winnipeg, Canada.

The following steps describe the data utilization:

- **Step-1:** Determine the geographical zones for the city of Winnipeg as shown in Figure 3.5. Ideally, this should be completed by considering the electrical and traffic network.
- **Step-2:** For each vehicle, identify i) trip start/end time, ii) trip start/end locations (GPS coordinates), and iii) day type (weekday/weekend).
- **Step-3:** For each vehicle, identify the geographical zones and parking location type from the GPS data. The location types considered are 1) RA, 2) WP, 3) CC, 4) SM, and 5) RL. The data is organized in two separate arrays which have geographical zones and parked location types in each time period t. 48-time intervals ($\Delta t = 30$ mins.) per day are considered. Figure 3.6 shows the representation of this concept where each vehicle status (geographical zone/location type) over different days is recorded for the purpose of necessary probability calculations. In Figure 3.6, the brown indication over the car represents the hidden state showing the geographical zone/travel state(s) and the green represents the visible states showing the parked location type(s).

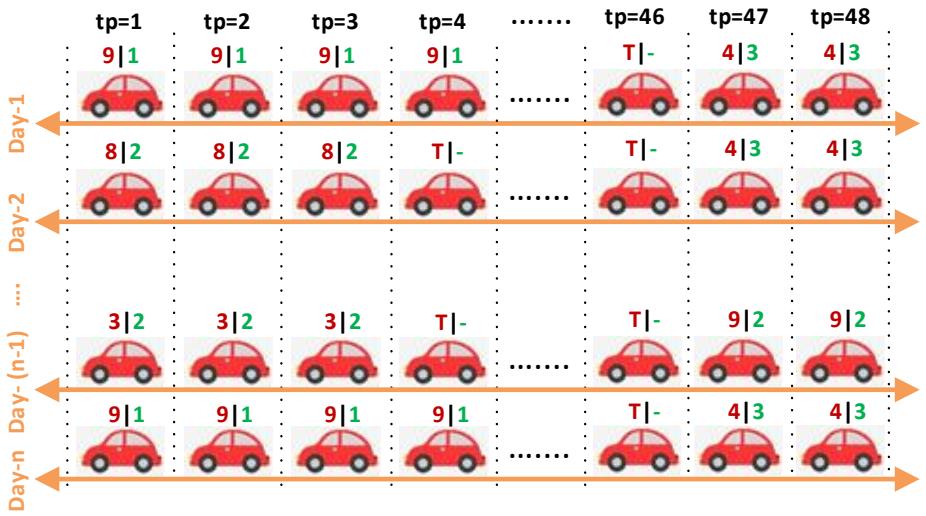

Figure 3.6 Schematic diagram illustrating the states of a vehicle.

- **Step-4:** Calculate the state transition matrix for each time period t using (3.21)-(3.22) and observation matrix probability values using (3.23).

$$\lambda^{t}_{S_i,S_i} = \frac{\sum_{p=1}^{SS} N^{t}_{S_{i\to i}}}{\sum_{p=1}^{SS} N^{t-1}_{S_i}} \qquad 3.21$$

$$\lambda^{t}_{S_i,S_j} = \frac{\sum_{p=1}^{SS} N^{t}_{S_{i\to j}}}{\sum_{p=1}^{SS} N^{t-1}_{S_i}} \quad i \neq j \qquad 3.22$$

$$\mu^{t}_{S_i,Y_j} = \frac{\sum_{k=1}^{TP} N^{t}_{Y_j \mid S_i}}{N^{t}_{TP}} \qquad 3.23$$

As per (3.21)-(3.22), the denominator counts the total number of S_i vehicle states in total vehicle states SS during the time period $t-1$. In (3.21), the numerator counts the total number of times the vehicle continued in the same state S_i whereas, (3.22) counts the number of times vehicle changed its state to S_j. The observation probability matrix values are computed using (3.23) where the numerator counts the number of times vehicle parked

at the location type Y_j provided that vehicle is at the state S_i and the denominator represents the total trips recorded N_{TP}^t during the time period t.

Sections (3.7.1.2)-(3.7.1.4) show the actual and simulated results pertaining to the model validation. For this probability matrices calculation example with data from Winnipeg, MB, nine geographical locations ($S_1 - S_9$) were assumed as shown in Figure 3.5 [94]. The in-movement state (S_M) is the hidden states of the designated model. Additionally, five visible states are assumed as different location types ($Y_1 - Y_5$) namely RA, WP, CC, SM, and RL respectively. Since more data points are available corresponding to weekdays, all evaluations are performed considering weekdays alone. The same procedure can be applied to weekends.

3.7.1.2. Hidden and visible states

Figure 3.7 (a) and (b) show the frequency of being in different hidden states (zones) at different times of the day, computed from the recorded vehicle data (160 data points) and the simulated data (2500 data points) respectively for one randomly selected vehicle.

It is visually observable that the model was able to capture the general trend in the vehicle state. Similarly, Figure 3.8 (c) and (d) show the frequency of being in different visible states at different times of the day, as obtained from the actual and simulated data respectively. The probability mass functions of hidden and visible states indicate the distribution of the probability of being in different hidden or visible states in an individual time period.

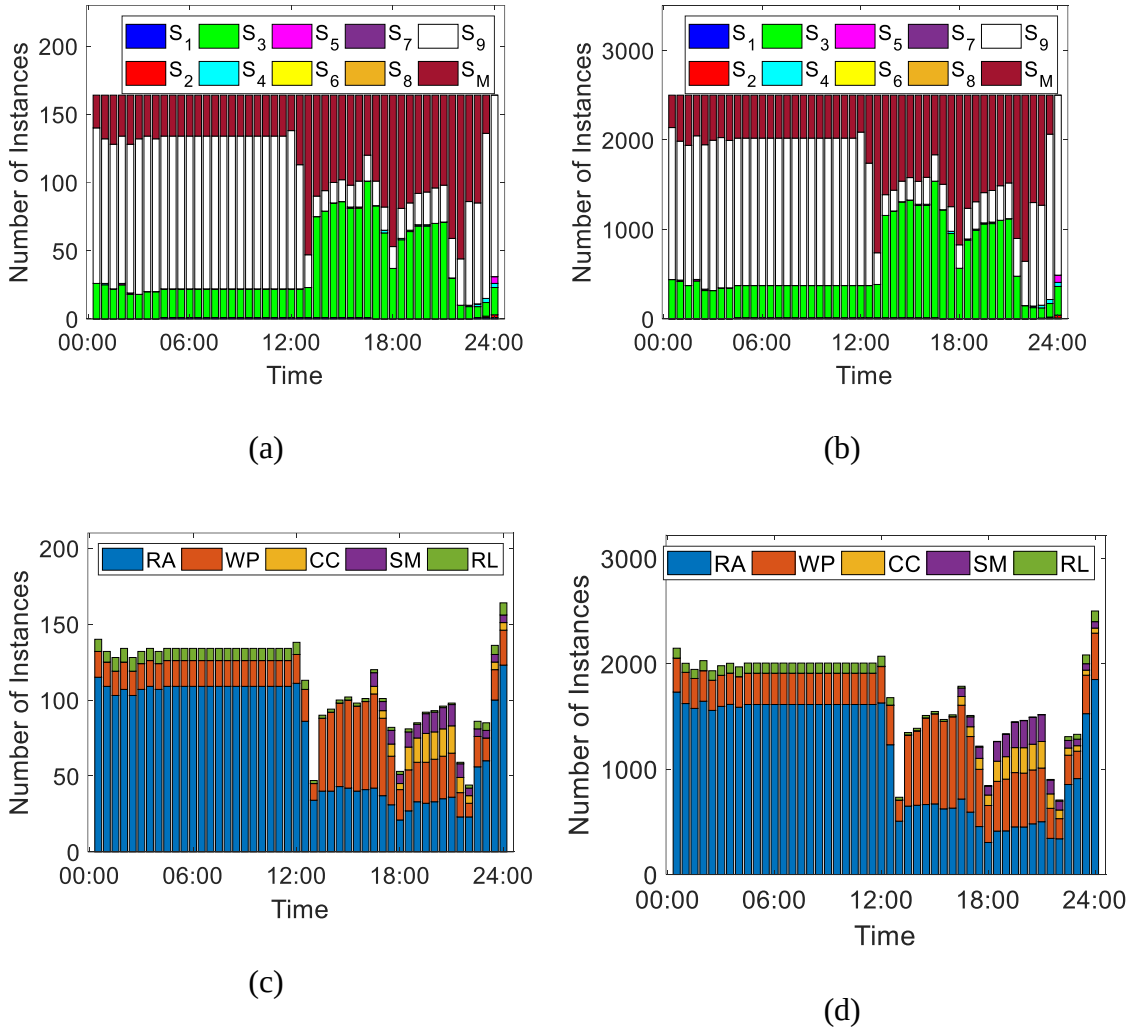

Figure 3.7 (a) Actual hidden states, (b) simulated hidden states, (c) observed visible states, (d) simulated visible states of a single vehicle,

Figure 3.8 (a) and (b) compare the samples of probability mass functions developed for time period $t = 40$ using actual and simulated data. As can be seen, the actual and simulated probability mass functions closely match each other, although there are some minor differences.

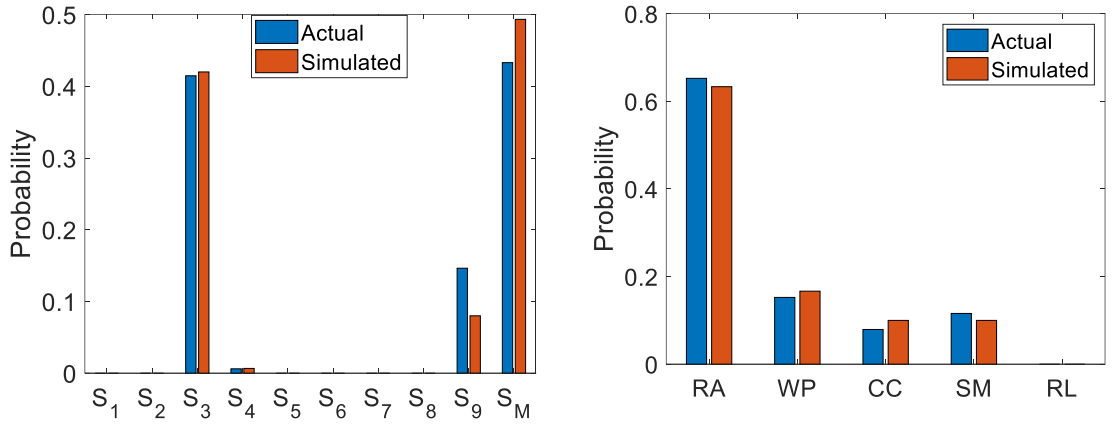

(a) (b)

Figure 3.8. (a) probability mass function of hidden states, and (b) visible state during the time period tp=40.

3.7.1.3. Transition and observation matrix values

After simulating a vehicle movement over a sufficient period of time, the data can be used to compute the state transition probability matrices (M^t) and the observation probability matrices (O^t) for different time steps. The time-dependent transition and observation probability values corresponding to those are shown in Figure 3.9 (a) and (b) for a randomly chosen vehicle. It can be seen from Figure 3.9 that the probability variations over time are very similar to those obtained from the actual data, as expected from a good model. This is indeed the main reason to have similar vehicle hidden states distributions in Figure 3.9 (a) and (b), and observable states distributions in Figure 3.9 (c) and (d). The similarity between the time variations of the actual and simulated transition probability matrix and observation probability matrix elements (all entries in M^t and O^t) were

evaluated using Pearson correlation coefficient (PCC). For the vehicle under consideration, the PCC for transition probabilities was 0.95, while the PCC for observation probabilities was 0.99. These PCC values show a good similarity between the actual and simulated vehicle travel pattern data.

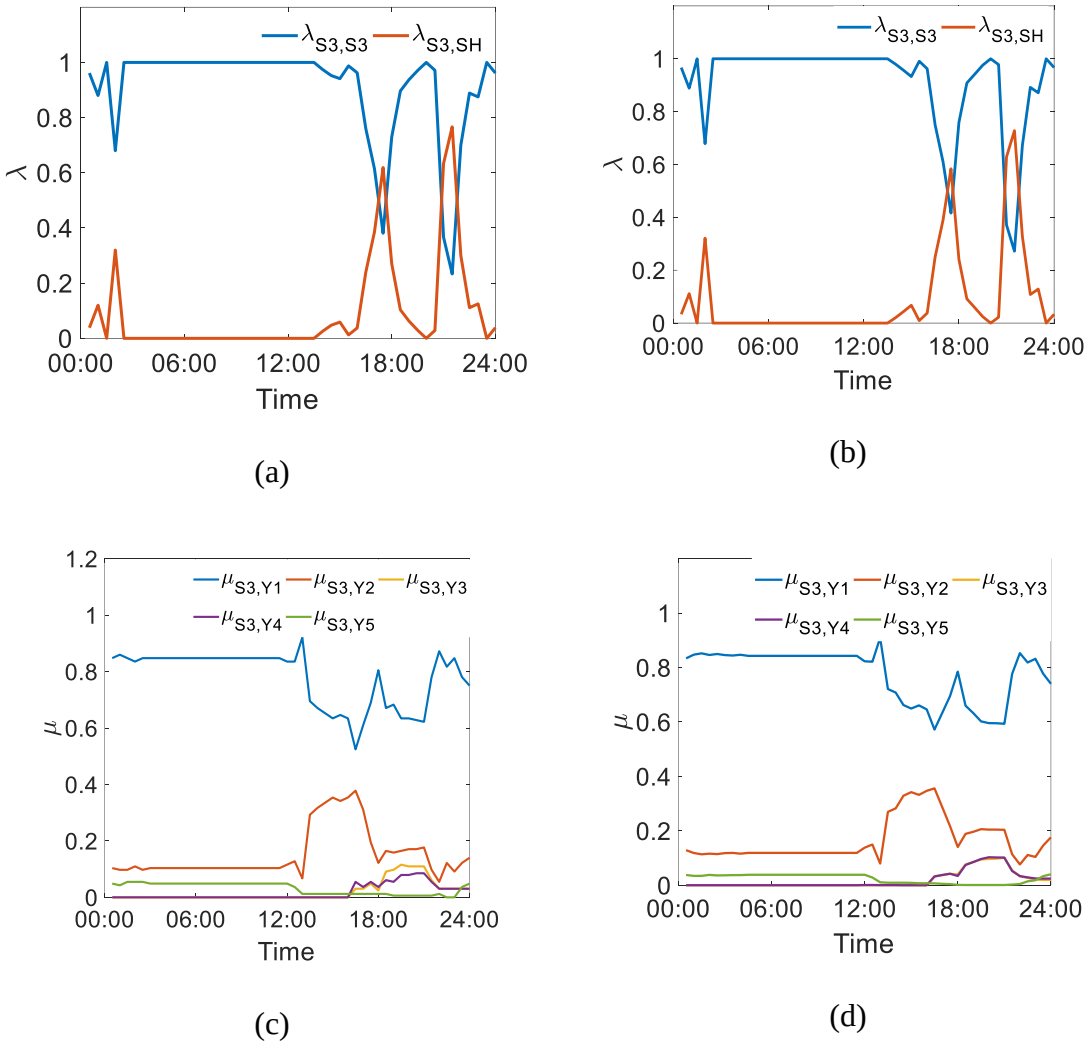

Figure 3.9 (a) Actual, (b) simulated values of transition matrix probabilities, (c) actual and (d) simulated values of observation matrix probabilities

3.7.1.4. Euclidean distances

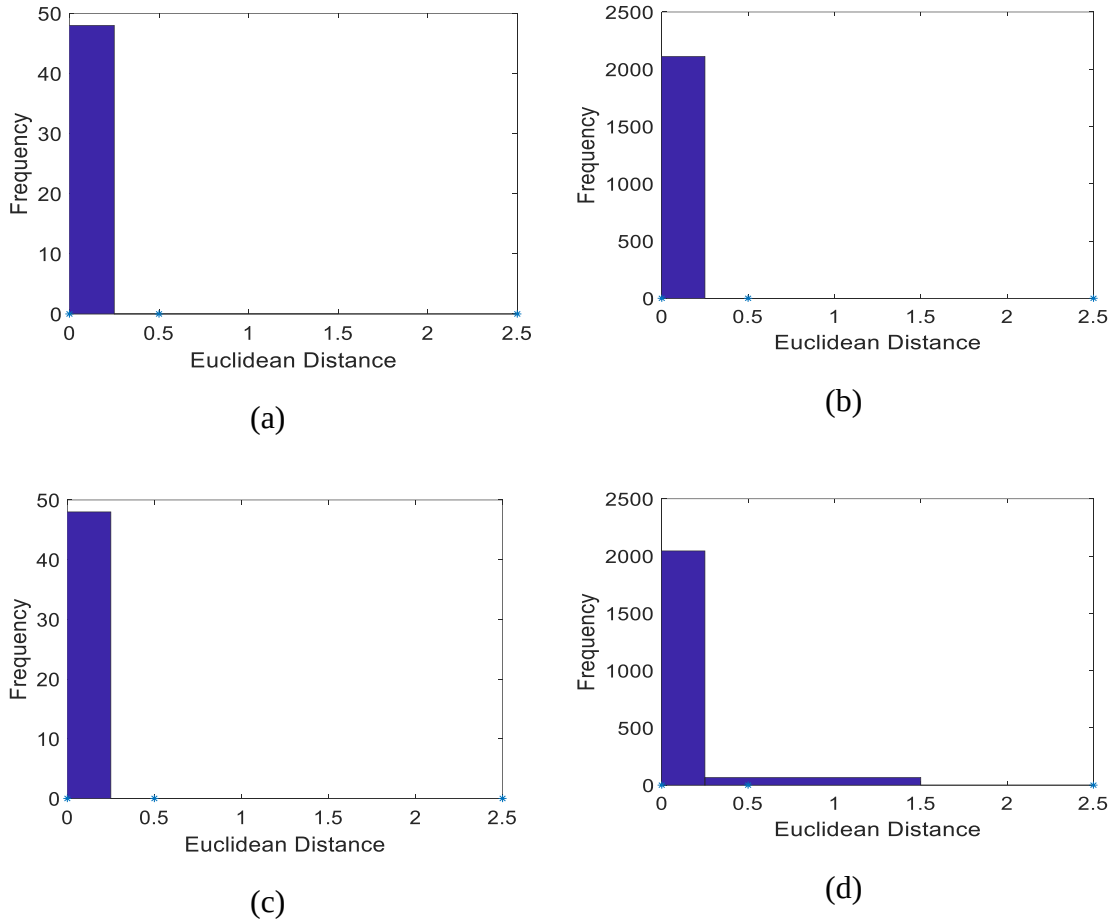

Figure 3.10 . Distributions of the Euclidean distances between (a) actual hidden states for one vehicle, (b) simulated hidden states for 50 vehicles, (c) actual visible states for one vehicle, and (d) simulated visible states for 50 vehicles

The distribution of Euclidean distances between the actual and simulated probability mass functions, computed for one single vehicle is shown in Figure 3.10 (a) and (c). It can be seen from Figure 3.10 (a) and (b) that most of the time distances are small (<0.3) indicating that the DHMM model reasonably well represents the actual vehicle movement

patterns. Additionally, the distribution of Euclidean distances for 50 different vehicles combined after generating their hidden and visible states separately for individual vehicles are shown in Figure 3.10 (c) and (d). The lower values of Euclidean distances in Figure 3.10 indicates the fidelity of the model to emulate the synthetic data closer to the actual recorded values. This further reveals the generic applicability of the model to preserve the spatial and temporal distributions for a group of vehicles.

3.7.2 Corroboration of traffic layer and electrical layer model combined

In order to examine the traffic layer model, the states of a single EV were tracked over two 24-hour periods on a weekday and a weekend. Figure 3.11 illustrates state transitions, associated distances traveled, the charging powers, and the variation of SOC during a weekday and a weekend day. It can be seen from the plot of (S_H), which illustrate the inter-zone transitions, that the EV follows the typical movement pattern of a driver who would have regular working hours on the weekdays and a more random movement on the weekend.

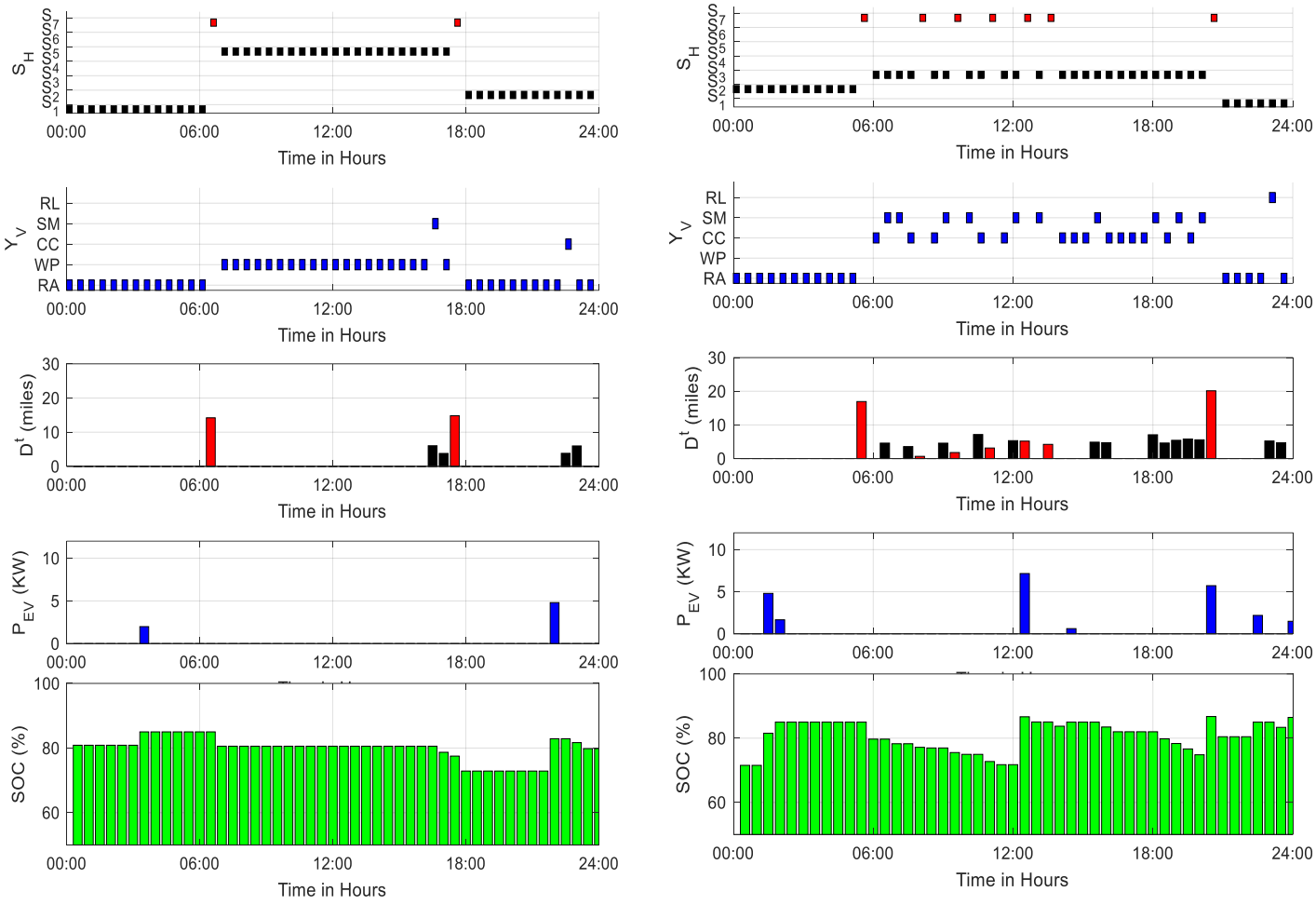

(a) (b)

Figure 3.11. A single EV state transitions, distance traveled, charging load and state of charge for a complete day during (a) weekday and (b) weekend

The plot of (Y_V) which illustrates the transitions among different location types also shows a similar pattern of more random movements on weekends. The inter-zone and intra-zone driving distances are indicated with red and black colours respectively in the graph of distance traveled (D^t). The variation of battery SOC is based on the distance traveled by

the EV and the charging levels at the respective charging locations. The variation in SOC levels can be seen while EV is involved in either traveling or charging.

The average charging power is estimated using the equations presented in Section 3.3.1.5. Considering the complexity of extracting and managing multiple vehicle parameter values from actual recorded vehicle data, the remaining results Section (3.7.3)-(3.7.5) use representative probability values for the transition/observation matrix and assumed six geographical zones in the traffic layer. A sample of representative transition and observation matrix probability values are provided in the Appendix. B.

3.7.3 Analysis of electrical network layer

Figure 3.12 illustrates the daily average charging load for various location types during weekdays and weekends for 250 EVs. A consistent residential charging during the initial and final hours can be observed for both weekdays and weekends, whereas workplace charging during the daytime of weekdays is noticeable in Figure 3.12 (a). On the other hand, a higher EV charging load can be seen at CC and SM during the weekend daytime. The peak charging load is much higher at the weekends, mainly due to contribution from the fast-charging stations in S_3. During the weekdays, the peak load including the charging load is 1625 kW while that on the weekend is 1460 kW. It can be seen from Figure 3.13 (b) that during weekends, there is a quick rise in the system load due to the increased volume of travel to CC and SM. The total daily average charging demand from 250 EVs and the total demand on the distribution system is shown in Figure 3.13.

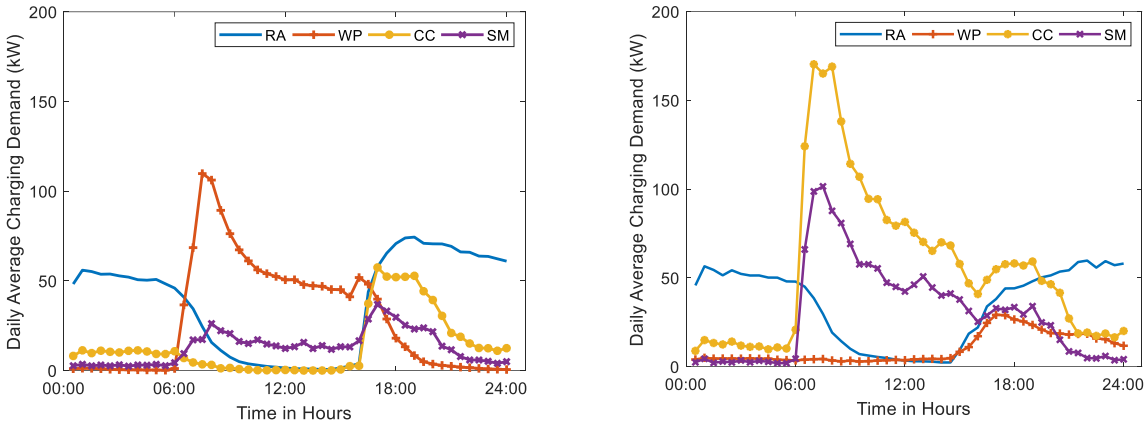

(a) (b)

Figure 3.12. Daily average EV charging demand for various location types for (a) weekday and (b) weekend for 250 EVs

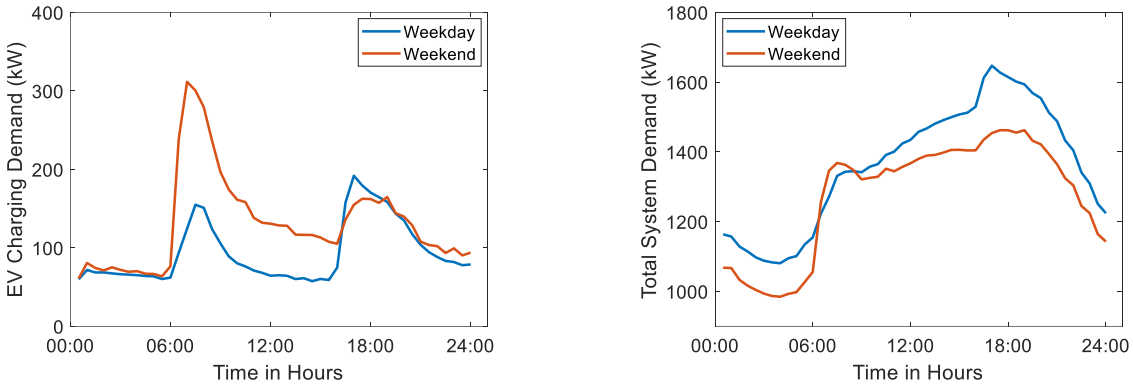

(a) (b)

Figure 3.13. Daily average total EV charging demand (a) and total system load (b) for 250 EVs penetration

To understand the impact of the penetration of EVs on the distribution system performance, the variations of the node voltage magnitudes were examined. Figure 3.14 (a) shows the observed node voltages at the busses farthest from the substation, Buses 18

and 33, for a sample weekday (WD) and a sample weekend day (WE) with 250 EVs. It can be observed that all node voltages are above the lower limit which is considered as 0.9 p.u. A significant difference in the minimum voltage can be seen between weekends and weekdays, which is anticipated due to a higher total system load observed during weekdays. The current flow through the main substation transformer is shown in Figure 3.14 (b) for a sample weekday and sample weekend day.

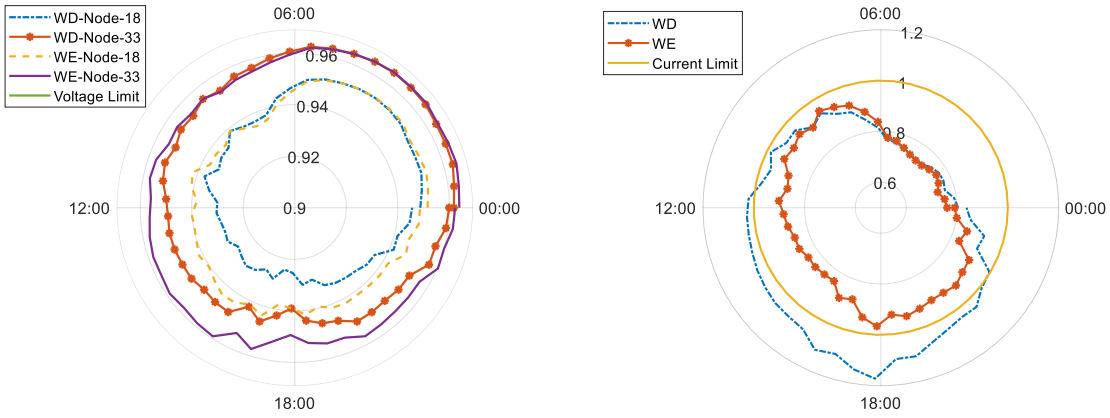

(a) (b)

Figure 3.14. (a) Voltage magnitudes in pu at the farthest Buses (18 and 33), (b) Main transformer current in kA for a sample weekend (WE) day and a sample weekday (WD)

According to Figure 3.14 (b), the transformer current violates the rated current limit during 11:00-21:00 hours for the weekday while no violations can be seen during the weekend. Even though the load curtailment is implemented to avoid the transformer overload and system voltage limit violations, there could be situations where the load shedding could reach its maximum potential, and it may finally result in transformer overloading as seen from Figure 3.14. The results indicate that system upgrades are

necessary to deal with the EV charging load. Although identification of the options for system upgrades is one of the major tasks in power system planning, it is beyond the scope of this work.

3.7.4 Reliability evaluation

Studies are performed to evaluate the impact of EV charging load on electric distribution system reliability including a range of sensitivity analysis. Table 3.8 summarizes the major parameters of the study cases and detailed descriptions are provided in the following.

Base Case: This study case considers 250 EVs with an approximately equal share for all EV models. The inter-zone driving distance values are assumed to be the same as in Table 3.2.

Case-A: To quantify the impact of higher-level EVs penetration, this study case assumes 500 EVs. The share of different EV models and the driving distance values will remain the same as the base case.

Case-B: The EVs with higher battery capacity can ensure a longer driving distance in one quick charging as opposed to the vehicles with lesser battery capacity, which may need more frequent charging from the network. To study the potential implications on the penetration of EVs with higher battery capacity, Case-B considered 90% of BEV 200 penetration which has 48 kWh battery capacity. The number of EVs and the driving distance values will remain the same as the base case.

Table 3.8 Summary of study cases

Study case	Sensitive parameter	Total Number of EVs	Percentage Penetration of Individual EV Model			Driving Distance
			PHEV 40	BEV 100	BEV 200	
Base Case		250	33%	33%	34%	Same values given in d_{inter}^{t}
Case-A	Increase in the EVs penetration	500	33%	33%	34%	Same values are given in d_{inter}^{t}
Case-B	Variation in the battery model	250	5%	5%	90%	Same values given in d_{inter}^{t}
Case-C	Variation in the inter-zone driving distance	500	33%	33%	34%	25% increase from the base case

Case-C: It may happen in reality that due to the increase in the number of EVs, the transportation infrastructure might have to be upgraded to accommodate more vehicles on the road resulting in an increased driving distance for individual EV owners. This could also interpret as representing the effect of increased driving time due to higher traffic congestions. Hence, Case-C considers a scenario of a 50% increase in the inter-zone driving distances as compared to the base case. The number of EVs is increased to 500, and the share of different EV models is the same as that in the base case.

Figure 3.15 illustrates the daily average EV charging profile and total system load for various study cases summarized in Table 3.8. A higher peak charging power demand can

be observed for Case-C and Case-A, which represent an increase in driving distance and higher EV penetration, respectively. These results are expected because the amount of energy consumed by an EV is proportional to its travel distance, and higher penetration of EVs would certainly imply a higher charging power demand.

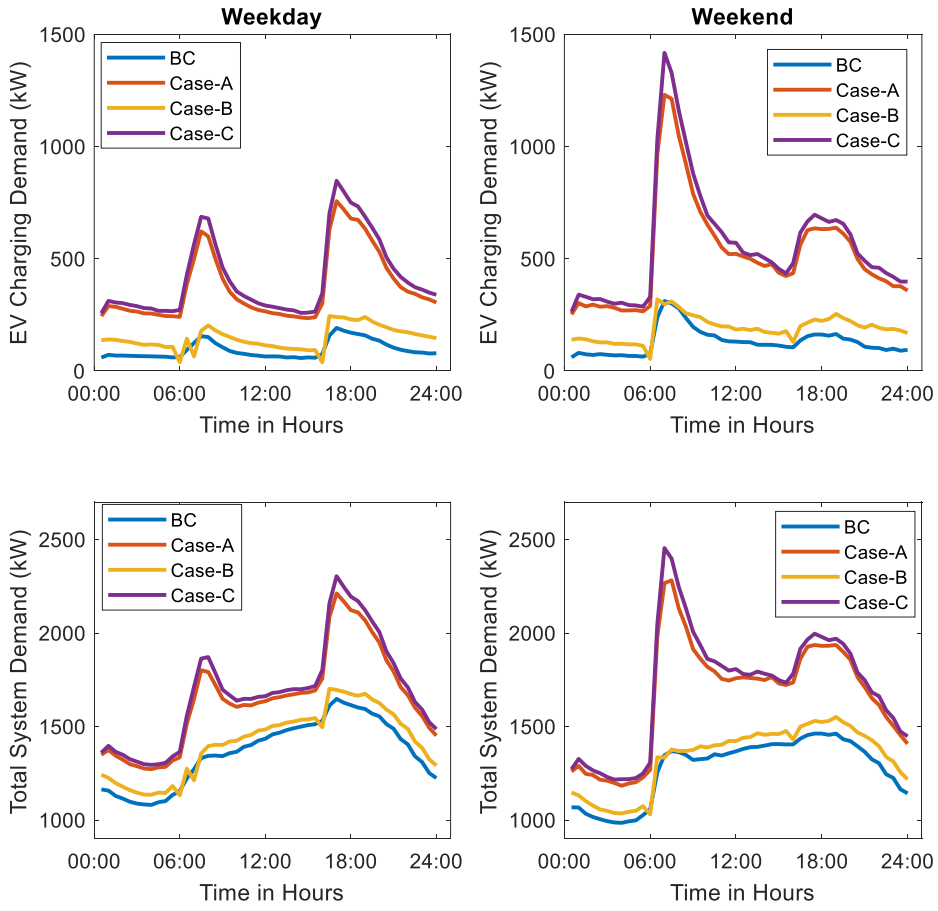

Figure 3.15. Daily average EV charging load and total system load for different cases

On the other hand, a notable reduction in charging load is evident for Case-B, which considers higher penetration of EVs having higher battery capacity. This is due to lesser

charging instances from vehicles like BEV 200, which can commute longer distances without frequent charging from the system. A simplified model is used in this work to calculate the energy consumption and more detailed models that take into account physical parameters of the EV, slopes along the route, driver behavior are available in [92], but for long-term planning, they may be overly complicated. The reliability indices calculated for various study cases are shown in Table 3.9. The following observations can be made:

Case-A: Due to increased penetration of EVs, there is an increase in the EV charging demand, which increased most of the reliability indices as compared with the Base Case indices. The increase in charging demand can be seen from the increase in EECL values from 104.7 KW to 417.9 KW. More than 400% increase was observed for SAIFI, SAIDI, and EENS values.

Table 3.9 Reliability indices values calculated for different cases

	Base Case (BC)	Case A	Case B	Case C
SAIFI (Interps/year/cust.)	0.07	0.35	0.12	0.37
SAIDI (mins/year/cust.)	142.4	710.2	248.5	758.28
EENS (MWh/year/cust.)	183.21	686.1	250.2	750.99
ASAI	1	0.99	1	0.99
EFECI (Charging inst./day/EV)	5.5	5.5	4.5	5.7
EDECI (Charging/mins/day/EV)	231.8	230.8	156.6	246.3
EECL (kW/day)	104.7	417.9	159.3	459

Case-B: The frequency and duration of EVs charging are reduced as compared to those of the Base Case. However, due to EVs with higher battery capacity, the power consumed

from the system by EVs is higher as can be seen from the slightly higher average daily charging demand measured in terms of EECL. The increase in SAIFI, SAIDI, and EENS values is marginal as compared to the Base Case.

Case-C: There is a substantial increase in the charging load due to the increase in the number of EVs along with the travel distance, which consumed more energy to complete the additional driving distances. An increase in the EV charging frequency, duration, and EECL is expected. Among all the study cases, the worst interruption frequency and duration indices were observed for Case-C, resulting in an increase of 400% while compared to the Base Case results.

3.7.5 Changes in EV penetration with time

Further studies are conducted to examine the impact of increased EV penetration over time. It is assumed that the number of EVs is increased by 5% annually over a five-year planning horizon. It is also assumed that 75% of the new EVs penetrating the system are of BEV 100 (50%) and BEV 200 (25%). The rest are PHVs. Therefore, the proportion of different EV types change over the planning horizon. Figure 3.16 depicts the changes in the average daily EV charging load. It can be seen from Figure 3.16 that the average EV charging load increases with increased EV penetration with time.

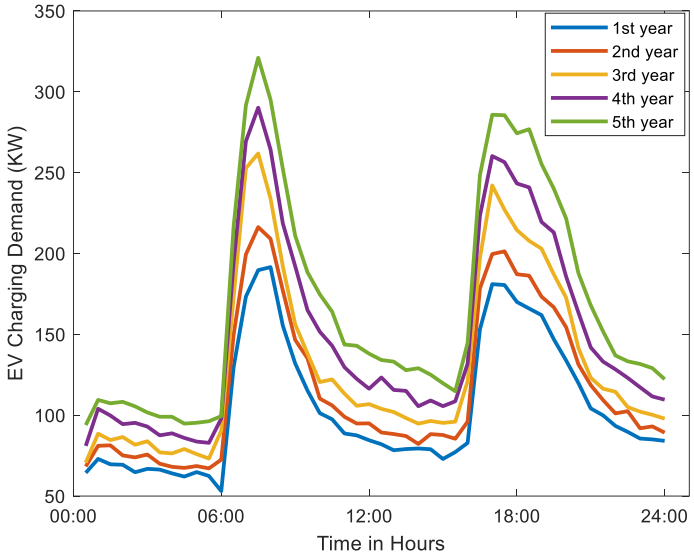

Figure 3.16. Daily average EV charging load for five years with 5% EV growth in each year

Table 3.10 shows the reliability indices calculated for five years assuming a growth rate of 5%. As anticipated, an increase in EECL values over the years corresponds with the increased EV charging load. The SAIFI, SAIDI, and EENS indices are rising over the years indicating the decreasing reliability (or increased frequency and duration of system interruptions) with the growth of EV charging load. One of the advantages of the proposed approach is its flexibility in the application of the model for any number of planning years considering not only the changes in the number of EVs but also the evolution of EV technology.

Table 3.10 Reliability indices values calculated for a five-year planning horizon

Year Number	1	2	3	4	5	Overall
SAIFI (Interps/year/cust.)	0.07	0.08	0.1	0.11	0.13	0.1
SAIDI (mins/year/cust.)	142.4	213.2	270.56	185.12	270.56	216.36
EENS (MWh/year/cust.)	183.21	205.9	233.87	267.45	305.45	239.17
ASAI	0.998	0.998	0.998	0.997	0.997	0.998
EFECI (Charging inst./day/EV)	4.96	5.07	5.33	5.25	5.24	5.17
EDECI (Charging/mins/day/EV)	207.13	214.41	229.64	229.43	227.7	221.66
EECL (kW/day)	104.46	116.7	131.14	149.14	167.41	133.77

3.8 Concluding remarks

In this chapter, a probabilistic reliability assessment method was developed to evaluate the impact of EVs on distribution system reliability performance. The method employees a two-layer stochastic EV charging demand estimation model to represent the traffic and the electrical network. A dynamic HMM was used to model the movements of EVs, considering their spatial-temporal aspects. The proposed method and models were used to analyze the reliability of an example system using a sequential MCS approach, and several useful reliability indices were calculated from the MCS process.

The proposed approach is validated for the traffic layer using real-world travel data and found that the model can mimic a travel pattern that is similar to a real-life scenario. In

correspondence to the parked locations, the EV charging demand for various location types is quantified in the electrical network layer. The EV charging decisions were simulated, considering the charge levels and preferred charging locations.

A series of reliability studies were performed to assess the reliability impacts of EVs on the electric distribution system considering variations in the EVs penetration, the battery model, and the inter-zone driving distance. Simulation results show that system reliability decrease with an increase in EV penetration and/or driving distances. An increase in the EVs with higher battery capacity also has a negative impact on the reliability performance of distribution systems. Studies are also performed to evaluate the impact of EV penetration over a particular planning horizon to demonstrate the applicability of the proposed approach in long-term planning.

Chapter 4

Distribution System Reliability Evaluation Considering Electric Vehicles and Distributed Energy Resources

4.1 Introduction

Chapter 3 presented a probabilistic reliability assessment method for evaluating the impact of EVs on distribution system reliability performance. The presence of PV and wind power generation introduces uncertainties and variabilities [95] in power systems. From a power system point of view, an EV can be considered as a randomly moving load [30], while PV and wind energy resources are stationary generations with random output depending on the availability of site resources [96], [97]. These characteristics make conventional deterministic methods unsuitable for the assessment of the reliability of distribution systems containing RESs and EVs. Hence, a great deal of effort has been

devoted to developing probabilistic approaches that appropriately model the stochastics nature of systems containing RESs, ESSs and EVs.

In this chapter, an appropriate methodology for performing a reliability-oriented distribution system analysis is proposed for capturing the complex interactions between EVs and PV power production. Stochastic models developed in Chapter 2 and Chapter 3 have been used to emulate the PV power generation and uncertain nature of EV charging loads respectively. MCS is used to analyze a range of scenarios for illustrating the applicability of the proposed method. Various computational models such as the EV charging station model, reliability evaluation model, and economic evaluation model are proposed to support the reliability and economic evaluation with necessary inputs. A sensitivity analysis is performed to illustrate the reliability and economic impact due to EV charging, PV power production and various operating strategies. An optimization algorithm is also used to choose the optimal resource sizes by minimizing charging station-related cost and cost of unreliability.

4.2 Background and literature review

As noted in Chapter 3 most of the models for the reliability assessment of power systems containing EVs [98]–[105] are proposed for studies focusing on the utilization of traditional grid power as the main source of power to meet the EV charging demand. Use of RESs and battery storage to augment the traditional grid supply in meeting the EV charging demand can be both economic and sustainable. Such decarbonization deserves serious attention as the contribution of EVs to emission reduction is more meaningful when

charging energy is from RESs, and the inherent storage in EVs can enable accommodating high renewable fraction into power grids. Feasibility and optimal designs that minimize the lifecycle cost of EV charging stations (EVCS) powered by PV, wind and diesel generation, battery energy storage, and electrical grid have been studied in [95], [106]-[107]. However, the representation of stochastic power production from solar and wind energy systems was limited to techniques such as monthly average values [106], fixed solar radiation and wind speed profiles [95], and normalized values [107]. Although these approaches are widely adapted in long-term planning, stochastic models that can account for the intermittencies associated with the RESs such as random cloud cover and variation in the wind speed [96], [97] are more desirable for probabilistic planning. Probabilistic planning approaches analyze a range of scenarios and result in more optimal outcomes compared to the designs based on the worst-case scenarios. There are long-term stochastic models suitable to generate synthetic solar radiation and wind speed profiles that can preserve the original characteristics of measured data [63].

Multi-objective optimization using MCS to determine the optimal size of the EVCS with RESs and ESSs considering various economic, environmental, and battery life aspects have been reported in the literature [33], [108]–[111]. In [33], a fast-charging station with RESs and ESSs is designed using MCS to estimate the EV charging demand and RESs. Optimal sizing of a green charging system that relies entirely on the RESs is discussed in [112] using a Markov model to capture the random solar power generation, and a queuing model to estimate the charging demand of EVs. A MCS procedure is proposed in [110] to

assess the influence of different PHEV usage conditions on EVCS sizing and operation in minimizing the total cost of EVCS considering the installation and operational constraints.

An EVCS can be fully grid-dependent, partially grid-dependent (grid connected-renewable based), or fully autonomous [111]. From a power system point of view, a fully or partially grid-dependent EVCS effectively appears as an additional intermittent load to the electrical system, and directly impacts the power supply reliability. But most of the planning and design studies that consider the combined evaluation of EV demand, RESs, and ESSs [25-35] haven't explicitly addressed the distribution system reliability in the design objectives. The focus of such studies includes a wide range of objectives such as maximizing the profits [114], [115] reducing the energy costs [116], [117], minimizing the power losses [29-30], minimizing the generation costs [120][121], reducing the peak loads [122], decongestion of the distribution network [123], and regulating the frequency [113], but not explicitly include the reliability aspects. This chapter tries to address the gap and examines the impact of fully and partially gird-dependent EVCS on the reliability of power distribution systems using appropriate stochastic models and MCS.

The modeling of a distribution system with EVCS equipped with PV systems and battery energy storage, referred to as distributed energy systems (DERs) is described and reliability evaluations have been performed using three different approaches. Firstly, an analysis is designed by varying the installed PV/ESSs capacity in different levels and their impact on the distribution system reliability is analyzed. Secondly, various predetermined operating strategies have been used to further examine their impacts on the distribution system reliability. Finally, a method using an optimization algorithm is presented to

optimally choose the resource sizes of EVCS equipped with DERs while minimizing the total cost.

The proposed planning framework involves many building blocks and is a natural progression of the work described in the previous chapters including i) the estimation of PV power production using the synthetic solar radiation generation model developed in Chapter 2 and ii) the estimation of the additional charging demand using two-layer stochastic EV model developed in Chapter 3. This chapter integrates these models and proposes a new comprehensive methodology for performing distribution system reliability evaluations considering the complex interactions among EVs, PV systems, and battery storage. A few new reliability indices are also proposed to quantify the perceived benefits of including DERs for EV charging.

4.3 Proposed framework

The overall framework consists of three major parts: (i) DERs based EV charging station model, (ii) reliability analysis model, and (iii) economic evaluation model. The DER-based EV charging station model is the most complex component and incorporates the sub-model of ESS and EVCS operating strategy. Details of the mathematical models and the simulation procedures are provided in the following subsections. A detailed description of the input data is given in Section 4.7.

It is assumed that the energy demand for an EV charging station can be supplied either by the main grid, a PV module, a battery, or any combination of the above sources. The operation of such a system needs to be carefully managed to maximize the use of renewable

power, and therefore pre-defined operating strategies can be used to ensure a coordinated operation of the available energy resources and energy storage. In actual operation, an EVCS energy management system may achieve this through a suitable optimization process, but in a long-term perspective, simplified representation such as a pre-defined operating strategy is adequate. The grid source is represented as a 100% reliable source in this study, as the motivation is to capture the effects of EV load and RESs, however, it is possible to represent the grid source with applicable outage characteristics if needed.

Due to the presence of multiple energy resources in a charging station, it is important to prioritize and optimally utilize the resources based on their availability. The following rule-based approach is proposed to represent the operating strategies for energy management and the coordinated operation of the available resources to meet the varying EV charging demand at each charging station. In reality, a power controller is needed to enforce these pre-defined energy management strategies while ensuring the physical constraints of various components are not violated.

- In a given simulation time-step Δt, the energy generated from the PV panels is primarily used for EV charging.
- When the available power from the PV panels P^{pv} is greater than the power demand P^{ev} to charge the EVs ($\Delta P^t > 0$), the excess energy is stored in the battery as described in (4.1)-(4.3), subject to the constraint that the total stored energy in the battery does not exceed the allowable maximum limit given in (4.5). The charging and discharging efficiencies (η_{ch} and η_{dch}) are taken into account and (4.2) enables establishing the battery SOC at the end of the time step. In (4.2), E^{bs} indicates the

energy stored in the battery storage, δ indicates the charge/discharge state of battery storage, and SOC_{max} shows the maximum allowed battery storage utilization.

- If the available energy from the PV panels is insufficient to meet the charging demand, the balance of power is drawn from the battery as described by (4.2) and (4.3), subject to the condition that the battery is not discharged below the allowable minimum battery limit given in (4.7) where SOC_{min} indicates the minimum allowed battery storage utilization.
- Any excess energy available from the PV system after recharging the batteries is exported to the grid is represented in (4.4) where E^{bs-r} represents the installed storage capacity and E^{pv2g} indicates total excess energy supplied to the utility grid.
- If the available PV energy and the energy stored in the battery is insufficient to meet the charging demand, the grid power will be used, as described by (4.6) where E^{g2cs} indicates the energy imported from the grid to the charging station.

$$\Delta P^t = P^{pv,t} - P^{ev,t} \tag{4.1}$$

$$E^{bs,t} = E^{bs,t-1} + \Delta P^t . \Delta t \left[(\delta(\Delta P^t) . \eta_{ch} + (1 - \delta(\Delta P^t)) . \frac{1}{\eta_{dch}}) \right] \tag{4.2}$$

$$\delta(\Delta P^t) = \begin{cases} 1 \ if \ \Delta P^t \geq 0 \\ 0 \ if \ \Delta P^t < 0 \end{cases} \tag{4.3}$$

$if \ E^{bs,t} \geq E^{bs-r} . SOC_{max}$

$$E^{pv2g,t} = (E^{bs-r} . SOC_{max}) - E^{bs,t} \tag{4.4}$$

$$E^{bs,t} = E^{bs-r} . SOC_{max} \tag{4.5}$$

$if \ E^{bs,t} < E^{bs-r} . SOC_{min}$

$$E^{g2cs,t} = E^{bs,t} - (E^{bs-r} . SOC_{min}) \quad 4.6$$

$$E^{bs,t} = E^{bs-r} . SOC_{min} \quad 4.7$$

4.4 Reliability analysis model

The total system demand, which includes the EV charging demand, can be calculated using the EV model developed in Chapter 3. The power demand due to non-EV loads (the baseload) is calculated by modeling the demand level factors as per [86]. Once the total system demand is determined, a power flow analysis is performed to evaluate the consequence of each possible state. If overload situations or voltage violations are found during the power flow analysis, an appropriate amount of load is shed to eliminate the issue by using a simple priority-based load shedding algorithm. It is assumed that the power utilities can agree with the consumer for curtailing the loads whenever necessary and the customers will be compensated with a fair incentive. The impact on system reliability due to EV charging and hybrid energy resources-based charging stations are quantified based on two sets of reliability indices. They are system-based reliability indices and EV-based reliability indices.

Four standard reliability indices as described in Equations (3.14)-(3.17) are used to evaluate the reliability performance of the power distribution system. Two new reliability indices are proposed to capture the reliability of supply for EV charging, as this is different from the system level supply reliability due to energy storage. These indices can be used to assess the impact of hybrid energy resources for EV charging. Expected Electric

Vehicles Grid Dependency (EEVGD) is proposed to measure the reliance of EVCS on the utility grid to satisfy the charging load.

$$EEVGD = \frac{\sum_{j=1}^{N_s}\left[\sum_{t=1}^{N_t} P^{grid,t} * \Delta t\right]}{N_s * N_{ev}} \quad 4.8$$

Expected Unserved Electric Vehicle Load (EUEVL) is proposed to measure customer satisfaction as a ratio of the actual energy supplied to an EV customer to the amount of energy requested by the EV customer (original EV load before the load shedding).

$$EUEVL = \frac{\sum_{j=1}^{N_s}\left[\sum_{t=1}^{N_t}\left(\overline{P^{ev,t}} - P^{ev,t}\right) * \Delta t\right]}{N_s * N_{ev}} \quad 4.9$$

where,

N_s	total number of MCS replications
N_t	total number of time steps
N_{ev}	number of EVs
P^{grid}	power provided from the utility grid (kW)
$\overline{P^{ev}}$	original EV charging demand (kW) associated with load curtailment
P^{ev}	estimated EV charging demand (kW)

4.5 Economic evaluation model

The costs associated with the installation and operation of charging stations with hybrid energy resources mainly involve a fixed capital cost to upgrade or build the charging facility and a variable service cost and maintenance cost related to operating the charging stations. Also, this work considers emission cost which accounts for the amount of carbon emitted by the non-renewable sources to meet the total system demand. Finally, the cost of

unreliability is also considered which is defined as a customer interruption cost resulting from loss of service to the customers due to system issues.

4.5.1 Charging station related cost

The capital cost C_{cap}^{t} is related to the installation of solar panels, battery storage, and a number of chargers in each charging station, and it can be calculated using (4.10).

$$C_{cap}^{t} = \sum_{b=1}^{B} C^{ch}.N^{ch,b}.P^{ch-rt} + C^{pv}.N^{pv,b} + C^{bs}.N^{bs,b} \tag{4.10}$$

where,

C^{ch}	cost of the charger ($/charger)
C^{pv}	cost of PV module ($/unit)
C^{bs}	cost of battery storage ($/unit)
N^{ch}	number of chargers
N^{pv}	number of PV modules
N^{bs}	number of battery storage units
P^{ch-rt}	rated charging power of the charging station (kW)
b	index for bus number equipped with DERs

The service cost $C_{service}$ is calculated as a difference between the cost of purchasing energy from the utility grid and the revenue received by exporting excess energy to the grid and serving the EV users for charging the vehicles.

$$C_{service}^{y} = \sum_{b=1}^{B} E^{g2cs}.C^{g2cs} - (E^{pv2g,y,b}.C^{pv2g} + E^{ev,y,b}.C^{cs2ev}) \tag{4.11}$$

where,

C^{g2cs} the purchase cost of energy from the utility grid ($/kWh)

C^{pv2g} the selling price for feeding power to the grid ($/kWh)

C^{cs2ev} cost of EV charging ($/kWh)

E^{pv2g} total energy supplied to the utility grid (kWh)

y index for planning years

The maintenance cost C^{y}_{maint} comprises the costs of maintaining EV chargers and solar array, which is considered as a fixed annual amount proportional to the installed capacity. The costs due to maintenance and degradation of batteries can be calculated using 4.12. The battery maintenance cost is calculated considering a fixed annual maintenance cost and a cost component proportional to the annual battery utilization. The annual battery utilization is considered as the ratio of annual energy derived by battery ($E^{dch,b,y}$) to the total energy that can be delivered through its rated cycle life ($E^{bs,cycles}$) [33]. x_{ch} and x_{pv} represents the fraction of capital cost accounted for annual maintenance cost of chargers and PV modules.

$$C^{y}_{maint} = x_{ch}.C^{ch,b}_{cap} + x_{pv}.C^{pv,b}_{cap} + \left[C^{m-bs,y} + \sum_{b=1}^{B}\left(\frac{E^{dch,b,y}}{E^{bs,cycles}}.C^{bs}.E^{bs-r,b}\right)\right] \quad 4.12$$

where,

x_{ch} the maintenance cost factor of the charger

x_{pv} the maintenance cost factor of PV array

C^{m-bs} the annual fixed maintenance cost of the battery storage system ($/year).

$E^{dch,b,y}$ total energy supplied by the storage system annually (kWh)

$E^{bs,cycles}$ total annual battery utilization expressed in kWh

E^{bs-r} installed storage capacity (kWh)

The emission cost is calculated based on the amount of carbon emissions that occurred by utilizing non-renewable energy resources to meet the total system demand as can be calculated using (4.13).

$$C^{y}_{emission} = E^{grid,y}.x_{nr}\ .y_{co2}\ .C^{ec} \qquad 4.13$$

where,

x_{nr} emission cost factor

y_{co2} carbon emission equivalent factor for non-renewable energy resources (tCo2e/MWh)

E^{grid} total energy consumed from the grid (kWh)

C^{ec} cost of carbon emissions ($/tCO2e)

4.5.2 Cost of unreliability

The cost of unreliability $C^{t,y}_{unrel}$ essentially represents the direct losses and the value of inconvenience caused to the customers due to the curtailment of their loads. This cost can be evaluated from the amount of unserved customer energy and the value of customer interruption cost $C^{EENS,l}$, which varies based on the location type l [124]. This cost value is calculated separately for EV loads and non-EVs using (4.14).

$$C_{unrel}^{y} = \sum_{l=1}^{L} EENS^{ev,l,y} * C^{EENS,l,y} + \sum_{l=1}^{L} EENS^{bl,l,y} * C^{EENS,l,y} \quad 4.14$$

4.5.3 Total cost

Thus, the total cost C_T after incorporating all the cost elements described above can be evaluated using (4.15). The net present value is calculated after including the total fixed cost, the total variable cost, and the cost of unreliability after considering a discount rate of i^d for Y planning years.

$$C_T = C_{cap}^{t} + \sum_{y=1}^{Y} \frac{\left(C_{service}^{y} + C_{maint}^{y} + C_{unrel}^{y} + C_{emission}^{y}\right)}{(1+i^d)^y} \quad 4.15$$

4.6 Overall procedure

The procedural flowchart for the reliability and economic assessment of power distribution systems containing EV charging stations with DERs is illustrated in Figure 4.1 and the step-by-step process is described as follows:

- **Step-1:** Prepare input data required for various models including the charging station model, reliability analysis model, and economic evaluation model.

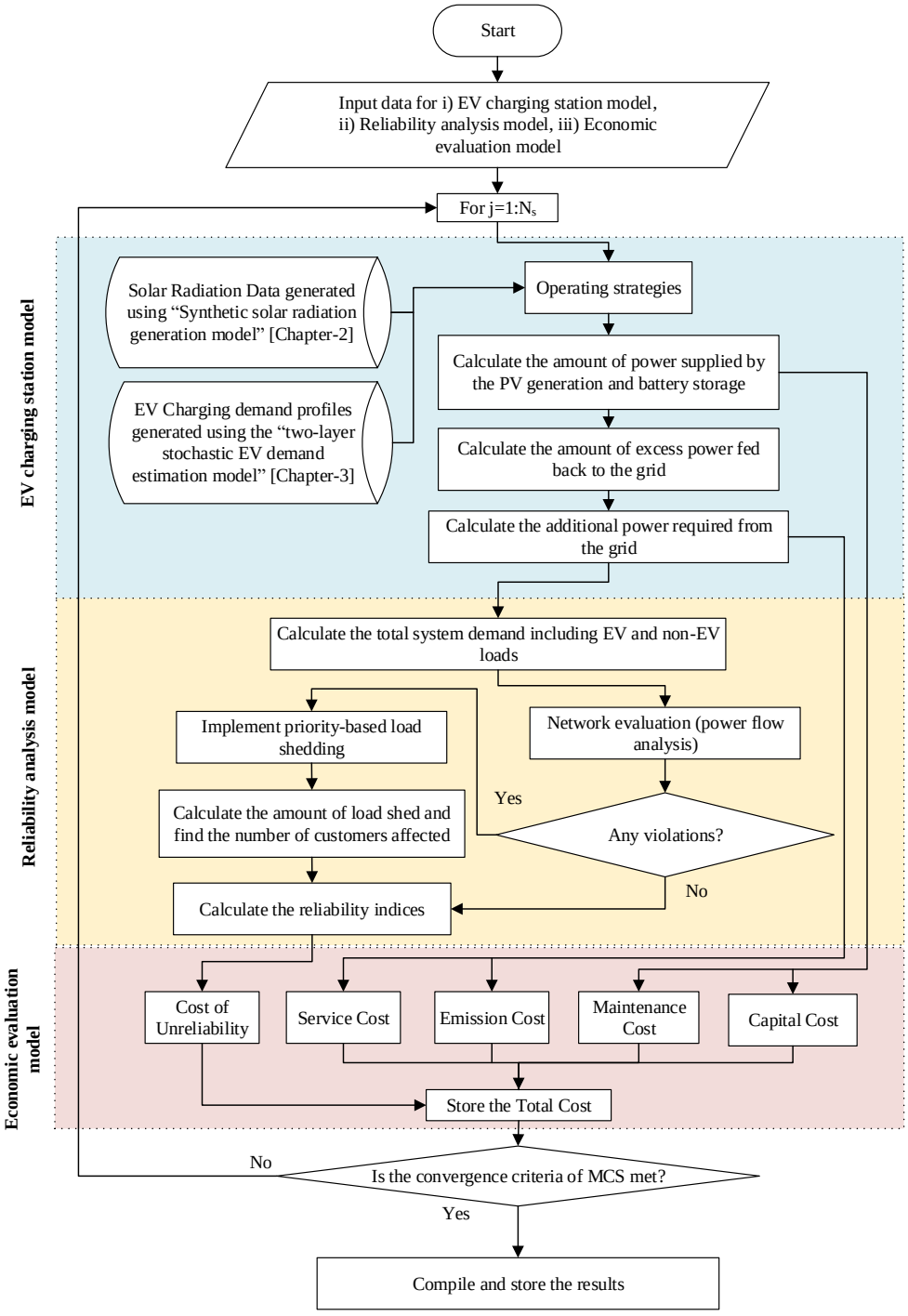

Figure 4.1. Procedural flowchart illustrating the overall framework

- **Step-2:** Simulate the operation of EVCSs with DERs using solar and EV models developed in Chapter 2 and Chapter 3 respectively for a specified duration. The simulation produces i) the amount of power supplied by the PV P^{pv2ev} or battery P^{bs2ev} to charge the EVs, ii) if applicable, the excess power that was fed back to the utility grid P^{pv2g}, and iii) the amount of power required from the grid to charge the EVs P^{g2cs} at each time step if applicable.
- **Step-3:** Compute the total system demand by adding the EV charging load computed in the previous time step to the non-EV loads and run a power flow. If any bus voltage limit violations or substation transformer overloading are noticed, priority-based load shedding is activated to remedy the situation. Record and accumulate all data needed for reliability and cost analysis.
- **Step-4:** At the end of each simulation run, calculate all annual cost components and reliability indices using the models described in Sections 4.4 and 4.5. Calculate the present worth of total cost at the specified discount rate.
- **Step-5:** Repeat simulations until the convergence of the MCS process. When the standard deviation of the total energy supplied to the loads becomes less than a threshold, MCS is considered converged.

4.7 Study system description and data inputs

The same modified IEEE 33 bus system described in Chapter 3 has been used to illustrate the applicability of the models and methodology presented in this chapter. The

area supplied by the electrical network was divided into six different geographical zones, and the load buses were classified into five different location types such as RA, WP, SM, CC and RL. These locations constitute 30 EV parking locations with charging facilities, some of which are equipped with DERs as marked in Figure 4.2. The EV charging power level and the range of charging power levels that can be accommodated at a given location type are shown in Table 4.1 and Table 4.2 respectively. The details of the electrical network can be found in [55], [85].

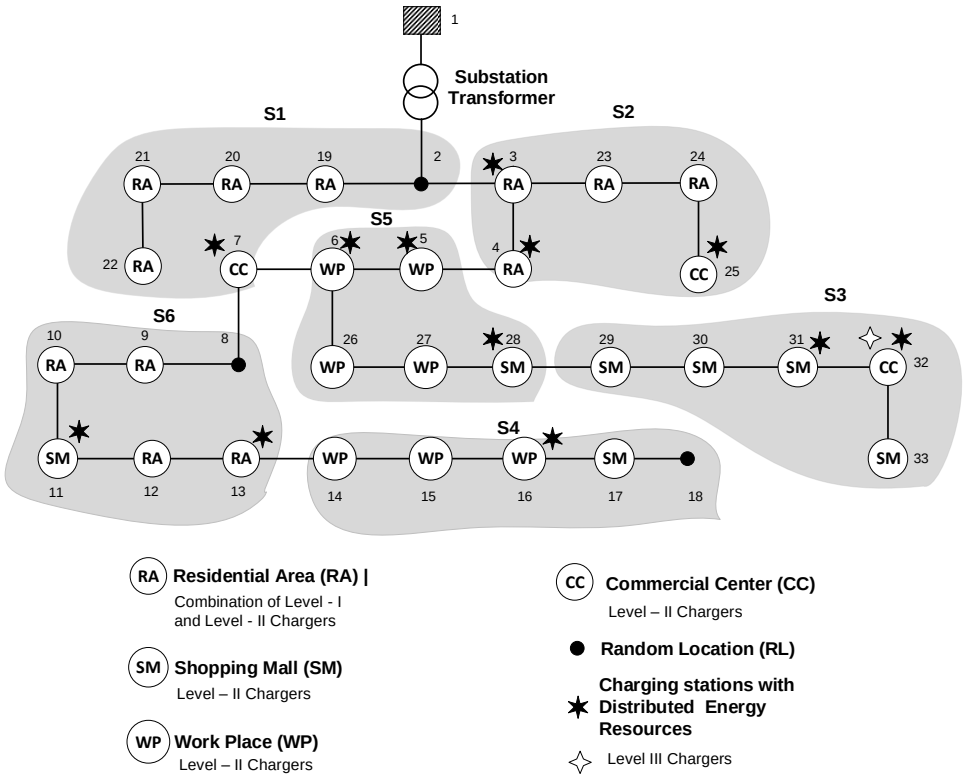

Figure 4.2. Electrical distribution system (modified IEEE 33 bus system) with geographical zones and EVCS locations

Table 4.1 EV charging power levels

Charging Type	**Charging Power Range (kW)**
Level-I Chargers	1.2-2
Level-II Chargers (Low)	2.8-8.8
Level-II Chargers (High)	8.8-19.2
Level-III Chargers	15-46*

*The maximum value for a Level-II charger is 96 kW [125]. However, 46 kW is chosen based on the maximum rated charging power of the EV model(s)

Table 4.2 Range of charging power levels acceptable at different location types

Location Type	**Possible Charging Power Levels**	**Locations (Bus Numbers)**
RA	Level-I/Level-II (Low)	3*, 4*, 9, 10, 12, 13*, 23, 24, 19, 20, 21, 22
WP	Level-II (High)/ Level-II (Low)/Level-III	5*, 6*, 14, 15, 16*, 26, 27
SM	Level-II (High)/Level-III	11*, 17, 28*, 29, 30, 31*, 33
CC	Level-II (High)/Level-III	7*, 25*, 32*

*Charging stations equipped with DERs

The restoration time r^t was considered as 30 minutes, and the capacity limits and the priority-based load shedding scheme used in [13] was adopted. The acceptable voltage limit was considered as ±10%. The input values of economic evaluation model are given in Table 4.3 [33], [124], [126]. A 10-year planning horizon ($Y = 10$) was considered in this work for the illustration of the proposed approach. The installation of the charging station is assumed in the 0^{th} year, and the charging station is assumed to be fully operational from the 1^{st} year.

Table 4.3 Input values of the economic evaluation model

Parameter	Value	Parameter	Value
C^{pv}	\$116/module	$C^{EENS,RA}$	\$0.8/kWh
C^{bs}	\$140/unit	$C^{EENS,WP}$	\$1.4/kWh
C^{ch}	\$740/unit	$C^{EENS,SM}$	\$2/kWh
C^{m}	\$1482	$C^{EENS,CC}$	\$2.4/kWh
C^{pv2g}	\$0.13/kWh	C^{ec}	\$50/tCO2e
C^{g2cs}	\$0.25/kWh	x_{ch}	5%
C^{cs2ev}	\$0.18/kWh	x_{pv}	10%
y_{co2}	0.499 tCO2e/MWh	x_{nr}	60%
Y	10	i^{d}	2.69%

The value of C^{pv2g} was assumed to be higher than C^{g2cs} to encourage renewable penetration on the network. The total energy consumed by the system was taken as the parameter to monitor the convergence of MCS. The simulation is considered to be converged if the standard deviation of annual total energy consumption is lower than 0.001 kW after completing a minimum number of 100 MCS trials.

4.8 Results and discussions

This section provides the simulation results obtained using the proposed approach presented in Section 4.6 and the data inputs described in Section 4.7. The first part of the results is devoted to verifying the simulation models and the latter part is devoted to highlighting the merits of the proposed planning approach.

4.8.1 Model validation

For the model validation, the size of the PV and battery was selected to some reasonable values (P^{pv-r}=72 kW, E^{bs-r}=40 kWh) for illustration purpose. These values will be optimized later. Figure 4.3 and Figure 4.4 illustrate the coordinated operation of the energy resources in a charging station equipped with DERs under the defined operating strategy during a randomly selected sunny day and a randomly selected cloudy day for a WP electrical bus. The WP bus has most of its EV charging demand in the daytime hours (07:00-18:00) and this trend closely aligns with the sunshine hours as evident from Figure 4.3. Hence, during a day with higher sunshine, most of its electrical load can be met through PV power production and the excess power can be stored in the battery (P^{pv2bs}) if required and the remaining power can be sent back to the grid (P^{pv2g}). The power that can be fed to the grid at a given bus is limited by the transformer capacity and hence P^{pv2g} remains at this maximum value when the PV power production is higher than the sum of the charging demand and the extra capacity sent back to the grid. It is also advantageous for the charging station to keep the battery SOC at maximum value when excess PV power is available as it could be used later to meet the charging demand when PV power is unavailable. This can, in turn, reduces grid dependency. The PV power production can be severely affected during a cloudy day as shown in Figure 4.4. Due to the lack of excess PV power, the battery SOC remains low towards the end of the day. Figure 4.4 also shows how the fluctuating PV power generation impacts the grid dependency to meet the EV charging demand.

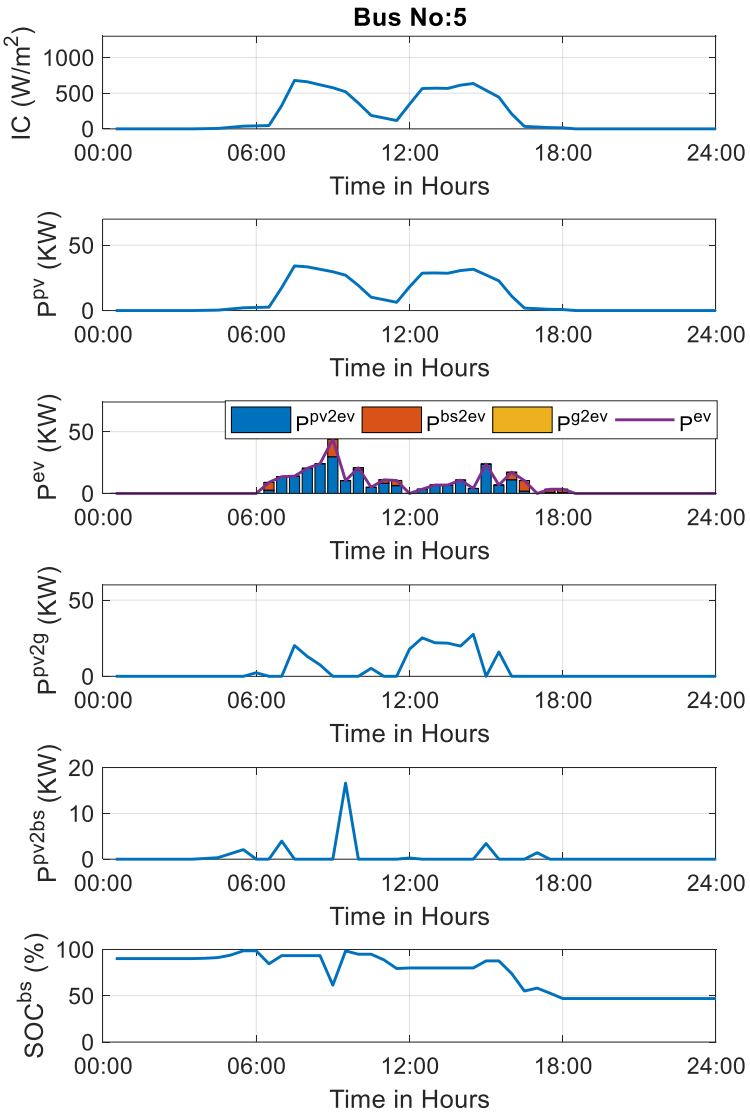

Figure 4.3. Coordinated operation of energy resources at the charging station Bus #5 during a sunny day

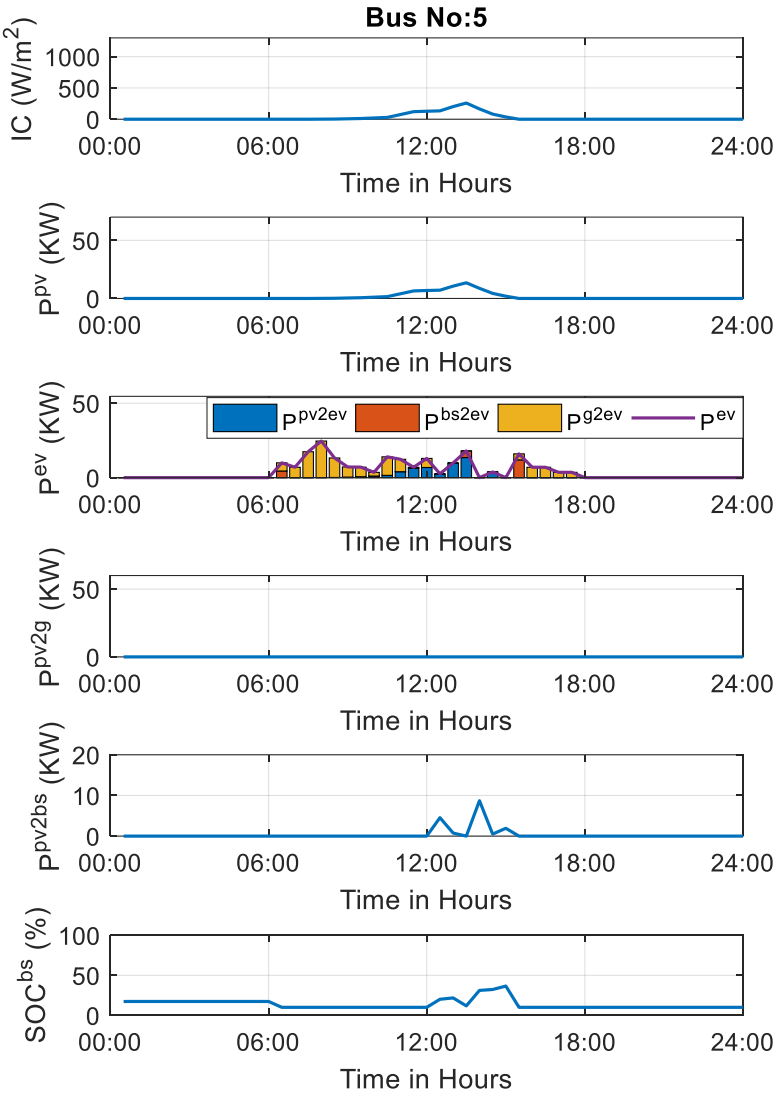

Figure 4.4. Coordinated operation of energy resources at the charging station Bus #5 during a cloudy day

Figure 4.5 shows the EV charging demand curve of various location types and the utilization of available energy resources to meet the changing needs of EVs for a randomly selected weekday and a weekend day. The distinctive charging curves for different location types can be recognized in Figure 4.5. RA location has most of its demand in the early

morning or late evening hours, and more or less remain the same for both weekdays and weekends. Hence, RA has met most of the EV charging demand through the battery and grid. WP mostly uses PV power, as the production aligns well with the daytime EV charging demand during the weekdays. During the weekend, SM and CC have their EV load surged compared to weekdays. While comparing with SM, CC has a much higher EV charging demand due to the presence of a fast-charging station at Bus #32. Overall, the support of the PV-battery combination can be used to reduce the reliance on the grid power for EV charging.

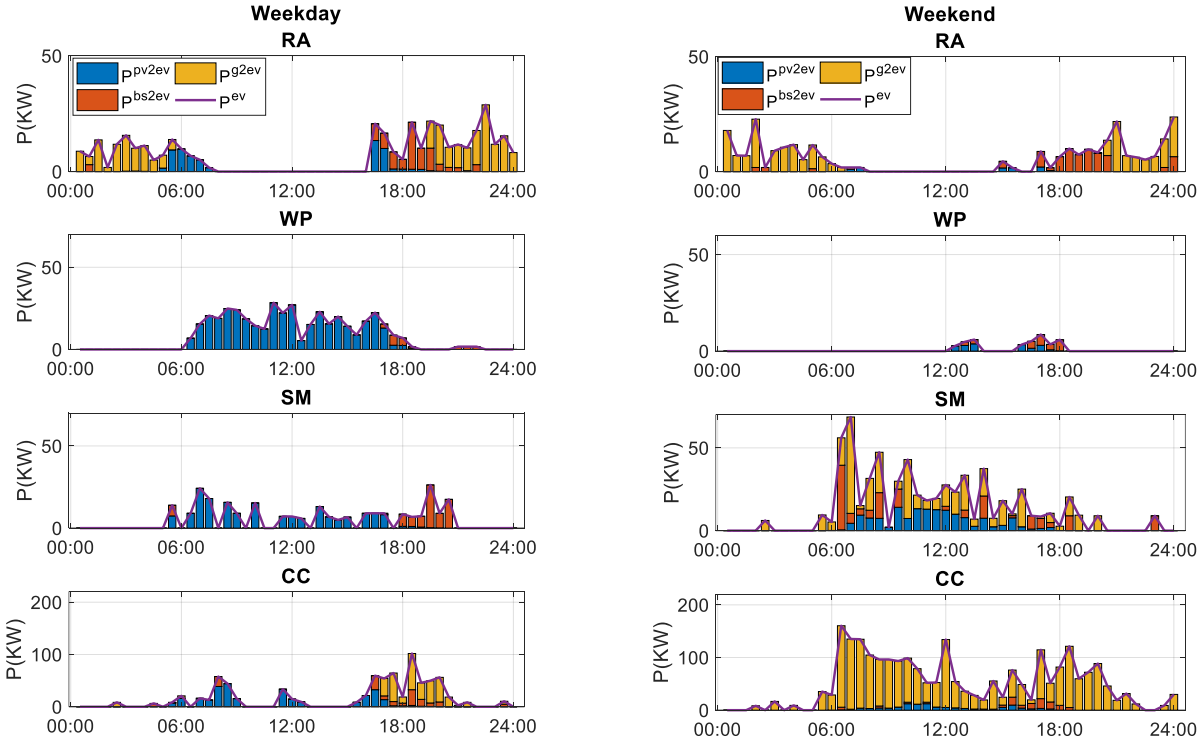

(a) (b)

Figure 4.5. Utilization of energy resources to meet the charging demand of various location types for a selected (a) weekday and (b) weekend

4.8.2 Reliability evaluation

The reliability of the distribution system is evaluated considering different combinations of the installed PV capacity (P^{pv-r}) and the installed battery storage capacity (E^{bs-r}). This analysis anticipates revealing the changes in the system reliability and the corresponding total cost of the distribution system under various levels of PV-battery penetration. The analysis considers three size variations for both resources: termed as low, medium, and high for installed PV capacity and termed as no storage, medium, and high for installed battery storage capacity. The medium installed capacities of PV represent an 80% increase of the low capacity whereas high capacity represents a 130% increase of the low capacity. The high battery storage capacities represent a 130% increase over respective low capacities. The same PV and battery storage capacities are assumed for all locations of a given location type. These size variations can be put in place using 3 × 3 matrices accommodating all 9 possible combinations as shown in Table 4.4. These configurations are compared with a base case where all the EV charging demand, as well as baseload, is satisfied with the grid power alone.

Table 4.4 PV and battery storage capacity combinations

		No Storage				**Low**				**High**			
		RA	WP	SM	CC	RA	WP	SM	CC	RA	WP	SM	CC
Low	P^{pv-r} (kW)	30	40	50	60	30	40	50	60	30	40	50	60
	E^{bs-r} (kWh)	0	0	0	0	30	40	50	60	69	92	115	138
Med	P^{pv-r} (kW)	54	72	90	108	54	72	90	108	54	72	90	108
	E^{bs-r} (kWh)	0	0	0	0	30	40	50	60	69	92	115	138
High	P^{pv-r} (kW)	69	92	115	138	69	92	115	138	69	92	115	138
	E^{bs-r} (kWh)	0	0	0	0	30	40	50	60	69	92	115	138

Table 4.5 and Table 4.6 show the reliability indices calculated for the base case and the

cases presented in Table 4.4. As expected, lower reliability can be observed for the base case due to a stressed distribution system resulted from the additional EV charging demand with no PV or battery storage available.

Table 4.5 Reliability indices calculated for the base case

	SAIFI (Interps/year/cust)	SAIDI (mins/year/cust)	EENS (Mwh/year/cust)	EEVGD (kWh/year/EV)	EUEVL (kWh/year/EV)
BC	0.080	144.57	210.61	6433.1	18.60

Table 4.6 Reliability indices calculated for the cases shown in Table 4.4

	$P^{pv\text{-}r}/E^{bs\text{-}r}$	No Storage	Low	High
SAIFI (Interps/year/cust)	Low	0.073	0.072	0.071
	Med	0.070	0.070	0.069
	High	0.070	0.069	0.068
SAIDI (mins/year/cust)	Low	130.57	129.76	128.51
	Med	126.48	125.14	124.10
	High	125.17	123.73	122.21
EENS (MWh/year/cust)	Low	156.1	151.8	146.7
	Med	140.5	133.9	129.4
	High	135.6	128.5	121.8
EEVGD (kWh/year/EV)	Low	5670.3	5272.6	4899.0
	Med	5456.7	5040.3	4670.8
	High	5333.9	4934.4	4547.8
EUEVL (kWh/year/EV)	Low	18.02	12.883	15.210
	Med	18.0	15.140	12.054
	High	17.900	16.392	12.461

Compared to the base case, a significant reduction in the frequency and duration of the interruptions (as indicated by SAIFI and SAIDI), as well as a reduction in EV grid dependency and unserved EV load (as indicated by EEVGD and EUEVL), can be seen even with low PV capacity with no energy storage (Ppv-r = low)/Ebs-r = no storage). This indicates the advantage of introducing PV power generation into the system. The reliability values further improved after deploying the battery storage along with the PV power generation, for example in the case of Ppv-r = low/Ebs-r = high. However, a significant improvement in the SAIFI/SAIDI values cannot be obtained for certain combinations such as Ppv-r = low/Ebs-r = low, and Ppv-r = low/Ebs-r = high. This advocates the ineffectiveness of having larger battery storage and smaller PV installed capacity if the battery storage is only charged from the excess PV power. Due to the excess PV power fed back from the EVCSs, the amount of annual unserved energy (EENS) has significantly reduced compared to the base case and this is evident from Ppv-r = low/Ebs-r = no storage case. The EENS values further reduced after introducing high capacity PV and battery storage, for example, the case of Ppv-r = high/Ebs-r = high. Additionally, EV-related reliability indices improved after introducing the PV and battery storage. The highest EEVGD and EUEVL values of 6433.1 kWh/year/EV and 18.6 kWh/year/EV are observed for the base case. These values have reduced to 5040.3.4 kWh/year/EV and 15.14 kWh/year/EV for the case of Ppv-r = med/ Ebs-r = low and the same values further reduced to 4547.8 kWh/year/EV and 12.46 kWh/year/EV respectively for the case of Ppv-r = high/ Ebs-r = high. Overall, a wide range of variation in the system and EV-related reliability

values concerning various PV and battery storage penetration levels can be observed from Table 4.5 and Table 4.6.

Table 4.7 and Table 4.8 shows the various cost components calculated for a 10-year planning horizon. Among various cases, the least capital and maintenance cost is observed for the base case due to the absence of PV and battery storage systems. These values increased significantly after deploying PV and battery storage. The emission costs were reduced after deploying the PV and battery storage. The least emission values were observed for the cases of $P^{pv\text{-}r}$ = *high*/$E^{bs\text{-}r}$ = *no storage* and $P^{pv\text{-}r}$ = *high*/$E^{bs\text{-}r}$ = *low* because these cases result in the highest excess PV power that can be fed back to the grid. The service cost is negative because the cost of energy purchased from the grid is less than the revenue earned for feeding excess PV power back to the grid and serving the EV load.

Among various cases, the least revenue is seen for the base case. However, the revenue increased significantly after deploying the PV and battery storage due to the revenue earned from the excess PV power fed to the grid and reduced use of grid power for EV charging. The lowest service cost is seen for $P^{pv\text{-}r}$= *high*/$E^{bs\text{-}r}$ = *no storage* because the battery storage is not present in this case, and all the excess PV power is fed back to the system earning higher revenue. As expected, the highest cost of unreliability is observed for the base case because more EV and system load is curtailed in this case.

Table 4.7 Total cost calculated for the base case

	Capital Cost, C_{cap}	Maintanence Cost, C_{maint}	Emission Cost $C_{emission}$	Service Cost, $C_{service}$	Cost of Unreliability C_{unrel}	Total Cost C_T
BC	256,188	22,570	1,358,033	- 106,476	859,267	2,389,582

Table 4.8 Total cost calculated for the cases shown in Table 4.4

	P^{pv-r}/E^{bs-r}	No Storage	Low	High
Capital Cost, C_{cap}	Low	603,840	681,540	782,340
	Med	881,962	959,662	1,060,462
	High	1,054,848	1,132,548	1,233,348
Maintanence Cost, C_{maint}	Low	370,222	567,636	583,756
	Med	648,344	844,953	862,532
	High	821,230	1,017,496	1,035,183
Emission Cost $C_{emission}$	Low	1,291,285	1,291,389	1,292,051
	Med	1,240,030	1,242,141	1,241,599
	High	1,214,108	1,218,092	1,218,726
Service Cost, $C_{service}$	Low	- 694,730	- 644,240	- 607,182
	Med	- 1,179,806	- 1,119,144	- 1,080,704
	High	- 1,433,630	- 1,350,400	- 1,298,187
Cost of Unreliability C_{unrel}	Low	649,461	611,630	595,425
	Med	585,503	555,213	522,091
	High	559,843	529,697	507,260
Total Cost C_T	Low	2,220,078	2,507,956	2,646,391
	Med	2,176,032	2,482,825	2,605,980
	High	2,216,398	2,547,433	2,696,331

The load curtailment can be reduced after introducing the PV and battery storage. The least cost of unreliability is observed for the case of P^{pv-r} = *high*/E^{bs-r} = *high*. Finally, the least total cost was observed for the case of P^{pv-r} = *med*/E^{bs-r} = *no storage* and the highest total cost was observed for P^{pv-r} = *high*/E^{bs-r} = *high*. The higher costs show the increase in the total cost for the increase in the resource sizes. Hence, it is worth considering optimally

choosing the size of PV capacity and battery storage resources to minimize the total cost including the costs of unreliability and emissions.

4.9 Impact of operating strategies on reliability and costs

In this work, three EVCS operating strategies (OS) are compared in terms of their impact on the distribution system reliability and the cost. For the comparison study, the sizes of installed PV and battery storage were fixed at the values corresponding to Ppv-r = *medium*/Ebs-r = *low* in Table 4.4.

- In OS -1, the EV charging demand is met through PV power generation, stored battery energy, and power available from the grid. However, the excess power from the PV power generation is not allowed to send back to the grid and the battery storage is charged only from the excess PV power.
- OS-2 is similar to OS-1, but the excess PV power generation can be fed back to the grid.
- OS-3 is similar to OS-2, except that the SOC of battery storage is always maintained above 50% at any given time period. To achieve this, unlike in OS-1 and OS-2, grid power is used to charge the battery when PV power is not sufficient. OS-3 is expected to improve the reliability of EV charging stations and possibly reduce the demand for grid power during peak hours, although it is not specifically targeting selected time slots.

Table 4.9 shows the reliability indices calculated for the three operating strategies considered. The lowest system reliability as indicated by SAIFI, SAIDI, and EENS was observed for OS-1. The use of grid power for EV charging and the curtailment of EV charging loads as indicated by EEVGD and EUEVL was also the highest for OS-1. A significant decrease in SAIFI, SAIDI, and EENS (i.e. improved system reliability) can be seen under OS-2 where the excess PV power can be used to meet the demand of other loads. Both EV-related reliability indices were improved as well. Under OS-3, the EV-related reliability indices were further improved, however contrary to the initial expectation, the system reliability deteriorated compared to OS-2. This is because the additional load excreted on the distribution grid due to battery storage charging is not sensitive to the total load demand of the grid, and battery storage only benefits EV charging loads.

Table 4.9 Reliability indices calculated considering different operating strategies

	SAIFI (Interps/year/cust)	SAIDI (mins/year/cust)	EENS (Mwh/year/cust)	EEVGD (kWh/year/EV)	EUEVL (kWh/year/EV)
OS-1	0.076	136.54	177.09	5037.18	15.19
OS-2	0.069	124.89	132.82	5044.32	14.89
OS-3	0.072	128.91	146.24	4243.15	10.74

Table 4.10 compares the various cost components for the three operating strategies. Since the size of the PV and battery storage is assumed to be the same for all strategies, the capital cost remained the same. The maintenance costs are also similar, but it is slightly higher in OS-3 due to increased cycle life degradation. As PV power is not allowed to feed

the grid, OS-1 incurred higher service, emission, and unreliability costs leading to the highest total cost. In OS-2, excess PV power can be fed back to the grid resulting in a decreased emission cost and cost of unreliability while gaining significant revenue from selling PV power. The total cost under OS-2 reduced by 31% compared to OS-1. In OS-3, after implementing a PV-grid combined battery charging, a slight decrease in the revenue can be seen as per the service cost. This strategy also creates an additional load on the system which slightly increased the cost of unreliability. OS-3 results in the lowest emission cost due to increased utilization of battery storage. However, the overall cost for OS-3 is slightly higher when compared with OS-2. This analysis demonstrates the capability of the proposed framework to facilitate the evaluation of the impact of different operating strategies on the distribution system reliability, emissions, and cost.

Table 4.10 Total cost calculated considering different operating strategies

Study Case	OS-1	OS-2	OS-3
Capital Cost, C_{cap} ($)	959,662	959,662	959,662
Maintenance Cost, $C_{maint\ (\$)}$	845,398	845,107	880,849
Emission Cost $C_{emission}$	1,330,883	1,241,262	1,223,358
Service Cost, $C_{service}$ ($)	- 226,741	- 1,118,145	- 1,108,424
Cost of Unreliability C_{unrel} ($)	710,436	560,051	594,689
Total Cost C_T ($)	3,619,637	2,487,937	2,550,135

4.10 Optimal resource sizing

The results presented in Section 4.8.2 pointed to the opportunity for optimizing the resource capacities by finding the right trade-off between the total charging stations related

cost (capital cost, maintenance cost, emission cost, and service cost) and the cost of unreliability. In this section, this possibility is demonstrated using the Particle Swarm Optimization (PSO) algorithm [127] to optimize the number of PV modules in the array, number of battery storage units, number of charging connectors, and the level (power rating) of the EV chargers for each EVCS. The optimization aims to minimize the value of the fitness function which in this case is the total cost C_T that comprises of the charging station related costs and the cost of unreliability.

$$Minimize\ C_T(N^{pv,b}, N^{bs,b}, N^{ch,b}, P^{ch-rt,b}) \tag{4.16}$$

The minimization is subject to constraints such as the power balance and ratings of the equipment. The range of values of the optimizing parameters (or the control variables) used in the optimization are: N^{pv} [0-250], N^{bs} [0-140], N^{cs} [0-50] and P^{ch-rt} [1.2-46 kW]. The total number of particles considered in PSO was 100. Each particle represents a possible solution, and its merit is evaluated using the framework presented in Section 4.6 using the inputs described in Section 4.7. Although demonstrated using PSO, any other nonlinear optimization routine can be applied.

Table 4.11 compares the optimized resource sizes with the base case (where no PV or battery storage). In the base case, the total charging capacity and the number of chargers (N^{cs}) for a given location was decided considering a standard charging rate and the observed maximum EV charging load. This results in a fewer number of chargers and a higher charging capacity for most of the EVCSs in the base case.

Table 4.11 Optimal resources size chosen for different study cases

		Base Case	Optimization Case		
		Pch × Ncs (kW)	$P^{pv\text{-}r}$ (kW)	$E^{bs\text{-}r}$ (kWh)	Pch × Ncs (kW)
RA	Bus #3	6 × 6	20	20	7 × 4
	Bus #4	6 × 7	46	35	1 × 30
	Bus #13	6 × 6	4	4	7 × 3
WP	Bus #5	6 × 9	120	5	10 × 4
	Bus #6	6 × 8	53	45	10 × 4
	Bus #16	6 × 10	4	4	8 × 4
SM	Bus #11	28 × 2	4	4	4 × 13
	Bus #28	28 × 3	10	4	6 × 7
	Bus #31	28 × 4	43	34	17 × 5
CC	Bus #7	28 × 4	173	138	22 × 3
	Bus #25	28 × 3	4	4	4 × 22
	Bus #32	55 × 5	248	19	15 × 17
Total Sizes		14091	729	316	12876

In the optimized solution, the charging rate of many charging stations has been reduced, and the number of chargers has been increased. For instance, the Level – III charger in Bus #32 was changed to a Level- II (high) charger after optimization. Since the charging capacity of the EVCSs in the base case was decided based on the maximum EV load, some of the charging capacity could be underutilized. After the optimization, the combined capacity of all EVCSs has been reduced by 8.62% compared to the base case. The results also show a more prudent selection of battery storage capacity. For example, the ratio of storage capacity to PV rating is higher for RA locations where charging mostly happens in the evening hours while that ratio is lower for WP locations where charging load coincides with the sunshine hours. In a SM location, Bus #32 has a relatively higher EV charging

demand and hence the selected PV array rating and the battery capacity are higher as seen from Table 4.11.

Table 4.12 compares the reliability indices for the base case and the optimized case. As expected, both system and EV-related reliability indices have been improved for the optimized case. However, these values are higher than the respective lowest values in Table 4.6, because the optimization is a compromise between the reliability and the cost.

Table 4.12 Reliability indices for the base case and the optimized case

	Base Case	Optimization Case
SAIFI (Interps/year/cust)	0.080	0.073
SAIDI (mins/year/cust)	144.25	130.89
EENS (Mwh/year/cust)	209.14	156.82
EEVGD (kWh/year/EV)	6413.60	5627.67
EUEVL (kWh/year/EV)	18.26	16.52

Table 4.13 compares the costs of the optimized system with the base case. Although there is a significant increase in the capital and maintenance costs due to the PV and battery storage deployment, the increased revenue from the PV power feeding back to the grid, the reduced emission cost, and the reduced cost of unreliability resulted in a lower total cost when optimized. There is a 20% reduction in the total cost compared to the base case. Also, the total cost of $1,909,723 observed in the optimized case is lower than any of the total cost values observed among other study cases presented in Table 4.8 and Table 4.10.

Table 4.13 Total cost calculated for the base case and the optimized case

Study Case	Base Case	Optimization Case
Capital Cost, C_{cap} ($)	256,188	673,824
Maintanence Cost, $C_{maint\ (\$)}$	22,570	688,215
Emission Cost $C_{emission}$	1,358,130	970,354
Service Cost, $C_{service}$ ($)	- 107,624	- 975,871
Cost of Unreliability C_{unrel} ($)	865,108	553,201
Total Cost C_T ($)	2,394,372	1,909,723

4.11 Concluding remarks

In this chapter, a comprehensive methodology to perform a distribution system reliability and cost analysis considering DERs and EVs are presented. To emulate the variable EV charging load and PV power production, earlier developed stochastic models are used to assess a range of scenarios. A flexible approach to model an EV charging station with PV power and ESSs is described. The model can accommodate different operating strategies and facilitate reliability and economic evaluations. The proposed reliability and economic evaluation involve running power flow to perform network impacts evaluation. The proposed method also considers various cost factors including the estimation of emissions.

The EVCS model, which forms the core of this work, is validated by illustrating the interaction between the energy resources present at a charging station under the predefined

operating strategy. The analyses performed considering different combinations of the PV ratings and the ESSs capacities demonstrate the usefulness of the EVCS, economic evaluation, and reliability evaluation models. This reliability and economic analysis show that incorporating PV power production and battery storage to EVCS can improve the distribution system reliability and reduce emission costs. The analyses also show that certain combinations such as high battery storage capacity with low PV rating are ineffective in improving the reliability despite the higher costs. It is demonstrated that the proposed framework can be easily integrated into any optimization routing to optimally select the PV and battery capacities as well as the configuration of EVCSs. Also, two new reliability indices are proposed to quantify the perceived benefits of integrating DERs for EV charging, and their application in power system planning is demonstrated.

Chapter 5

Conclusions, Contributions and Future Work

5.1 Summary of the thesis and conclusions

This thesis proposes the necessary models and methodology to perform a reliability-centred distribution system analysis considering the role of RESs, ESSs, and EVs. The conclusions made from the studies presented in each chapter are presented here, accompanied by a summary.

A synthetic global horizontal solar irradiance generation model usable for Monte Carlo simulation-based long-term energy planning studies is presented in Chapter 2. It is revealed that the first-order differences of solar irradiance calculated at a given hour have a characteristic distribution that does not tend to vary from year to year. Hence the solar irradiance generation model is built utilizing this characteristic distribution function. Furthermore, it is shown that the first-order differences of solar irradiance of a particular hour in a given year can be represented in terms of a trend component and a stochastic

component characterized using a cumulative distribution function obtained from the historical data. Additionally, an extended model is also presented utilizing the strong correlation between hourly to sub-hourly values to generate 30-mins solar irradiance values from hourly solar irradiance values. Based on the study results presented in Chapter 2, the following conclusions are drawn:

- A strong correlation exists between the hourly solar irradiance over long persistence time periods. Hence, the current hour solar irradiance is highly relevant when generating the next hour of solar irradiance.
- The first-order difference in solar irradiance introduced in this thesis has annual probability distributions that are identical and predictable. This property can be used as an additional measure to evaluate the ability of the synthetic solar irradiance data generating algorithms to preserve the original characteristics of measured data.
- Characteristics of solar irradiance within 31 days centred around the current day are found to be similar. Hence a window of 31 days centred around the current day is appropriate to obtain the probability distributions of the first-order differences.
- The autocorrelation and partial correlation functions of the simulated data from the proposed model are similar to those of the measured solar irradiance data.
- The proposed model is able to reproduce the probability distributions of first-order difference in solar irradiance much better than two other models (SISIM and SHSRM) described in the existing literature.

- The hourly solar irradiance can be used to predict 30-mins solar irradiance values based on the strong correlation that exists between the average hourly solar irradiance and the 30-mins solar irradiance.

The impact of EV penetration on the distribution system reliability is examined in Chapter 3. A new probabilistic approach that primarily utilizes a novel two-layer stochastic EV charging demand estimation model is described. The model comprises a traffic layer representing the spatial-temporal distributions of EVs and an electrical network layer describing the EVs charging demand. A DHMM is used to capture the EV movements in the traffic layer. EV travel patterns and charging demand are simulated using a sequential Monte Carlo simulation approach considering the vehicle distance traveled, the type of charging location and the driver class. The proposed method and models are used to analyze the reliability of an example system and several useful reliability indices are calculated to quantify the reliability impact of EV charging. In correspondence to the parked locations, the EV charging demand for various location types is quantified in the electrical network layer. The EV charging decisions are simulated, considering the charge levels and preferred charging locations. Based on the study results presented in Chapter 3, the following conclusions are reached:

- The concept of geographical zones in the traffic network layer is capable of capturing the spatial distribution of EVs in a reasonable manner. By separating inter-zone and intra-zone EV movements, model complexity is reduced to a manageable level in the proposed traffic network model.

- The DHMM in the traffic layer is capable of emulating the time-dependent random travel patterns of EV drivers. The model parameters can be conveniently obtained from traffic survey data.
- The electrical network layer model is proven to be efficient to perform various operations such as performing power flow, limit checking, reliability analysis, and simulation of corrective actions such as load shedding.
- The EV energy consumption patterns simulated using the proposed model show clear distinctions depending on the location type, the time of the day, drivers charging preferences, and day type.
- For the case study presented, a significant increase in the peak load is observed during the weekend mainly due to the demand from the fast-charging stations in commercial centers.
- It is observed that system reliability decreases with an increase in EV penetration and driving distances. Also, an increase in the EVs with higher battery capacity has shown a negative impact on the reliability performance of distribution systems due to higher power consumption to satisfy battery charging needs.

A comprehensive methodology to perform a distribution system reliability and cost analysis considering DERs and EVs is presented in Chapter 4. Stochastic models developed in Chapter 2 and Chapter 3 have been used to emulate the PV power generation and uncertain nature of EV charging loads. Various computational models such as the EV charging station model, reliability evaluation model, and economic evaluation model are proposed to support the reliability and economic evaluation with necessary inputs. A range

of scenarios is analyzed using the proposed approach for illustrating the applicability. Sensitivity analyses are also performed to illustrate the reliability and economic impact due to EV charging, PV power production and various operating strategies. An optimization algorithm is used to choose the optimal resource sizes considering the minimization of charging station-related cost and cost of unreliability. Based on the investigations described in Chapter 4, the following conclusions are made:

- The presented comprehensive methodology was able to capture complex interactions among EVs, PV systems, and battery storage while performing distribution system reliability evaluations.
- The reliability and economic analysis show that the incorporation of PV power production and battery storage to EVCS can improve the distribution system reliability and reduce emission costs.
- The analyses also show that certain combinations such as high battery storage capacity with low PV rating are ineffective in improving the system reliability while resulting in higher costs.
- The proposed framework was proven to be flexible to implement an optimization framework using MCS and Particle Swam Optimization to choose optimal HER sizes while minimizing the total cost.

5.2 Major contributions of the research

The main objectives of the proposed research are to develop appropriate models for accurate and realistic evaluation of the reliability of distribution networks considering the

roles of DERs, ESSs, and EVs. The major contributions made while fulfilling these objectives are presented in this section. The first contribution of this thesis is the development of a novel synthetic global horizontal irradiance generation model for simulating solar resources. This model is used to quantify the available power from the PV arrays in the overall simulation process. The second contribution is the development of a two-layer stochastic EV charging demand estimation model. This model is used to simulate the EV travel patterns and charging demand considering the distance traveled, the type of charging location and the driver class. The third contribution is the incorporation of various computational models such as the EV charging station model, reliability evaluation model and economic evaluation model to perform comprehensive reliability and economic evaluation for distribution systems.

The developed models and methodology can benefit end-users like power distribution system planners to quantify long-term distribution system reliability impact under EVs and DERs penetration and determine the optimal sizes of resources to meet a certain power distribution system reliability criterion. Designated models and methodology may also benefit the distribution system owners to understand the cost of maintaining system reliability and life cycle costs associated with new EVCSs.

Electrification of the transportation sector is rapidly growing associated with a very dynamic technology transformation. With the increased penetration of different types of autonomous electrical transportation such as buses, delivery vehicles, and trucks, the adaptability of the proposed models would be questioned. Since the developed EV model efficiently captures vehicle movements and charging behaviour of each EV user, the

proposed models are sophisticated enough to accommodate any new vehicle type by providing necessary EV model input values pertaining to the vehicle specifications, vehicle travel pattern, and vehicle/user charging behaviour.

5.3 Potential future extensions of the research

This thesis presented models and methodologies to perform reliability and economic assessment of distribution systems considering EVs, DERs, and ESSs. However, there are many aspects to further studies. Some directions for future extensions that arise from the research described in this thesis are:

1. It may also be necessary to develop methodologies to identify zones using geographical information systems (GIS) of both municipal traffic and utility network. The application of machine learning-based clustering techniques may be considered for this purpose.
2. The development of an automated system to calculate the transition matrix and observation matrix probability values from the EV fleet monitoring system would be a very useful tool for the practical implementation of the proposed modelling concepts.
3. Presently it is assumed that the distribution system components are 100% reliable. Some of the future work could be extended to consider a failure of power system components.

4. Future developments need to incorporate V2G technology in the proposed framework to understand its perceived benefits on the distribution system reliability and total cost reduction.

References

[1] V. Viswanathan, D. Zehe, J. Ivanchev, D. Pelzer, A. Knoll, and H. Aydt, "Simulation-Assisted Exploration of Charging Infrastructure Requirements For Electric Vehicles In Urban Environments," *J. Comput. Sci.*, vol. 12, pp. 1–10, 2016.

[2] M. Govardhan and R. Roy, "Generation Scheduling in Smart Grid Environment Using Global Best Artificial Bee Colony Algorithm," *Int. J. Electr. Power Energy Syst.*, vol. 64, pp. 260–274, Jan. 2015.

[3] A. Papavasiliou and S. S. Oren, "Large-Scale Integration of Deferrable Demand and Renewable Energy Sources," *IEEE Trans. Power Syst.*, vol. 29, no. 1, pp. 489–499, 2014.

[4] A. Soroudi, M. Aien, and M. Ehsan, "A Probabilistic Modeling of Photo Voltaic Modules and Wind Power Generation Impact on Distribution Networks," *IEEE Syst. J.*, vol. 6, no. 2, pp. 254–259, 2012.

[5] A. Arias, M. Granada, and C. Castro, "Optimal Probabilistic Charging of Electric Vehicles in Distribution Systems," *IET Electr. Syst. Transp.*, vol. 7, no. 3, pp. 246–251, 2017.

[6] A. R. Malekpour, T. Niknam, A. Pahwa, and A. K. Fard, "Multi-Objective Stochastic Distribution Feeder Reconfiguration in Systems with Wind Power Generators and Fuel Cells using the Point Estimate Method," *IEEE Trans. Power Syst.*, vol. 28, no. 2, pp. 1483–1492, 2013.

[7] V. Tavakoli Bina and D. Ahmadi, "Stochastic Modeling for Scheduling the Charging Demand of EV In Distribution Systems using Copulas," *Int. J. Electr. Power Energy Syst.*, vol. 71, pp. 15–25, 2015.

[8] W. Su, J. Wang, and J. Roh, "Stochastic Energy Scheduling in Microgrids With Intermittent Renewable Energy Resources," *IEEE Trans. Smart Grid*, vol. 5, no. 4, pp. 1876–1883, 2014.

[9] A. Soroudi and M. Ehsan, "A Possibilistic–Probabilistic Tool for Evaluating the Impact of Stochastic Renewable And Controllable Power Generation on Energy Losses in Distribution Networks—A Case Study," *Renew. Sustain. Energy Rev.*, vol. 15, no. 1, pp. 794–800, 2011.

[10] S. F. Abdelsamad, W. G. Morsi, and T. S. Sidhu, "Impact of Wind-Based Distributed Generation on Electric Energy in Distribution Systems Embedded With Electric Vehicles," *IEEE Trans. Sustain. Energy*, vol. 6, no. 1, pp. 79–87, 2015.

[11] D. Božič and M. Pantoš, "Impact of Electric-Drive Vehicles on Power System Reliability," *Energy*, vol. 83, pp. 511–520, 2015.

[12] N. Z. Xu and C. Y. Chung, "Reliability Evaluation of Distribution Systems Including Vehicle-to-Home and Vehicle-to-Grid," *IEEE Trans. Power Syst.*, vol. 31, no. 1, pp. 1–10, 2015.

[13] J. García-Villalobos, I. Zamora, J. I. San Martín, F. J. Asensio, and V. Aperribay, "Plug-In Electric Vehicles in Electric Distribution Networks: A Review of Smart Charging Approaches," *Renew. Sustain. Energy Rev.*, vol. 38, pp. 717–731, Oct. 2014.

[14] M. B. Arias and S. Bae, "Prediction of Electric Vehicle Charging-Power Demand in Realistic Urban Traffic Networks," *Appl. Energy*, vol. 195, pp. 738–753, 2017.

[15] K. Hou *et al.*, "A Reliability Assessment Approach for Integrated Transportation and Electrical Power Systems Incorporating Electric Vehicles," *IEEE Trans. Smart Grid*, vol. 3053, no. c, pp. 1–1, 2016.

[16] D. Tang and P. Wang, "Probabilistic Modeling of Nodal Charging Demand Based on Spatial-Temporal Dynamics of Moving Electric Vehicles," *IEEE Trans. Smart Grid*, vol. 7, no. 2, pp. 627–636, 2016.

[17] J. L. Bowman and M. E. Ben-Akiva, "Activity-Based Disaggregate Travel Demand Model System with Activity Schedules," *Consort. Newsl.*, vol. 35, p. 11, 1999.

[18] Y. Wang and D. Infield, "Markov Chain Monte Carlo Simulation of Electric Vehicle use For Network Integration Studies," *Int. J. Electr. Power Energy Syst.*, vol. 99, no. March 2017, pp. 85–94, 2018.

[19] C. Paper *et al.*, "A stochastic model to simulate electric vehicles motion and quantify the energy required from the grid," *2011 17th Power Syst. Comput. Conf.*, no. February 2014, 2011.

[20] A. Ul-Haq, C. Cecati, and E. El-Saadany, "Probabilistic Modeling of Electric Vehicle Charging Pattern in a Residential Distribution Network," *Electr. Power Syst. Res.*, vol. 157, pp. 126–133, 2018.

[21] G. Hill, P. T. Blythe, and C. Higgins, "Deviations in Markov Chain Modeled Electric Vehicle Charging Patterns from Real World Data," *IEEE Conf. Intell. Transp. Syst. Proceedings, ITSC*, pp. 1072–1077, 2012.

[22] M. P. Anand, A. Rajapakse, and Bagen B, “Stochastic Model for Generating Synthetic Hourly Global Horizontal Solar Radiation Data Sets Based on Auto Regression Characterization,” *Int. Energy J.*, vol. 20, pp. 181–200, 2020.

[23] J. Polo, L. F. Zarzalejo, R. Marchante, and A. A. Navarro, “A Simple Approach to the Synthetic Generation of Solar Irradiance Time Series with High Temporal Resolution,” *Sol. Energy*, vol. 85, no. 5, pp. 1164–1170, 2011.

[24] A. P. Grantham, P. J. Pudney, L. A. Ward, M. Belusko, and J. W. Boland, “Generating Synthetic Five-Minute Solar Irradiance Values from Hourly Observations,” *Sol. Energy*, vol. 147, pp. 209–221, 2017.

[25] J. M. Bright, O. Babacan, J. Kleissl, P. G. Taylor, and R. Crook, “A Synthetic, Spatially Decorrelating Solar Irradiance Generator and Application to a LV Grid Model With High PV Penetration,” *Sol. Energy*, vol. 147, pp. 83–98, 2017.

[26] H. Morais, T. Sousa, Z. Vale, and P. Faria, “Evaluation of the Electric Vehicle Impact in the Power Demand Curve in a Smart Grid Environment,” *Energy Convers. Manag.*, vol. 82, pp. 268–282, Jun. 2014.

[27] T. Wu, Q. Yang, Z. Bao, and W. Yan, “Coordinated Energy Dispatching in Microgrid With Wind Power Generation and Plug-in Electric Vehicles,” *IEEE Trans. Smart Grid*, vol. 4, no. 3, pp. 1453–1463, Sep. 2013.

[28] T. Sousa, H. Morais, J. Soares, and Z. Vale, “Day-Ahead Resource Scheduling in Smart Grids Considering Vehicle-to-Grid and Network Constraints,” *Appl. Energy*, vol. 96, pp. 183–193, Aug. 2012.

[29] A. Zakariazadeh, S. Jadid, and P. Siano, “Stochastic Multi-Objective Operational

Planning of Smart Distribution Systems Considering Demand Response Programs," *Electr. Power Syst. Res.*, vol. 111, pp. 156–168, Jun. 2014.

[30] J. Munkhammar, J. Wid, and J. R. En, Pia Grahn, "Optimal Probabilistic Charging of Electric Vehicles in Distribution Systems," *IEEE Trans. Smart Grid*, vol. 6, no. 2, pp. 1–5, Dec. 2016.

[31] S. Pazouki and A. Mohsenzadeh, "Simultaneous Planning of PEV Charging Stations and DGs Considering Financial , Technical , and Environmental Effects Planification simultanée des stations de recharge de PEV et des DG en considérant les critères," *Can. J. Electr. Comput. Eng.*, vol. 38, no. 3, pp. 238–245, 2015.

[32] G. Carpinelli, P. Caramia, and P. Varilone, "Multi-Linear Monte Carlo Simulation Method for Probabilistic Load Flow of Distribution Systems With Wind and Photovoltaic Generation Systems," *Renew. Energy*, vol. 76, pp. 283–295, 2015.

[33] J. A. Domínguez-Navarro, R. Dufo-López, J. M. Yusta-Loyo, J. S. Artal-Sevil, and J. L. Bernal-Agustín, "Design of an Electric Vehicle Fast-Charging Station with Integration of Renewable Energy and Storage Systems," *Int. J. Electr. Power Energy Syst.*, vol. 105, no. July 2018, pp. 46–58, 2019.

[34] S. F. Abdelsamad, W. G. Morsi, and T. S. Sidhu, "Probabilistic Impact of Transportation Electrification on the Loss-of-Life of Distribution Transformers in the Presence of Rooftop Solar Photovoltaic," *IEEE Trans. Sustain. Energy*, vol. 6, no. 4, pp. 1565–1573, 2015.

[35] M. Hopkins and A. Pahwa, "Monte-Carlo Simulation of Energy Production by a Small Wind Generator," *40th North Am. Power Symp.*, pp. 1–6, 2008.

[36] H. Sharma, B. Bora, S. Sharma, R. Kumar, and R. Jain, “Reliability Study of Solar PV Power Production In Terms Of Weather Parameters Using Monte Carlo Simulation,” *Int. J. Eng. Res. Appl.*, vol. 07, no. 07, pp. 37–45, 2017.

[37] M. J. Reno and C. Hansen, “Global Horizontal Irradiance Clear Sky Models: Implementation and Analysis,” *Sandia Rep.*, no. January, 2014.

[38] B. Y. H. Liu and R. C. Jordan, “The Interrelationship and of Direct, Diffuse and Characteristic Distribution Total Solar Radiation,” *Sol. Energy*, vol. 4, no. 3, pp. 1–19, 1960.

[39] H. Morf, “A stochastic solar irradiance model adjusted on the Ångström-Prescott regression,” *Sol. Energy*, vol. 87, no. 1, pp. 1–21, 2013.

[40] E. De Alfragide, “Tag : a Time-Dependent , Autoregressive , Gaussian Model for Generating Synthetic Hourly Radiation,” *Sol. Energy*, vol. 49, pp. 167–174, 1992.

[41] Kristijan Brecl and Marko TopiI, “Development of a Stochastic Hourly Solar Irradiation Model,” *Int. J. Photoenergy*, vol. 2014, 2014.

[42] R. J. Aguiar, M. Collares-Pereira, and J. P. Conde, “Simple Procedure for Generating Sequences of Daily Radiation Values using a Library of Markov Transition Matrices,” *Sol. Energy*, vol. 40, no. 3, pp. 269–279, 1988.

[43] V. A. Graham and K. G. T. Hollands, “A Method to Generate Synthetic Hourly Solar Radiation Globally,” *Sol. Energy*, vol. 44, no. 6, pp. 333–341, 1990.

[44] H. Suehrcke and P. G. McCormick, “The Frequency Distribution of Instantaneous Insolation Values,” *Sol. Energy*, vol. 40, no. 5, pp. 413–422, 1988.

[45] C. M. Fernández-Peruchena, M. Gastón, M. Sánchez, J. García-Barberena, M.

Blanco, and A. Bernardos, “MUS: A Multiscale Stochastic Model for Generating Plausible Meteorological Years Designed for Multiyear Solar Energy Yield Simulations,” *Sol. Energy*, vol. 120, pp. 244–256, 2015.

[46] F. Besharat, A. A. Dehghan, and A. R. Faghih, “Empirical Models for Estimating Global Solar Radiation: A Review And Case Study,” *Renew. Sustain. Energy Rev.*, vol. 21, pp. 798–821, 2013.

[47] B. O. Ngoko, H. Sugihara, and T. Funaki, “Synthetic Generation of High Temporal Resolution Solar Radiation Data using Markov Models,” *Sol. Energy*, vol. 103, pp. 160–170, 2014.

[48] J. M. Bright, C. J. Smith, P. G. Taylor, and R. Crook, “Stochastic Generation of Synthetic Minutely Irradiance Time Series Derived from Mean Hourly Weather Observation Data,” *Sol. Energy*, vol. 115, pp. 229–242, 2015.

[49] J. A. Duffie and W. A. Beckman, *Solar Engineering of Thermal Processes, Fourth Edition*. Wiley, 2013.

[50] M. A. Azzouz, M. F. Shaaban, and E. F. El-Saadany, “Real-Time Optimal Voltage Regulation for Distribution Networks Incorporating High Penetration of PEVs,” *IEEE Trans. Power Syst.*, no. November, 2015.

[51] J. M. Gordon and T. A. Reddy, “Time Series Analysis of Daily Horizontal Solar Radiation,” *Sol. Energy*, vol. 41, no. 3, pp. 215–226, 1988.

[52] M. C. Peel, B. L. Finlayson, and T. A. McMahon, “Updated World Map of the Köppen-Geiger Climate Classification,” *Hydrol. Earth Syst. Sci.*, vol. 11, no. 5, pp. 1633–1644, Oct. 2007.

[53] Joakim Munkhammar, “Polynomial Probability Distribution Estimation with the Method-of-Moments - File Exchange - MATLAB Central.” [Online]. Available: https://www.mathworks.com/matlabcentral/fileexchange/62520-polynomial-probability-distribution-estimation. [Accessed: 03-Jul-2018].

[54] A. P. Grantham, P. J. Pudney, and J. W. Boland, “Generating Synthetic Sequences of Global Horizontal Irradiation,” *Sol. Energy*, vol. 162, no. November 2017, pp. 500–509, 2018.

[55] M. P. Anand, B. Bagen, and A. Rajapakse, “Probabilistic Reliability Evaluation of Distribution Systems Considering the Spatial and Temporal Distribution of Electric Vehicles,” *Int. J. Electr. Power Energy Syst.*, vol. 117, no. July 2019, p. 105609, 2020.

[56] G. M. Masters, *Renewable and Efficient Electric Power Systems*. Wiley - Interscience, 2004.

[57] K. Mertens, *Photovoltaics Fundamentals, Technology, and Practice.* John Wiley & Sons, Incorporated, 2018.

[58] F. Fazelpour, M. Vafaeipour, O. Rahbari, and M. A. Rosen, “Intelligent Optimization to Integrate a Plug-In Hybrid Electric Vehicle Smart Parking Lot with Renewable Energy Resources and Enhance Grid Characteristics,” *Energy Convers. Manag.*, vol. 77, pp. 250–261, 2014.

[59] “Engineering Climate Datasets-Canada.” [Online]. Available: http://climate.weather.gc.ca/prods_servs/engineering_e.html. [Accessed: 24-Nov-2017].

[60] “SolarAnywhere - Accurate & Scalable Solar Data.” [Online]. Available: https://data.solaranywhere.com/Account/Login?ReturnUrl=%2F. [Accessed: 24-Nov-2017].

[61] R. Perez, R. Seals, P. Ineichen, R. Stewart, and D. Menicucci, “A New Simplified Version of the Perez Diffuse Irradiance Model for Tilted Surfaces,” *Sol. Energy*, vol. 39, no. 3, pp. 221–231, Jan. 1987.

[62] “R2017a - MATLAB & Simulink.” [Online]. Available: https://www.mathworks.com/help/symbolic/release-notes-R2017a.html. [Accessed: 18-Jun-2018].

[63] V. Chamola and B. Sikdar, “Synthetic Generation of Hourly Solar Irradiance Using a Multi-State Markov Model,” *IEIE/IEEE ICEIC, Singapore*, vol. 1, pp. 1–3, 2015.

[64] “Environment and natural resources - Canada.ca.” [Online]. Available: https://www.canada.ca/en/services/environment.html. [Accessed: 20-Feb-2020].

[65] A. Resistance, “300 W – 320 W Poly-crystalline Solar Module,” *Www.Sunceco.Com*.

[66] M. P. Anand, S. Golshannavaz, W. Ongsakul, and A. Rajapakse, “Incorporating Short-Term Topological Variations in Optimal Energy Management of MGs Considering Ancillary Services by Electric Vehicles,” *Energy*, vol. 112, pp. 241–253, 2016.

[67] K. Sun, M. R. Sarker, and M. A. Ortega-Vazquez, “Statistical Characterization of Electric Vehicle Charging in Different Locations of the Grid,” *IEEE Power Energy Soc. Gen. Meet.*, vol. 2015-Septe, 2015.

[68] F. J. Soares, J. A. P. Lopes, and P. M. R. Almeida, “A Stochastic Model to Simulate Electric Vehicles Motion and Quantify the Energy Required from The Grid,” *2011 17th Power Syst. Comput. Conf.*, no. 1, pp. 22–26, 2011.

[69] S. Guo and H. Zhao, “Optimal Site Selection of Electric Vehicle Charging Station by using Fuzzy TOPSIS Based on Sustainability Perspective,” *Appl. Energy*, vol. 158, pp. 390–402, 2015.

[70] I. J. Ramirez-Rosado and J. a. Dominguez-Navarro, “Possibilistic Model Based on Fuzzy Sets for the Multiobjective Optimal Planning of Electric Power Distribution Networks,” *IEEE Trans. Power Syst.*, vol. 19, no. 4, pp. 1801–1810, 2004.

[71] A. S. Masoum, S. Deilami, S. Member, M. a S. Masoum, and S. Member, “Fuzzy Approach for Online Coordination of Plug-In Electric Vehicle Charging in Smart Grid,” *IEEE Trans. Sustain. Energy*, vol. 6, no. 3, pp. 1112–1121, 2015.

[72] Z. Liu, D. Wang, H. Jia, N. Djilali, and W. Zhang, “Aggregation and Bidirectional Charging Power Control of Plug-in Hybrid Electric Vehicles: Generation System Adequacy Analysis,” *IEEE Trans. Sustain. Energy*, vol. 6, no. 2, pp. 325–335, 2015.

[73] H. R. Galiveeti, A. K. Goswami, and N. B. Dev Choudhury, “Impact of Plug-In Electric Vehicles and Distributed Generation on Reliability of Distribution Systems,” *Eng. Sci. Technol. an Int. J.*, vol. 21, no. 1, pp. 50–59, 2018.

[74] S. Shojaabadi, S. Abapour, M. Abapour, and A. Nahavandi, “Optimal Planning of Plug-In Hybrid Electric Vehicle Charging Station in Distribution Network Considering Demand Response Programs and Uncertainties,” *IET Gener. Transm. Distrib.*, vol. 10, no. 13, pp. 3330–3340, 2016.

[75] P. Berkhin, “Survey of Clustering Data Mining Techniques,” *Group. Multidimens. Data Recent Adv. Clust.*, vol. 10, pp. 25–71, 2006.

[76] C. M. Grinstead and J. L. Snell, “Markov Chains,” *Introd. to Probab.*, pp. 1–66, 2010.

[77] N. Angiuli, “An Introduction to Hidden Markov Models,” *Vis. Ethnogr.*, vol. 6, no. 2, pp. 239–249, 2017.

[78] T. Pamuła and W. Pamuła, “Estimation of The Energy Consumption of Battery Electric Buses for Public Transport Networks using Real-World Data And Deep Learning,” *Energies*, vol. 13, no. 9, 2020.

[79] International Energy Agency, “Global EV Outlook 2017: Two million and counting,” *IEA Publ.*, pp. 1–71, 2017.

[80] K. Sun, M. R. Sarker, and M. A. Ortega-Vazquez, “Statistical Characterization of Electric Vehicle Charging in Different Locations of the Grid,” *2015 IEEE Power Energy Soc. Gen. Meet.*, pp. 1–5, 2015.

[81] L. Gong, W. Cao, and J. Zhao, “Load Modeling Method for EV Charging Stations Based on Trip Chain,” *2017 IEEE Conf. Energy Internet Energy Syst. Integr. EI2 2017 - Proc.*, vol. 2018-Janua, pp. 1–5, 2018.

[82] X. Hu, H. Jiang, F. Feng, and B. Liu, “An Enhanced Multi-State Estimation Hierarchy for Advanced Lithium-Ion Battery Management,” *Appl. Energy*, vol. 257, no. October 2019, p. 114019, 2020.

[83] X. Hu, F. Feng, K. Liu, L. Zhang, J. Xie, and B. Liu, “State Estimation for Advanced Battery Management: Key Challenges and Future Trends,” *Renew. Sustain. Energy*

Rev., vol. 114, no. April, p. 109334, 2019.

[84] J. a M. Rupa and S. Ganesh, "Power Flow Analysis for Radial Distribution System Using Backward / Forward Sweep Method," *Int. J. Electr. Comput. Energ. Electron. Commun. Eng.*, vol. 8, no. 10, pp. 1537–1541, 2014.

[85] B. F. F. Mew E, "Network Reconfiguration In Distribution Systems For Loss Reduction And Load Balancing," *Justice Syst. J.*, vol. 13, no. 3, pp. 79–385, 1988.

[86] A. Soroudi, R. Caire, N. Hadjsaid, and M. Ehsan, "Probabilistic Dynamic Multi-Objective Model for Renewable and Non-Renewable Distributed Generation Planning," *IET Gener. Transm. Distrib.*, vol. 5, no. 11, p. 1173, 2011.

[87] "ERCOT-Hourly Load Data Archives." [Online]. Available: http://www.ercot.com/gridinfo/load/load_hist/. [Accessed: 09-Feb-2018].

[88] "Electric Powertrains: Opportunities and Challenges in the U.S. Light-Duty Vehicle Fleet | MIT Energy Initiative." [Online]. Available: http://energy.mit.edu/publication/electric-powertrains-opportunities-and-challenges-in-the-u-s-light-duty-vehicle-fleet/. [Accessed: 30-May-2018].

[89] A. Zakariazadeh, S. Jadid, and P. Siano, "Multi-Objective Scheduling of Electric Vehicles in Smart Distribution System," *Energy Convers. Manag.*, vol. 79, pp. 43–53, Mar. 2014.

[90] A. Dubey, S. Member, and S. Santoso, "Electric Vehicle Charging on Residential Distribution Systems : Impacts and Mitigations," *IEEE Access*, pp. 1871–1893, 2015.

[91] E. Bibeau, "Winnipeg duty cycle," 01-Jan-2012. [Online]. Available:

mspace.lib.umanitoba.ca/xmlui/handle/1993/8131?show=full. [Accessed: 05-Sep-2017].

[92] N. G. Omran and S. Filizadeh, "Location-Based Forecasting of Vehicular Charging Load on The Distribution System," *IEEE Trans. Smart Grid*, vol. 5, no. 2, pp. 632–641, 2014.

[93] S. Shahidinejad, S. Filizadeh, and E. Bibeau, "Profile of Charging Load on the Grid Due to Plug-In Vehicles," *IEEE Trans. Smart Grid*, vol. 3, no. 1, pp. 135–141, 2012.

[94] M. P. Anand, A. Rajapakse, S. Muthukumarana, and B. Bagen, "Evaluation of a Stochastic Vehicle Travel Pattern Generation Model with the Real-World Travel Data," *2020 IEEE Electr. Power Energy Conf.*, vol. 3, pp. 8–13, 2020.

[95] O. Hafez and K. Bhattacharya, "Optimal Design of Electric Vehicle Charging Stations Considering various Energy Resources," *Renew. Energy*, vol. 107, pp. 576–589, 2017.

[96] E. Akarslan and F. O. Hocaoglu, "A Novel Adaptive Approach for Hourly Solar Radiation Forecasting," *Renew. Energy*, vol. 87, pp. 628–633, 2016.

[97] L. Dong, L. Wang, S. F. Khahro, S. Gao, and X. Liao, "Wind Power Day-Ahead Prediction with Cluster Analysis of NWP," *Renew. Sustain. Energy Rev.*, vol. 60, pp. 1206–1212, 2016.

[98] Z. Xu, Z. Hu, Y. Song, Z. Luo, K. Zhan, and J. Wu, "Coordinated Charging Strategy for PEVs Charging Stations," *IEEE Power Energy Soc. Gen. Meet.*, pp. 1–8, 2012.

[99] P. Zhang, K. Qian, C. Zhou, B. G. Stewart, and D. M. Hepburn, "A Methodology for Optimization of Power Systems Demand Due to Electric Vehicle Charging

Load," *IEEE Trans. Power Syst.*, vol. 27, no. 3, pp. 1628–1636, 2012.

[100] Y. Cao *et al.*, "An Optimized EV Charging Model Considering TOU Price and SOC Curve," *IEEE Trans. Smart Grid*, vol. 3, no. 1, pp. 388–393, 2012.

[101] P. Sadeghi-Barzani, A. Rajabi-Ghahnavieh, and H. Kazemi-Karegar, "Optimal Fast Charging Station Placing and Sizing," *Appl. Energy*, vol. 125, pp. 289–299, 2014.

[102] G. Wang, Z. Xu, F. Wen, and K. P. Wong, "Traffic-Constrained Multiobjective Planning of Electric-Vehicle Charging Stations," *IEEE Trans. Power Deliv.*, vol. 28, no. 4, pp. 2363–2372, 2013.

[103] Y. Xiang, J. Liu, R. Li, F. Li, C. Gu, and S. Tang, "Economic Planning of Electric Vehicle Charging Stations Considering Traffic Constraints and Load Profile Templates," *Appl. Energy*, vol. 178, pp. 647–659, 2016.

[104] S. Su, Y. Hui, D. Ning, and P. Li, "Spatial-Temporal Distribution Model of Electric Vehicle Charging Demand Based on a Dynamic Evolution Process," *2nd IEEE Conf. Energy Internet Energy Syst. Integr. EI2 2018 - Proc.*, pp. 1–8, 2018.

[105] Z. Zhou and T. Lin, "Spatial and Temporal Model for Electric Vehicle Rapid Charging Demand," *2012 IEEE Veh. Power Propuls. Conf. VPPC 2012*, pp. 345–348, 2012.

[106] H. J. Vermaak and K. Kusakana, "Design of a Photovoltaicewind Charging Station for Small Electric Tuketuk in D.R.Congo," *Renew. Energy*, vol. 67, pp. 40–45, 2014.

[107] S. J. Gunter, K. K. Afridi, and D. J. Perreault, "Optimal Design of Grid-Connected PEV Charging Systems with Integrated Distributed Resources," *IEEE Trans. Smart Grid*, vol. 4, no. 2, pp. 956–967, 2013.

[108] T. Li *et al.*, "An Optimal Design and Analysis of a Hybrid Power Charging Station for Electric Vehicles Considering Uncertainties," *Proc. IECON 2018 - 44th Annu. Conf. IEEE Ind. Electron. Soc.*, vol. 1, pp. 5147–5152, 2018.

[109] J. Ugirumurera and Z. Haas, "Optimal Sizing of a Completely Green Charging System for Electric Vehicles," *IEEE Trans. Transp. Electrif.*, vol. 3, no. 3, pp. 1–1, 2017.

[110] B. Aluisio, M. Dicorato, G. Forte, and M. Trovato, "A Monte-Carlo Based Procedure for Optimal Sizing of Integrated Electric Vehicle Supply Infrastructure Benedetto," *2017 IEEE PES Innov. Smart Grid Technol. Conf. Eur. ISGT-Europe 2017 - Proc.*, vol. 2018-Janua, pp. 1–6, 2017.

[111] O. Hafez and K. Bhattacharya, "Optimal Design of Electric Vehicle Charging Stations Considering various Energy Resources," *Renew. Energy*, vol. 107, pp. 576–589, 2017.

[112] J. Ugirumurera and Z. Haas, "Optimal Sizing of a Completely Green Charging System for Electric Vehicles," *IEEE Trans. Transp. Electrif.*, vol. 7782, no. c, pp. 1–1, 2017.

[113] F. J. Soares, P. M. R. Almeida, and J. A. P. Lopes, "Quasi-Real-Time Management of Electric Vehicles Charging," *Electr. Power Syst. Res.*, vol. 108, pp. 293–303, 2014.

[114] C. Hutson, G. K. Venayagamoorthy, and K. A. Corzine, "Intelligent Scheduling of Hybrid and Electric Vehicle Storage Capacity in a Parking Lot for Profit Maximization in Grid Power Transactions," *2008 IEEE Energy 2030 Conf.*

ENERGY 2008, 2008.

[115] S. Han, S. Han, and K. Sezaki, "Development of an Optimal Vehicle-to-Grid Aggregator for Frequency Regulation," *IEEE Trans. Smart Grid*, vol. 1, no. 1, pp. 65–72, 2010.

[116] I. K. A. Aswantara, K. S. Ko, and D. K. Sung, "A Centralized EV Charging Scheme Based on User Satisfaction Fairness and Cost," *2013 IEEE Innov. Smart Grid Technol. - Asia, ISGT Asia 2013*, pp. 19–22, 2013.

[117] D. T. Nguyen and L. B. Le, "Joint Optimization of Electric Vehicle and Home Energy Scheduling Considering User Comfort Preference," *IEEE Trans. Smart Grid*, vol. 5, no. 1, pp. 188–199, 2014.

[118] M. H. K. Tushar, C. Assi, M. Maier, and M. F. Uddin, "Smart Microgrids: Optimal Joint Scheduling for Electric Vehicles and Home Appliances," *IEEE Trans. Smart Grid*, vol. 5, no. 1, pp. 239–250, 2014.

[119] S. Acha, T. C. Green, and N. Shah, "Effects of Optimised Plug-in Hybrid Vehicle Charging Strategies on Electric Distribution Network Losses," *2010 IEEE PES Transm. Distrib. Conf. Expo. Smart Solut. a Chang. World*, pp. 1–6, 2010.

[120] J. Huang, V. Gupta, and Y. F. Huang, "Scheduling Algorithms for PHEV Charging in Shared Parking Lots," *Proc. Am. Control Conf.*, pp. 276–281, 2012.

[121] M. G. Vaya and G. Andersson, "Centralized and Decentralized Approaches to Smart Charging of Plug-in Vehicles," *IEEE Power Energy Soc. Gen. Meet.*, pp. 1–8, 2012.

[122] T. N. Le, S. Al-Rubaye, H. Liang, and B. J. Choi, "Dynamic Charging and Discharging for Electric Vehicles in Microgrids," *2015 IEEE Int. Conf. Commun.*

Work. ICCW 2015, pp. 2018–2022, 2015.

[123] S. Huang, Q. Wu, S. S. Oren, R. Li, and Z. Liu, "Distribution Locational Marginal Pricing Through Quadratic Programming for Congestion Management in Distribution Networks," *IEEE Trans. Power Syst.*, vol. 30, no. 4, pp. 2170–2178, 2015.

[124] G. Wacker and G. Tollefson, "Electric Power System Customer Interruption Cost Assessment," *Reliab. Eng. Syst. Saf.*, vol. 46, no. 1, pp. 75–81, 1994.

[125] M. R. Mozafar, M. H. Amini, and M. H. Moradi, "Innovative appraisement of smart grid operation considering large-scale integration of electric vehicles enabling V2G and G2V systems," *Electr. Power Syst. Res.*, vol. 154, pp. 245–256, 2018.

[126] W. Cole and A. W. Frazier, "Cost Projections for Utility- Scale Battery Storage Cost Projections for Utility- Scale Battery Storage," *Natl. Renew. Energy Lab.*, no. June, p. NREL/TP-6A20-73222, 2019.

[127] A. H. Fathima and K. Palanisamy, "Optimization in Microgrids with Hybrid Energy Systems - A Review," *Renew. Sustain. Energy Rev.*, vol. 45, pp. 431–446, 2015.

Appendices

Appendix A: Network data of IEEE 33 bus system

Bus Number	From Bus	To Bus	R (Ohm)	X (Ohm)	PL (kW)	QL (kvar)	|V|*2
1	1	2	0.0922	0.047	100	60	0.9927
2	2	3	0.493	0.2511	90	40	0.9574
3	3	4	0.366	0.1864	120	80	0.9374
4	4	5	0.3811	0.1941	60	30	0.9176
5	5	6	0.819	0.707	60	20	0.8707
6	6	7	0.1872	0.6188	200	100	0.8641
7	7	8	0.7114	0.2351	200	100	0.855
8	8	9	1.03	0.74	60	20	0.8432
9	9	10	1.044	0.74	60	20	0.8324
10	10	11	0.1966	0.065	45	30	0.8308
11	11	12	0.3744	0.1238	60	35	0.828
12	12	13	1.468	1.155	60	35	0.8161
13	13	14	0.5416	0.7129	120	80	0.8125
14	14	15	0.591	0.526	60	10	0.8099
15	15	16	0.7463	0.545	60	20	0.8074
16	16	17	1.289	1.721	60	20	0.8037
17	17	18	0.732	0.574	90	40	0.8026
18	2	19	0.164	0.1565	90	40	0.9916
19	19	20	1.5042	1.3554	90	40	0.9845
20	20	21	0.4095	0.4784	90	40	0.9831
21	21	22	0.7089	0.9373	90	40	0.9818
22	3	23	0.4512	0.3083	90	50	0.9504
23	23	24	0.898	0.7091	420	200	0.9373
24	24	25	0.896	0.7011	420	200	0.9309
25	6	26	0.203	0.1034	60	25	0.8643
26	26	27	0.2842	0.1447	60	25	0 .8557
27	27	28	1.059	0.9337	60	20	0.8201
28	28	29	0.8042	0.7006	120	10	0.7945
29	29	30	0.5075	0.2585	200	600	0.7816
30	30	31	0.9744	0.963	150	70	0.7739
31	31	32	0.3105	0.3619	210	100	0.7723
32	32	33	0.341	0.53	60	40	0.7717

Appendix B: Transition and Observation Matrix Probability Values

B.1. Sample transition matrix probability values (between zones and zone to travel) for an EV during a weekday

	S_1		S_2		S_3		S_4		S_5		S_6	
tp	$\lambda_{S1,S1}$	$\lambda_{S1,SH}$	$\lambda_{S2,S2}$	$\lambda_{S2,SH}$	$\lambda_{S3,S3}$	$\lambda_{S3,SH}$	$\lambda_{S4,S4}$	$\lambda_{S4,SH}$	$\lambda_{S5,S5}$	$\lambda_{S5,SH}$	$\lambda_{S6,S6}$	$\lambda_{S6,SH}$
1	0.98	0.02	0.98	0.02	0.02	0.98	0.02	0.98	0.02	0.98	0.98	0.02
2	0.98	0.02	0.98	0.02	0.02	0.98	0.02	0.98	0.02	0.98	0.98	0.02
3	0.98	0.02	0.98	0.02	0.02	0.98	0.02	0.98	0.02	0.98	0.98	0.02
4	0.98	0.02	0.98	0.02	0.02	0.98	0.02	0.98	0.02	0.98	0.98	0.02
5	0.98	0.02	0.98	0.02	0.02	0.98	0.02	0.98	0.02	0.98	0.98	0.02
6	0.98	0.02	0.98	0.02	0.02	0.98	0.02	0.98	0.02	0.98	0.98	0.02
7	0.98	0.02	0.98	0.02	0.02	0.98	0.02	0.98	0.02	0.98	0.98	0.02
8	0.98	0.02	0.98	0.02	0.02	0.98	0.02	0.98	0.02	0.98	0.98	0.02
9	0.98	0.02	0.98	0.02	0.02	0.98	0.02	0.98	0.02	0.98	0.98	0.02
10	0.98	0.02	0.98	0.02	0.02	0.98	0.02	0.98	0.02	0.98	0.98	0.02
11	0.2	0.8	0.2	0.8	0.02	0.98	0.02	0.98	0.02	0.98	0.2	0.8
12	0.2	0.8	0.2	0.8	0.02	0.98	0.02	0.98	0.02	0.98	0.2	0.8
13	0.1	0.9	0.1	0.9	0.02	0.98	0.02	0.98	0.02	0.98	0.1	0.9
14	0.1	0.9	0.1	0.9	0.02	0.98	0.02	0.98	0.02	0.98	0.1	0.9
15	0.02	0.98	0.02	0.98	0.02	0.98	0.98	0.02	0.98	0.02	0.02	0.98
16	0.02	0.98	0.02	0.98	0.02	0.98	0.98	0.02	0.98	0.02	0.02	0.98
17	0.02	0.98	0.02	0.98	0.02	0.98	0.98	0.02	0.98	0.02	0.02	0.98
18	0.02	0.98	0.02	0.98	0.02	0.98	0.98	0.02	0.98	0.02	0.02	0.98
19	0.02	0.98	0.02	0.98	0.02	0.98	0.98	0.02	0.98	0.02	0.02	0.98
20	0.02	0.98	0.02	0.98	0.02	0.98	0.98	0.02	0.98	0.02	0.02	0.98
21	0.02	0.98	0.02	0.98	0.02	0.98	0.98	0.02	0.98	0.02	0.02	0.98
22	0.02	0.98	0.02	0.98	0.02	0.98	0.98	0.02	0.98	0.02	0.02	0.98
23	0.02	0.98	0.02	0.98	0.02	0.98	0.98	0.02	0.98	0.02	0.02	0.98
24	0.02	0.98	0.02	0.98	0.02	0.98	0.98	0.02	0.98	0.02	0.02	0.98
25	0.02	0.98	0.02	0.98	0.02	0.98	0.98	0.02	0.98	0.02	0.02	0.98
26	0.02	0.98	0.02	0.98	0.02	0.98	0.98	0.02	0.98	0.02	0.02	0.98
27	0.02	0.98	0.02	0.98	0.02	0.98	0.98	0.02	0.98	0.02	0.02	0.98
28	0.02	0.98	0.02	0.98	0.02	0.98	0.98	0.02	0.98	0.02	0.02	0.98
29	0.9	0.1	0.9	0.1	0.02	0.98	0.98	0.02	0.98	0.02	0.9	0.1
30	0.9	0.1	0.9	0.1	0.02	0.98	0.98	0.02	0.98	0.02	0.9	0.1
31	0.2	0.8	0.2	0.8	0.8	0.2	0.1	0.9	0.1	0.9	0.2	0.8
32	0.2	0.8	0.2	0.8	0.8	0.2	0.1	0.9	0.1	0.9	0.2	0.8
33	0.8	0.2	0.8	0.2	0.8	0.2	0.1	0.9	0.1	0.9	0.8	0.2
34	0.8	0.2	0.8	0.2	0.8	0.2	0.1	0.9	0.1	0.9	0.8	0.2
35	0.8	0.2	0.8	0.2	0.8	0.2	0.1	0.9	0.1	0.9	0.8	0.2
36	0.8	0.2	0.8	0.2	0.8	0.2	0.1	0.9	0.1	0.9	0.8	0.2
37	0.9	0.1	0.9	0.1	0.8	0.2	0.1	0.9	0.1	0.9	0.9	0.1
38	0.9	0.1	0.9	0.1	0.8	0.2	0.1	0.9	0.1	0.9	0.9	0.1
39	0.98	0.02	0.98	0.02	0.5	0.5	0.02	0.98	0.02	0.98	0.98	0.02
40	0.98	0.02	0.98	0.02	0.5	0.5	0.02	0.98	0.02	0.98	0.98	0.02
41	0.98	0.02	0.98	0.02	0.1	0.9	0.02	0.98	0.02	0.98	0.98	0.02
42	0.98	0.02	0.98	0.02	0.1	0.9	0.02	0.98	0.02	0.98	0.98	0.02
43	0.98	0.02	0.98	0.02	0.02	0.98	0.02	0.98	0.02	0.98	0.98	0.02
44	0.98	0.02	0.98	0.02	0.02	0.98	0.02	0.98	0.02	0.98	0.98	0.02
45	0.98	0.02	0.98	0.02	0.02	0.98	0.02	0.98	0.02	0.98	0.98	0.02
46	0.98	0.02	0.98	0.02	0.02	0.98	0.02	0.98	0.02	0.98	0.98	0.02
47	0.98	0.02	0.98	0.02	0.02	0.98	0.02	0.98	0.02	0.98	0.98	0.02
48	0.98	0.02	0.98	0.02	0.02	0.98	0.02	0.98	0.02	0.98	0.98	0.02

B.2. Sample transition matrix probability values (travel to travel, travel to other zones) for an EV during a weekday

	$\lambda_{SH,Sn}$						
tp	$\lambda_{SH,S1}$	$\lambda_{SH,S2}$	$\lambda_{SH,S3}$	$\lambda_{SH,S4}$	$\lambda_{SH,S5}$	$\lambda_{SH,S6}$	$\lambda_{SH,SH}$
1	0.33	0.33	0	0	0	0.33	0.01
2	0.33	0.33	0	0	0	0.33	0.01
3	0.33	0.33	0	0	0	0.33	0.01
4	0.33	0.33	0	0	0	0.33	0.01
5	0.33	0.33	0	0	0	0.33	0.01
6	0.33	0.33	0	0	0	0.33	0.01
7	0.33	0.33	0	0	0	0.33	0.01
8	0.33	0.33	0	0	0	0.33	0.01
9	0.33	0.33	0	0	0	0.33	0.01
10	0.33	0.33	0	0	0	0.33	0.01
11	0	0	0	0.5	0.5	0	0
12	0	0	0	0.5	0.5	0	0
13	0	0	0	0.5	0.5	0	0
14	0	0	0	0.5	0.5	0	0
15	0	0	0	0.5	0.5	0	0
16	0	0	0	0.5	0.5	0	0
17	0	0	0	0.5	0.5	0	0
18	0	0	0	0.5	0.5	0	0
19	0	0	0	0.5	0.5	0	0
20	0	0	0	0.5	0.5	0	0
21	0	0	0	0.5	0.5	0	0
22	0	0	0	0.5	0.5	0	0
23	0	0	0	0.5	0.5	0	0
24	0	0	0	0.5	0.5	0	0
25	0	0	0	0.5	0.5	0	0
26	0	0	0	0.5	0.5	0	0
27	0	0	0	0.5	0.5	0	0
28	0	0	0	0.5	0.5	0	0
29	0.26	0.26	0.2	0	0	0.26	0.02
30	0.26	0.26	0.2	0	0	0.26	0.02
31	0.26	0.26	0.2	0	0	0.26	0.02
32	0.26	0.26	0.2	0	0	0.26	0.02
33	0.26	0.26	0.2	0	0	0.26	0.02
34	0.26	0.26	0.2	0	0	0.26	0.02
35	0.26	0.26	0.2	0	0	0.26	0.02
36	0.26	0.26	0.2	0	0	0.26	0.02
37	0.26	0.26	0.2	0	0	0.26	0.02
38	0.26	0.26	0.2	0	0	0.26	0.02
39	0.33	0.33	0	0	0	0.33	0.01
40	0.33	0.33	0	0	0	0.33	0.01
41	0.33	0.33	0	0	0	0.33	0.01
42	0.33	0.33	0	0	0	0.33	0.01
43	0.33	0.33	0	0	0	0.33	0.01
44	0.33	0.33	0	0	0	0.33	0.01
45	0.33	0.33	0	0	0	0.33	0.01
46	0.33	0.33	0	0	0	0.33	0.01
47	0.33	0.33	0	0	0	0.33	0.01
48	0.33	0.33	0	0	0	0.33	0.01

B.3. Sample observation matrix probability values for an EV during a weekday

	S_1					S_2					S_3					S_4					S_5					S_6				
	RA	**WP**	**CC**	**SM**	**RL**	**RA**	**WP**	**CC**	**SM**	**RL**	**RA**	**WP**	**CC**	**SM**	**RL**	**RA**	**WP**	**CC**	**SM**	**RL**	**RA**	**WP**	**CC**	**SM**	**RL**	**RA**	**WP**	**CC**	**SM**	**RL**
1	0.95	0	0.05	0	0	0.95	0	0.05	0	0	0	0	0.2	0.8	0	0	0	0	0.05	0.95	0	0.5	0	0.5	0	0.99	0	0	0.01	0
2	0.95	0	0.05	0	0	0.95	0	0.05	0	0	0	0	0.2	0.8	0	0	0	0	0.05	0.95	0	0.5	0	0.5	0	0.99	0	0	0.01	0
3	0.95	0	0.05	0	0	0.95	0	0.05	0	0	0	0	0.2	0.8	0	0	0	0	0.05	0.95	0	0.5	0	0.5	0	0.99	0	0	0.01	0
4	0.95	0	0.05	0	0	0.95	0	0.05	0	0	0	0	0.2	0.8	0	0	0	0	0.05	0.95	0	0.5	0	0.5	0	0.99	0	0	0.01	0
5	0.95	0	0.05	0	0	0.95	0	0.05	0	0	0	0	0.2	0.8	0	0	0	0	0.05	0.95	0	0.5	0	0.5	0	0.99	0	0	0.01	0
6	0.95	0	0.05	0	0	0.95	0	0.05	0	0	0	0	0.2	0.8	0	0	0	0	0.05	0.95	0	0.5	0	0.5	0	0.99	0	0	0.01	0
7	0.95	0	0.05	0	0	0.95	0	0.05	0	0	0	0	0.2	0.8	0	0	0	0	0.05	0.95	0	0.5	0	0.5	0	0.99	0	0	0.01	0
8	0.95	0	0.05	0	0	0.95	0	0.05	0	0	0	0	0.2	0.8	0	0	0	0	0.05	0.95	0	0.5	0	0.5	0	0.99	0	0	0.01	0
9	0.95	0	0.05	0	0	0.95	0	0.05	0	0	0	0	0.2	0.8	0	0	0	0	0.05	0.95	0	0.5	0	0.5	0	0.99	0	0	0.01	0
10	0.95	0	0.05	0	0	0.95	0	0.05	0	0	0	0	0.2	0.8	0	0	0	0	0.05	0.95	0	0.5	0	0.5	0	0.99	0	0	0.01	0
11	0.8	0	0.2	0	0	0.8	0	0.2	0	0	0	0	0.2	0.8	0	0	0.9	0	0.1	0	0	0.8	0	0.2	0	0.8	0	0	0.2	0
12	0.8	0	0.2	0	0	0.8	0	0.2	0	0	0	0	0.2	0.8	0	0	0.9	0	0.1	0	0	0.8	0	0.2	0	0.8	0	0	0.2	0
13	0.8	0	0.2	0	0	0.8	0	0.2	0	0	0	0	0.2	0.8	0	0	0.9	0	0.1	0	0	0.8	0	0.2	0	0.8	0	0	0.2	0
14	0.8	0	0.2	0	0	0.8	0	0.2	0	0	0	0	0.2	0.8	0	0	0.9	0	0.1	0	0	0.8	0	0.2	0	0.8	0	0	0.2	0
15	0.8	0	0.2	0	0	0.8	0	0.2	0	0	0	0	0.2	0.8	0	0	0.9	0	0.1	0	0	0.8	0	0.2	0	0.8	0	0	0.2	0
16	0.8	0	0.2	0	0	0.8	0	0.2	0	0	0	0	0.2	0.8	0	0	0.9	0	0.1	0	0	0.8	0	0.2	0	0.8	0	0	0.2	0
17	0.8	0	0.2	0	0	0.8	0	0.2	0	0	0	0	0.2	0.8	0	0	0.9	0	0.1	0	0	0.8	0	0.2	0	0.8	0	0	0.2	0
18	0.8	0	0.2	0	0	0.8	0	0.2	0	0	0	0	0.2	0.8	0	0	0.9	0	0.1	0	0	0.8	0	0.2	0	0.8	0	0	0.2	0
19	0.8	0	0.2	0	0	0.8	0	0.2	0	0	0	0	0.2	0.8	0	0	0.9	0	0.1	0	0	0.8	0	0.2	0	0.8	0	0	0.2	0
20	0.8	0	0.2	0	0	0.8	0	0.2	0	0	0	0	0.2	0.8	0	0	0.9	0	0.1	0	0	0.8	0	0.2	0	0.8	0	0	0.2	0
21	0.8	0	0.2	0	0	0.8	0	0.2	0	0	0	0	0.2	0.8	0	0	0.9	0	0.1	0	0	0.8	0	0.2	0	0.8	0	0	0.2	0
22	0.8	0	0.2	0	0	0.8	0	0.2	0	0	0	0	0.2	0.8	0	0	0.9	0	0.1	0	0	0.8	0	0.2	0	0.8	0	0	0.2	0
23	0.8	0	0.2	0	0	0.8	0	0.2	0	0	0	0	0.2	0.8	0	0	0.9	0	0.1	0	0	0.8	0	0.2	0	0.8	0	0	0.2	0
24	0.8	0	0.2	0	0	0.8	0	0.2	0	0	0	0	0.2	0.8	0	0	0.9	0	0.1	0	0	0.8	0	0.2	0	0.8	0	0	0.2	0
25	0.8	0	0.2	0	0	0.8	0	0.2	0	0	0	0	0.2	0.8	0	0	0.9	0	0.1	0	0	0.8	0	0.2	0	0.8	0	0	0.2	0
26	0.8	0	0.2	0	0	0.8	0	0.2	0	0	0	0	0.2	0.8	0	0	0.9	0	0.1	0	0	0.8	0	0.2	0	0.8	0	0	0.2	0
27	0.8	0	0.2	0	0	0.8	0	0.2	0	0	0	0	0.2	0.8	0	0	0.9	0	0.1	0	0	0.8	0	0.2	0	0.8	0	0	0.2	0
28	0.8	0	0.2	0	0	0.8	0	0.2	0	0	0	0	0.2	0.8	0	0	0.9	0	0.1	0	0	0.8	0	0.2	0	0.8	0	0	0.2	0
29	0.8	0	0.2	0	0	0.8	0	0.2	0	0	0	0	0.2	0.8	0	0	0.9	0	0.1	0	0	0.8	0	0.2	0	0.8	0	0	0.2	0
30	0.8	0	0.2	0	0	0.8	0	0.2	0	0	0	0	0.2	0.8	0	0	0.9	0	0.1	0	0	0.8	0	0.2	0	0.8	0	0	0.2	0
31	0.8	0	0.2	0	0	0.8	0	0.2	0	0	0	0	0.2	0.8	0	0	0.9	0	0.1	0	0	0.8	0	0.2	0	0.8	0	0	0.2	0
32	0.8	0	0.2	0	0	0.8	0	0.2	0	0	0	0	0.2	0.8	0	0	0.9	0	0.1	0	0	0.8	0	0.2	0	0.8	0	0	0.2	0
33	0.8	0	0.2	0	0	0.8	0	0.2	0	0	0	0	0.2	0.8	0	0	0.9	0	0.1	0	0	0.8	0	0.2	0	0.8	0	0	0.2	0
34	0.8	0	0.2	0	0	0.8	0	0.2	0	0	0	0	0.2	0.8	0	0	0.9	0	0.1	0	0	0.8	0	0.2	0	0.8	0	0	0.2	0
35	0.8	0	0.2	0	0	0.8	0	0.2	0	0	0	0	0.2	0.8	0	0	0.9	0	0.1	0	0	0.8	0	0.2	0	0.8	0	0	0.2	0
36	0.8	0	0.2	0	0	0.8	0	0.2	0	0	0	0	0.2	0.8	0	0	0.9	0	0.1	0	0	0.8	0	0.2	0	0.8	0	0	0.2	0
37	0.8	0	0.2	0	0	0.8	0	0.2	0	0	0	0	0.2	0.8	0	0	0.9	0	0.1	0	0	0.8	0	0.2	0	0.8	0	0	0.2	0
38	0.8	0	0.2	0	0	0.8	0	0.2	0	0	0	0	0.2	0.8	0	0	0.9	0	0.1	0	0	0.8	0	0.2	0	0.8	0	0	0.2	0
39	0.8	0	0.2	0	0	0.8	0	0.2	0	0	0	0	0.2	0.8	0	0	0.9	0	0.1	0	0	0.8	0	0.2	0	0.8	0	0	0.2	0
40	0.95	0	0.05	0	0	0.95	0	0.05	0	0	0	0	0.2	0.8	0	0	0	0	0.05	0.95	0	0.4	0	0.3	0	0.99	0	0	0.01	0
41	0.95	0	0.05	0	0	0.95	0	0.05	0	0	0	0	0.2	0.8	0	0	0	0	0.05	0.95	0	0.4	0	0.3	0	0.99	0	0	0.01	0
42	0.95	0	0.05	0	0	0.95	0	0.05	0	0	0	0	0.2	0.8	0	0	0	0	0.05	0.95	0	0.4	0	0.3	0	0.99	0	0	0.01	0
43	0.95	0	0.05	0	0	0.95	0	0.05	0	0	0	0	0.2	0.8	0	0	0	0	0.05	0.95	0	0.4	0	0.3	0	0.99	0	0	0.01	0
44	0.95	0	0.05	0	0	0.95	0	0.05	0	0	0	0	0.2	0.8	0	0	0	0	0.05	0.95	0	0.4	0	0.3	0	0.99	0	0	0.01	0
45	0.95	0	0.05	0	0	0.95	0	0.05	0	0	0	0	0.2	0.8	0	0	0	0	0.05	0.95	0	0.4	0	0.3	0	0.99	0	0	0.01	0
46	0.95	0	0.05	0	0	0.95	0	0.05	0	0	0	0	0.2	0.8	0	0	0	0	0.05	0.95	0	0.4	0	0.3	0	0.99	0	0	0.01	0
47	0.95	0	0.05	0	0	0.95	0	0.05	0	0	0	0	0.2	0.8	0	0	0	0	0.05	0.95	0	0.4	0	0.3	0	0.99	0	0	0.01	0
48	0.95	0	0.05	0	0	0.95	0	0.05	0	0	0	0	0.2	0.8	0	0	0	0	0.05	0.95	0	0.4	0	0.3	0	0.99	0	0	0.01	0